공학박사학위논문

고체상 수소화붕소나트륨을 통한 고출력 수소생산시스템에 관한 연구

Study on the Hydrogen Generation System for High-power Fuel Cell Applications based on Hydrolysis of Solid-state Sodium Borohydride

2023년 2월

서울대학교 대학원

기계항공공학부

고 재 선

고체상 수소화붕소나트륨을 통한 고출력 수소생산시스템에 관한 연구

Study on the Hydrogen Generation System for High-power Fuel Cell Applications based on Hydrolysis of Solid-state Sodium Borohydride

지도교수 김 민 수

이 논문을 공학박사 학위논문으로 제출함

2022년 10월

서울대학교 대학원

기계항공공학부

고 재 선

고재선의 공학박사 학위논문을 인준함

2022년 12월

위 원 장 : _____ **(인)**

부위원장 : _____ **(인)**

위 원 : _____ **(인)**

위 원 : _____ **(인)**

위 원 : _____ **(인)**

Abstract

Study on the Hydrogen Generation System for High-power Fuel Cell Applications based on Hydrolysis of Solid-state Sodium Borohydride

Jae Seon Koh

Department of Mechanical and Aerospace Engineering

The Graduate School

Seoul National University

To alleviate the climate crisis, global efforts are underway to reduce greenhouse gases and achieve carbon neutrality, and fossil fuel reduction is the most important aspect of achieving these goals. Hydrogen has been revealed the most remarkable clean and efficient energy carrier to replace fossil fuels. Accordingly, hydrogen-powered fuel cells are attracting significant attention as power generators for various applications, from portable devices to high-power applications (such as heavy-duty vehicles, electricity generators). These new

fuel cell applications will require the production, storage, and transportation of hydrogen suitable for their desired properties. Hydrogen storage methods include compression, liquefaction, absorption, and chemical hydride, the first two of which are currently the preferred methods for high-power fuel cell applications. However, liquified hydrogen has critical problems, such as excessive energy consumption during liquefication and continuous loss due to vaporization. When compressed, the density of hydrogen at 70 MPa is relatively low (38 kg/m^3) and a substantial amount of compression work is also consumed. For these reason, chemical hydrides (including metal-borohydride, ammonia borane, and methanol) are promising candidates to handle the aforementioned issues. In particular, sodium borohydride ($NaBH_4$, SBH) has been regarded as one of the leading chemical hydrides due to its high hydrogen storage capacity (10.6 wt.%).

Hydrolysis of SBH is the most commonly used method to generate hydrogen from SBH. In ambient conditions, the conversion of SBH via self-hydrolysis is only 7%–8% and it is too slow for utilization in any fuel cell applications. Therefore, the hydrolysis of SBH needs a way to accelerate. In particular, the process can be accelerated by using acid or metal catalysts. The hydrolysis of SBH using metal catalysts can facilitate a continuous reaction at a relatively low temperature and pressure. However, in most cases of using

metal catalysts, SBH should be prepared as an aqueous solution and its solubility issues, SBH concentration should be <16 g per 100 g of water to keep the reaction product liquid. This implies that when a metal catalyst is used, the gravimetric hydrogen storage capacity is only 2–3 wt.%. Moreover, given the limited active sites of the metal catalyst and the low concentration of SBH, it is difficult to obtain sufficient hydrogen generation rates for high-power fuel cell applications. In contrast, acid-accelerated hydrolysis offers several advantages, such as high activity under optimum conditions, no catalyst recovery and recycling, minimum side reactions, low cost, ease of injection and usage, and high controllability. For these reasons, acid-accelerated hydrolysis of SBH is more suitable for hydrogen generation systems for high-power fuel cell applications. Moreover, in the acid-accelerated hydrolysis process, SBH can be prepared either in an aqueous solution or a solid-state. For this reason, hydrolysis of solid-state SBH with acid-acceleration enables to achieve high hydrogen storage density and high-flow rate hydrogen generation for high-power fuel cell applications.

In Chapter 2, The characteristics of the SBH hydrogen generation system were analyzed by experiments according to various parameters. In addition, ^{11}B solid NMR spectroscopy and viscosity measurement were conducted to analyze the composition and properties of the reaction product. In 5% concentration

feed experimental cases, the conversion of SBH was ≥95%, and a maximum of 6.71 wt.% gravimetric hydrogen storage density was achieved. The experimental results indicated that it is possible to control the rate of hydrogen generation through the feed injection rate. In addition, as a result of experiments according to the reactant temperature, it was demonstrated that the lower the reactant temperature, the less hydrogen produced, and the greater amount of unreacted dissolved SBH. Moreover, when the stoichiometric number increased, the gravimetric hydrogen storage density decreased. This reduced the viscosity of the reaction product and the amount of unreacted dissolved SBH observed when the reaction was conducted at low reactant temperatures. As a result of the viscosity measurement by rheometer, the reaction product showed gel-solution transition characteristics which has gel or solution state depending on their temperature, suggesting that discharge of the reaction product is virtually impossible at the temperature below the gel-solution transition temperature. Since the gel-solution transition temperature can be significantly lowered by injecting a little additional feed, it is possible to consider increasing the stoichiometric number for practical purposes.

In Chapter 3, The reaction and thermal management simulation of the SBH hydrogen generation system, which has been neglected so far, was performed. Since the hydrolysis of SBH is the exothermic reaction, thermal management

is important in case of hydrogen generation system for high-power applications. The reaction and thermal management modeling were performed to confirm such as evaluating the maximum hydrogen generation rate that were difficult to confirm through experiments. The simulation was validated through the experimental results and showed relatively high accuracy. In particular, except for the initial stage of reaction when the reactant was not homogeneous, the reactant temperature showed an error of 5% or less. Base on the simulation result of the reactant temperature, stable operation was possible up to the feed injection rate of 175 mL/min, which can operate about 12 kW of fuel cell applications.

In Chapter 4, The operation strategies for more efficient utilization of hydrogen generation system in this study were analyzed. First, the on-board operation feasibility considering the transportability of SBH was evaluated. As a result of conducting experiments by changing the feed injection rate within a single batch reaction, the hydrogen generation rate was also increased or decreased according to the increase or decrease of the feed injection rate. Also, it was confirmed that it is possible to change the hydrogen generation rate multiple times within a single batch reaction if there is sufficient reaction time. Based on this result, it was shown that on-board operation of the hydrogen generation system in this study is possible. In addition, it was evaluated whether

it was possible to improve the hydrogen storage density by reducing acid usage. As a result of the experiment according to the acid concentration of feed in Chapter 2, based on the similar tendency of hydrogen generation rates of 2.5% concentration feed and 5% concentration feed at the initial stage of the reaction, experiments that a certain ratio of the reaction was conducted with 2.5% concentration feed and the rest ratio of the reaction was conducted with 5% concentration feed was conducted to maximize hydrogen generation and reduce acid usage. As results of experiments, even when 2.5% concentration feed was used in the smallest proportion, the conversion and hydrogen storage density were lower than when only 5% concentration feed was used, and the unreacted agglomerated SBH observed when using 2.5% concentration feed was increased as the ratio of the reaction conducting 2.5% concentration feed increased. However, when replacing water used for feed with the water generated from fuel cell, using 2.5% concentration feed during the initial 25% reaction progress ratio showed a 1% lower conversion than using only 5% concentration feed, but acid usage can be reduced by 12.5% so it can be considered to reduce fuel cost.

Through this study, the factors affecting the performance of the hydrogen generation system for high-power fuel cell applications based on hydrolysis of solid-state SBH were evaluated and the operation strategies were presented.

Also, the hydrogen generation system in this study can contribute to the revitalization of the hydrogen society by extending the scope of hydrogen applications.

Keyword: Hydrogen generation system, Sodium borohydride ($NaBH_4$), Formic acid, Acid-accelerated hydrolysis of SBH, Semi-batch reactor thermal management, Operation optimization, Hydrogen storage density, ^{11}B solid nuclear magnetic resonance (NMR) spectroscopy,

***Identification Number*: 2013-20642**

Contents

Abstract ..... **i**

Contents ..... **viii**

List of Figure ..... **xi**

List of Table ..... **xvi**

Nomenclature ..... **xvii**

Chapter 1. Introduction **1**

1.1. Background of the study 1

1.2. Literature survey 11

1.2.1. Hydrogen generation system based on hydrolysis of SBH 11

1.2.2. Simulation of hydrogen generation system based on hydrolysis of SBH 18

1.3. Objectives and scopes 21

Chapter 2. Experimental study of SBH hydrogen generation system **24**

2.1. Introduction 24

2.2. Experimental apparatus of hydrogen generation system 28

2.2.1. Experimental setup 28

2.2.2. Accuracy of measuring devices and uncertainty analysis 34

2.2.3. Experiment procedure 36

2.2.4. Analytical techniques 39

2.3. Experimental analysis of factors affecting hydrogen generation characteristics 40

2.3.1. Effect of the reactant temperature 40
2.3.2. Effect of the feed injection rate 50
2.3.3. Effect of the stoichiometric number 55
2.3.4. Effect of the feed concentration 63
2.3.5. Hydrogen conversion of the liquid hydrolysis of solid SBH..... 74
2.4. Summary.....77
Chapter 3. Thermal simulation of SBH hydrogen generation system.....80
3.1. Introduction 80
3.2. Model description.....83
3.2.1. Hydrolysis reaction modeling 83
3.2.2. Heat transfer modeling of cooling system..... 94
3.3. Results and discussion 110
3.3.1. Simulation validation 110
3.3.2. Limit hydrogen generation ability evaluation 119
3.4. Summary.....132
Chapter 4. Operation strategy of SBH hydrogen generation system 134
4.1. Introduction 134
4.2. Experimental condition.....137
4.3. Experimental results and discussion.....140
4.3.1. 'On-board' operability evaluation 140
4.3.2. Maximize hydrogen storage density..... 146
4.4. Summary.....155
Chapter 5. Concluding remarks.....158

Reference.....163

국 문 초 록 184

List of Figure

Figure 1.1 Hydrogen storage method and their advantages and disadvantages 2

Figure 1.2 Gravimetric and Volumetric hydrogen density of some selected metal and chemical hydride 4

Figure 2.1 Theoretical gravimetric hydrogen storage density (in wt.% H_2) according to moles of H_2O per mole of SBH. 25

Figure 2.2 Experimental apparatus of hydrogen generation system based on acid-accelerated liquid hydrolysis of solid SBH at elevated temperature and pressure..... 29

Figure 2.3 Schematic diagram of experimental apparatus 30

Figure 2.4 CAD perspective view of the reactor (Coil position and shape are approximate and not exact) 31

Figure 2.5 Sensing point of multi-point thermocouple and position of cooling coil..... 33

Figure 2.6 Reactant temperature over time in case of RT#1, RT#2, and RT#3 41

Figure 2.7 Cumulative hydrogen generation over time in case of RT#1, RT#2, and RT#3 (a) entire experiment (Section 1 ~ Section 3) (b) stable operation section (Section 2)..... 43

Figure 2.8 Hydrogen generation amount by section in case of RT#1, RT#2, and RT#3..... 44

Figure 2.9 ^{11}B solid NMR spectroscopy results of reaction product in case of

(a) RT#1 (b) RT#2 (c) RT#3 47
Figure 2.10 X-ray diffractometer result of reaction product of RT#3 49
Figure 2.11 Experimental results according to feed injection rate, in case of 250 g SBH charging (a) hydrogen mass flow rate, (b) cumulative hydrogen generation amount 53
Figure 2.12 Experimental results according to feed injection rate, in case of 500 g SBH charging (a) hydrogen mass flow rate, (b) cumulative hydrogen generation amount 54
Figure 2.13 Cumulative hydrogen generation amount overtime according to stoichiometric number (a) 160 ℃ reactant temperature (RT#1, SN#1) (b) 180 ℃ reactant temperature (RT#2, SN#2) 56
Figure 2.14 ^{11}B solid NMR spectroscopy results of reaction product in case of (a) SN#1 (b) SN#2 59
Figure 2.15 Rheometer results of reaction product in case of RT#1, RT#2, SN#1, and SN#2 at sheer rate 1 /s 60
Figure 2.16 Reactant temperature over time in case of FC#1, FC#2, and FC#3 65
Figure 2.17 Cumulative hydrogen generation over time in case of FC#1, FC#2, and FC#3 (a) entire experiment (Section 1 ~ Section 3) (b) initial section (Section 1) (c) stable operation section (Section 2) 66
Figure 2.18 Hydrogen generation amount by section in case of FC#1, FC#2, and FC#3 67
Figure 2.19 Example of the unreacted agglomerated SBH after experiment 70
Figure 2.20 ^{11}B solid NMR spectroscopy results of reaction product in case of

(a) FC#1 (b) FC#2 (c) FC#3 72

Figure 3.1 Specific heat value with temperature change of reaction component 88

Figure 3.2 Cumulative hydrogen generation (mol) of experiments RT#1, RT#2, and RT#3 in homogeneous condition..... 92

Figure 3.3 Arrehnius plot of 5% acid concentration experiment (RT#1, RT#2, RT#3) 93

Figure 3.4 The shape and dimension symbols of the reactor and helical cooling coil..... 95

Figure 3.5 Control volume of the reactor and vertically helical coil..... 97

Figure 3.6 The schemetic diagram of heat transfer in helical cooling coil.... 99

Figure 3.7 Experimental data of SV#1 inputed in the simulation (a) coolant and hydrogen mass flow rate, (b) coolant inlet temperature.....112

Figure 3.8 Experimental data of SV#2 inputed in the simulation (a) coolant and hydrogen mass flow rate, (b) coolant inlet temperature.....113

Figure 3.9 Experiment and simulation comparison of SV#1 (a) reactant temperature, (b) coolant outlet temperature 114

Figure 3.10 Experiment and simulation comparison of SV#2 (a) reactant temperature, (b) coolant outlet temperature 115

Figure 3.11 Error between experiment and simulation of the reactant temperature and coolant outlet temperature (a) SV#1 (b) SV#2 118

Figure 3.12 Experimental results of (a) hydrogen generation rate according to feed injection rate over normalized time (b) hydrogen generation

rate per 1 mL/min feed injection over normalized time 120

Figure 3.13 Hydrogen generation rate per 1 mL/min feed injection rate over normalized time applied to the simulation 122

Figure 3.14 Simulation results in case of 150 mL/min feed injection rate (a) the reactant temperature (b) the heat release by the cooling coil .. 123

Figure 3.15 Simulation results in case of 175 mL/min feed injection rate (a) the reactant temperature (b) the heat release by the cooling coil .. 124

Figure 3.16 Simulation results in case of 200 mL/min feed injection rate (a) the reactant temperature (b) the heat release by the cooling coil .. 125

Figure 3.17 Simulation results when controlling the coolant mass flow rate proportionally (a) the reactant temperature (b) the coolant mass flow rate 127

Figure 3.18 Simulation results when controlling the coolant mass flow rate proportionally (a) the heat release by the cooling coil (b) the coolant outlet temperature..... 128

Figure 3.19 Simulation results when controlling the coolant mass flow rate proportionally (50 g/s maximum coolant mass flow rate) (a) the reactant temperature (b) the coolant mass flow rate 130

Figure 3.20 Simulation results when controlling the coolant mass flow rate proportionally (50 g/s maximum coolant mass flow rate) (a) the heat release by the cooling coil (b) the coolant outlet temperature 131

Figure 4.1 Experimenet result of OB#1 (a) hydrogen mass flow rate over normalized time (b) cumulative hydrogen generation amount over

reaction time..... 143

Figure 4.2 Experimenet result of OB#2 (a) hydrogen mass flow rate over normalized time (b) cumulative hydrogen generation amount over reaction time..... 144

Figure 4.3 Experimenet result of OB#3 (a) hydrogen mass flow rate over normalized time (b) cumulative hydrogen generation amount over reaction time..... 145

Figure 4.4 Experimenet result of HD#1 (a) hydrogen mass flow rate over time (b) cumulative hydrogen generation amount over time 148

Figure 4.5 Experimenet result of HD#2 (a) hydrogen mass flow rate over time (b) cumulative hydrogen generation amount over time 149

Figure 4.6 Experimenet result of HD#3 (a) hydrogen mass flow rate over time (b) cumulative hydrogen generation amount over time 150

Figure 4.7 ^{11}B solid NMR spectroscopy results of reaction product in case of (a) HD#1 (b) HD#2 (c) HD#3..... 153

Figure 4.8 Picture of the unreacted agglomerated SBH after experiment (a) HD#1, (b) HD#2, (c) HD#3 154

List of Table

Table 1.1 Approximate prices of several metal-borohydride..... 6

Table 2.1 Accuracies of measuring devices..... 35

Table 2.2 Experimental conditions 37

Table 2.3 Feed injection amount by experimental condition (g/100 g SBH) 38

Table 2.4 Hydrogen generation amount according to reactant temperature .. 45

Table 2.5 Hydrogen generation amount according to stoichiometric number 57

Table 2.6 Hydrogen generation amount according to reactant temperature in case of 2.5 % feed concentration..... 68

Table 2.7 Hydrogen generation amount and conversion of experiments..... 76

Table 3.1 Correlations and conditions used in inner convection heat transfer coefficient calculation 102

Table 3.2 Correlations and conditions used in outer convection heat transfer coefficient calculation 107

Table 3.3 Experimental conditions for simulation validation.....111

Table 4.1 Experiments conditions for ‘on-board’ operability evaluation and optimization of hydrogen storage density 138

Table 4.2 Experimental results of HD#1, HD#2, HD#3 147

Nomenclature

a	thermal coefficient of resistance (1/°C)
A	area (m^2)
C_i	concentration of component i
Cp	specific heat capacity (J/kg)
D_{rin}	reactor inner diameter (m)
D_{rout}	reactor outer diameter (m)
D_c	coil diameter (m)
d_{cin}	coil tube inner diameter (m)
d_{cout}	coil tube outer diameter (m)
Dn	Dean number
E	energy (J)
E_a	activation energy (kJ/mol)
F	Faraday constant
f	feed injection rate (mL/min)
Gr	Grashof number (-)
g	gravitational acceleration due to Earth (m/s^2)
ΔH	standard enthalpy change of formation (kJ)
h_{cs}	distance between reactor bottom and coil (m)
h_i	convection heat transfer coefficient of inside coil ($W/m^2 \cdot K$)
h_o	convection heat transfer coefficient of outside coil ($W/m^2 \cdot K$)
k	thermal conductivity ($W/m \cdot K$)
k_0	the Arrhenius coefficient (-)

L	coil length (m)
M	molar mass (kg/mol)
m	mass (kg)
$\dot{m}$	mass flow rate (kg/s)
n_i	number of moles of component i
Nu	Nusselt number (-) ($= hL/k$)
P	pressure (Pa)
p	coil pitch (m)
Pr	Prandtl number (-) ($= c_p\mu/k$)
$\dot{Q}$	heat transfer rate (W)
r	rate of reaction (mol/s)
Ra	Rayleigh number (-)
Re	Reynolds number (-) ($= \rho vL/\mu$)
T	temperature (°C)
t_w	thickness of reactor wall (m)
U_i	inner overall heat transfer coefficient of coil (W/K)
U_o	inner overall heat transfer coefficient of coil (W/K)
V	volume (m^3)
v	velosity (m/s)

Greek Letters

α	thermal diffusivity (m^2/s)
α_i	partial order of component i (-)

β	volumetric thermal expansion coefficient (K^{-1})
γ	reaction progress ratio (-)
ζ	friction factor
ρ	density (kg/m^3)
μ	viscosity (Pa/s)
ν	kinematic viscosity (m^2/s)
ρ	density (kg/m^3)

Subscripts

0	initial state
c	coil
f	coolant in coil
feed	feed
H2	hydrogen
l	liquid state
prod	reaction product
r	reactant
SBH	sodium borohydride
w	reactor wall

Abbreviations

SBH	Sodium borohydride

STP	Standarad temperatrue and pressure
DOE	U.S. Department of Energy
NMR	Nuclear megnetic resonance
XRD	X-ray diffractometer

Chapter 1. Introduction

1.1. Background of the study

To alleviate the climate crisis, global efforts are underway to reduce greenhouse gases and achieve carbon neutrality, and fossil fuel reduction is the most important aspect of achieving these goals. Studies have revealed that hydrogen is the most remarkable clean and efficient energy carrier to replace fossil fuels [1, 2]. Accordingly, hydrogen-powered fuel cells are attracting significant attention as power generators for various applications, from portable devices to high-power applications (such as electricity generators) [3-5]. In particular, these fuel cells could be beneficial for the electrification of heavy-duty vehicles, which is expected to be difficult because of their long driving range and reduced transport capacity due to battery weight [6, 7]. These new fuel cell applications will require the production, storage, and transportation of hydrogen suitable for their desired properties. As shown in Figure 1.1, hydrogen storage methods include compression, liquefaction, absorption, and chemical hydride, the first two of which are currently the preferred methods for high-power fuel cell applications [8]. However, liquified hydrogen has critical

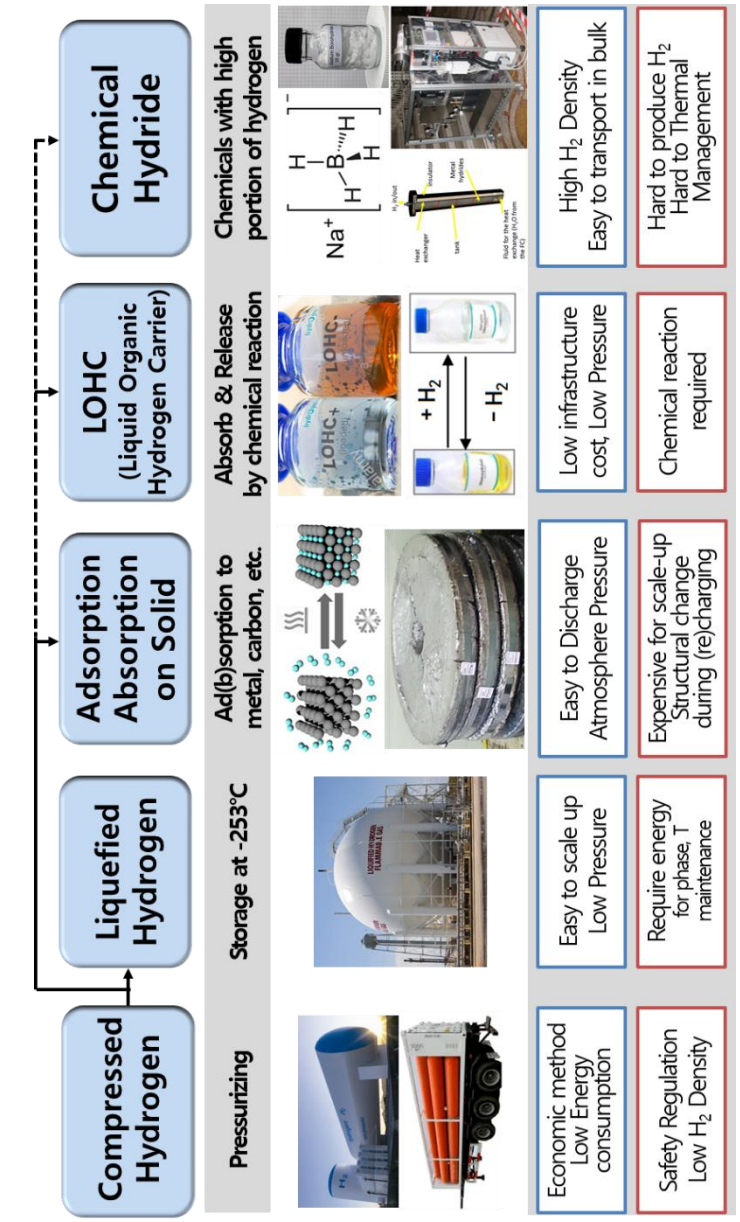

Figure 1.1 Hydrogen storage method and their advantages and disadvantages

problems, such as excessive energy consumption during liquefication and continuous loss due to vaporization [9]. When compressed, the density of hydrogen at 70 MPa is relatively low (38 kg/m^3) and a substantial amount of compression work is also consumed [10, 11]. With regard to transportation, hydrogen tube trailers and cryogenic liquid hydrogen trucks play important roles. Tube trailers are capable of delivering approximately 400 kg at 20 MPa, while cryogenic tanks delivered by semi-trucks operate at 1.1 MPa and are capable of transporting 3,200–4,500 kg of hydrogen [12]. However, these transportation methods cannot be considered long-term delivery solutions for the expected future hydrogen demands, because their low hydrogen transportation capacity would necessitate too many deliveries [13].

Chemical hydrides (including metal-borohydride, ammonia borane, and methanol) are promising candidates to handle the aforementioned issues [14]. These carriers could be used for mass transportation of hydrogen, which could then be released either before distribution or by the final customer. Even Sartbaeva et al. [1] concluded that light element hydrides are the only viable method of achieving a high gravimetric & volumetric hydrogen storage density.

As shown in Figure 1.2, due to the high hydrogen proportion in the borohydride ion (BH_4^-), in general, metal-borohydrides have a high gravimetric hydrogen storage density. Especially sodium borohydride ($NaBH_4$, SBH) has

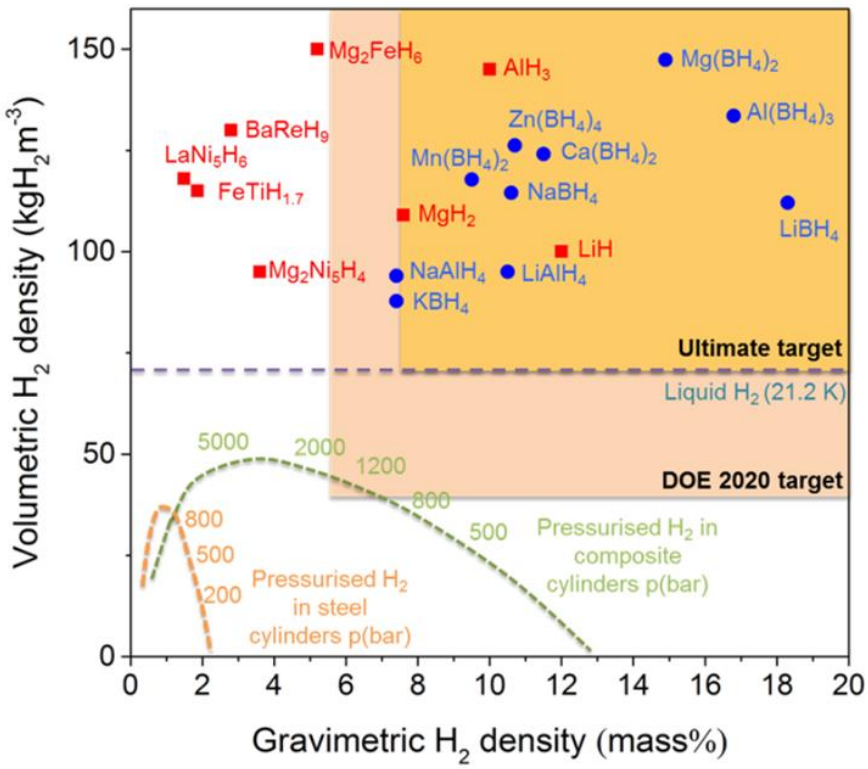

Figure 1.2 Gravimetric and Volumetric hydrogen density of some selected metal and chemical hydride

been regarded as one of the leading chemical hydrides due to its high hydrogen storage capacity (10.6 wt.%) [15-17]. Moreover, SBH has several further advantages, such as nonflammability, simple hydrolysis and recycling processes, stable reaction by-products that are environmentally benign, and low cost (compared to other hydrogen storage materials) [18]. There are also metal-borohydrides with a higher gravimetric hydrogen storage density than SBH, such as lithium borohydride ($LiBH_4$), magnesium borohydride ($Mg(BH_4)_2$), aluminum borohydride ($Al(BH_4)_3$), but a hydrogen generation method using them has not yet been established, and it is expected that commercialization will be difficult due to their high price as shown in Table 1.1.

Hydrogen stored in SBH can be dehydrogenated via thermolysis or hydrolysis [19]. However, thermolysis of SBH has several limitations, such as high decomposition temperature (300–600 ℃) [20], impure gas generation, and slow hydrogen release kinetics. Accordingly, SBH hydrolysis is the most commonly used method to generate hydrogen from SBH. The self-hydrolysis of SBH is a spontaneous and exothermic reaction. According to the hydrolysis reaction stoichiometry, 1 g of $NaBH_4$, fully hydrolyzed, will produce 2.37 L of hydrogen at standard temperature and pressure (STP). On a reactants-only basis, this gives a gravimetric hydrogen storage capacity of 10.8 wt.%, which more than satisfies the U.S. Department of Energy (DOE) storage density targets.

Table 1.1 Approximate prices of several metal-borohydride

Material	Price ($/kg)
Sodium borohydride (SBH)	3
Lithium borohydride ($LiBH_4$)	600
Magnesium borohydride ($Mg(BH_4)_2$)	100
Aluminum borohydride ($Al(BH_4)_3$)	3000

However, in ambient conditions, the conversion of SBH via self-hydrolysis is only 7%–8% and is too slow for utilization in any fuel cell applications [21-23]. In other words, the hydrolysis of SBH needs a way to accelerate. In particular, the process can be accelerated by using acid or metal catalysts [24, 25]. The hydrolysis of SBH using metal catalysts can facilitate a continuous reaction at a relatively low temperature and pressure. However, in most cases, SBH should be prepared as an aqueous solution and its solubility (55 g SBH per 100 g of water, 1.46 mol SBH per 5.56 mol of water, at 25 ℃) can result in low gravimetric hydrogen storage density [26]. Even the reaction product ($NaBO_2$) is less soluble than SBH (28 g $NaBO_2$ per 100 g of water at 25 ℃). This means that SBH concentration should be <16 g SBH per 100 g of water to keep the reaction product liquid, which precipitation of the reaction product could block the active site of the catalyst and cause losses in catalytic performance [27, 28]. This implies that when a metal catalyst is used, the gravimetric hydrogen storage capacity is only 2–3 wt.% [22]. Moreover, given the limited active sites of the metal catalyst and the low concentration of SBH, it is difficult to obtain sufficient hydrogen generation rates for high-power fuel cell applications. In contrast, acid-accelerated hydrolysis offers several advantages, such as high activity under optimum conditions, no catalyst recovery and recycling, minimum side reactions, low cost, ease of injection and usage, and high

controllability [29]. For these reasons, acid-accelerated hydrolysis of SBH is more suitable for hydrogen generation systems for high-power fuel cell applications. Moreover, in the acid-accelerated hydrolysis process, SBH can be prepared either in an aqueous solution or a solid state. This is in contrast to when a metal catalyst is used, where SBH must be prepared in an aqueous solution in most cases. Although SBH in an aqueous solution can be easily supplied through a pump, the advantages of acid-acceleration are lost, because it should be stabilized with a basic substance to prevent self-hydrolysis [26, 30]. Moreover, since solid SBH is difficult to supply quantitatively, SBH hydrolysis is conducted in a semi-batch reactor, rendering a continuous reaction difficult.

Hydrogen generation from SBH is illustrated by many papers published since the early 2000s. In a review paper published by Demirci et al. in 2009 [15], more than 50 papers using metal catalysts were reported, but only 5 papers using acid catalysts were reported. Furthermore in the review paper published by Abdelhamid H.N. [25] in 2021, more than 200 papers using metal catalysts have been reported, but only under 10 papers using acid catalysts have been reported. This is due to the advantages of using metal catalysts described above, but also to the impact of a major decision made by the DOE In November 2007, DOE has decided to make a no-go recommendation for SBH as an on-board hydrogen storage device for hydrogen vehicles, which is the most

representative high-power fuel cell application [31]. This decision had the effect of making SBH-based hydrogen storage devices confined to low-power fuel cell applications. Most of the subsequent studies have also focused on being applied to portable devices or niche applications [32], and in that case, since it is difficult to operate at high temperatures, studies focusing on metal catalysts have been conducted. The DOE cited the following reasons when deciding on a no-go recommendation.

i) Low hydrogen storage capacity performance targets for DOE target for 2007 and later: in general, achievable hydrogen storage density of 2-3 wt.% is the most critical issue.

ii) Net system cost will be higher than compressed hydrogen or liquified hydrogen

iii) Energy consumption and cost of regenerating reaction products ($NaBO_2$) back to fuel (SBH)

iv) Engineering issue of accumulating solid reaction products that are hard to discharge from reactor.

This decision was made more than 10 years ago, and nowadays, it can be said that there are more incentives to overcome these limitations that the demand for the transportation to a hydrogen society is increasing even more than at the time. Since the use of hydrogen becomes more widespread and the

demand for hydrogen increases, it will be emphasized that the transportation and storage of SBH is convenient and energy-efficient. This could alleviate concerns about energy consumption and cost. Therefore, the biggest problem is the low hydrogen storage density. If this can be solved through an engineering approach, the hydrogen production system based on SBH can also show potential for high-power fuel cell applications.

In this study, Hydrolysis of solid SBH with liquid water at elevated temperature and pressure in acid-accelerated condition was performed to increase hydrogen storage density and obtain sufficient hydrogen generation rate. Also, the practical feasibility of an SBH-based hydrogen generation system was shown for applying to high-power fuel cell applications by controlling the reaction heat released and analyzing the hydrogen generation characteristics according to various parameters

1.2. Literature survey

1.2.1. Hydrogen generation system based on hydrolysis of SBH

Researches on the hydrolysis of SBH began with metal-based catalysts due to easy to control reaction process and low reaction temperature. A large number of metals have been shown to be active in the hydrolysis of $NaBH_4$ in alkaline solutions under various temperature conditions, including Co and Ni and their borides, as well as noble metal-based catalysts such as Pt, Pd, Pt–Ru, and Pt–Pd. To increase the reaction rate and decrease the catalyst load required, it is important to ensure a small particle size and good dispersion to maximize the contact area between the catalyst and the $NaBH_4$ solution. Since noble metals are expensive and scarce, simple separation and reuse methods are highly required and the development of noble metal-free catalysts is a subject of current research, and most of these studies are devoted to the cobalt-based catalysts [33, 34], nickel based-catalysts [34, 35], metal salts ($NiCl_2$, $CoCl_2$) [36], colloidal platinum [37], active carbon [38], Raney nickel [39], Ru supported on ion-exchange resin beads [40], and fluorinated particles of based materials [24], as well as cobalt and nickel borides [41]. Among them, Ru-based catalysts are known to be the most effective for promoting H_2 generation [42]. The first metal-based materials used are metal salts [43-45]. Schlesinger et al.

[43] had tested $MnCl_2$, $FeCl_2$, $CoCl_2$, $NiCl_2$, $CuCl_2$. They reported that particularly striking was the catalytic effect of certain metal salts, especially that of $CoCl_2$. Liu et al. [44] compared $CoCl_2$, $NiCl_2$, and for the first time NiF_2. The highest reactivity of the Co-based salt was confirmed but the hydrogen generation rate was much lower than the rates obtained in other studies. This may be explained by the fact that they stabilized the aqueous solution with 10 wt.% NaOH. This shows that the performance of the catalyst may be lowered due to the influence of the aqueous solution stabilized with the base. Liu et al. [45] reported hydrogen generation rates of about 11 $L(H_2)/min \cdot g(Co)$ for $CoCl_2$ and gravimetric hydrogen storages up to 6–7 wt.%. This performance is likely the best reported for the metal salt. It should be noted that the result of Liu et al. [45] was also obtained by adding a catalyst solution to solid SBH, not preparing SBH as an aqueous solution. Noble metal-based catalysts such as Pt, Pd, Ru, and Rh can be characterized by superior catalytic activity towards the hydrolysis of SBH with high hydrogen generation rate [46-49]. Transition metal-based catalysts were considered to be an alternative to noble metals. Some of the transitional metals displayed better catalytic activity, especially Co is the most promising non-noble metal for hydrogen generation via the hydrolysis of SBH [33, 50]. Metal catalysts is needed the catalyst support to keep a certain shape in practical use and reduce the amount of metal materials.

The support improves the dispersion of the catalyst and it increases the active sites on the material's surface area and prevents the aggregation or agglomeration. It can also be used for processing into a thin film and three dimensional [51]. Several material types were reported as support including carbon nanotubes, graphene, ionic liquids (ILs), polymers, metal oxide, metal form and mesh, zeolite, and metal-organic frameworks (MOFs) etc. [25]. Metal catalysts are being studied focusing on obtaining maximum catalytic activity while using minimum metal through inexpensive support materials. Research on hydrogen generation system based on SBH, not simply measuring the effects or performance of catalysts, started in earnest in 2000 with the research of Amendola et al [52, 53]. Since then, there have been many studies on hydrogen production systems based on hydrolysis of SBH using metal catalyst [54-64]. Some notable studies are as follows. Richardson, et al. [55], reported a flow reactor. This reactor comprised a hollow tube with top and bottom end caps, and aimed for the continuous generation of hydrogen in the order of 500 W. In their fixed bed reactor, sodium borohydride was fed through a catalyst bed. Their experiment used a series of reactors to study this approach. The hydrogen generation system consisted of a catalytic reactor, pump, feed solution vessel, by-product catch vessel, and a heat exchanger. The heat exchanger was used to cool the hydrogen gas before it entered the fuel cell. Their results demonstrated

a steady-state load of 500 W and a peak capability of 2 kW. Zhang, et al. [56], studied a 1 kWe sodium borohydride hydrogen generation system, comprising a packed-bed reactor in which sodium borohydride solution is pumped through the bed to initiate the hydrolysis reaction. Using a gas–liquid separator, the gaseous hydrogen and liquid $NaBO_2$ solution were separated from the product stream. A large amount of water vapor entered into the high-temperature hydrogen stream, and to condense the water vapor a heat exchange process was used. Research of Kojima, Y. et al. [60] was one of the few studies that scale up systems up to 10kW using metal catalysts. They used a honeycomb monolith coated with Pt-LiCoO2 catalyst and feed SBH aqueous solution of maximum concentration of 25 wt.%. They achieved hydrogen generation rate of 10.8 g/min equivalent to 12 kW fuel cell operation. However, gravimetric hydrogen storage density was only 2 wt.%. Ferreira, M.J.F [61] conduct hydrolysis of solid SBH with solid nickel-ruthenium based catalyst. Their system has the advantage of not having to be stabilized with a base because solid SBH and a solid catalyst were used. They achieved maximum gravimetric hydrogen storage density of 6.3 wt.%. It indicates that the system using solid SBH certainly has a high gravimetric hydrogen storage density. However, it is expected that it is difficult to treat reaction products mixed with catalysts for reuse of catalyst when practical application. Marchionni et al. [64] aimed to

feed a 2 kW scale PEMFC stack by developing an apparatus for H_2 generation via hydrolysis of SBH. The reactor comprised a cylindrical stainless-steel chamber. A replaceable head piece with a stainless-steel rod whose vertical movement was controlled by a stepper motor was located on the top. The warm water was circulated inside the reactor. The initial temperature of the solution was controlled by a copper coil. The seal of the reactor was tested prior to any experiments using H_2 up to a pressure of 10 bars. Throughout all of the experiments, the catalyst was totally immersed in the solution. At 5 bar pressures, the catalyst was capable of generating up to 35 L H_2/min · $g_{catalyst}$. In this paper, an internal coil is installed inside the reactor. However, the internal coil was not used for thermal management, but for warm-up early in the reaction. As described in Chapter 1.1, hydrogen generation based on the hydrolysis of SBH is mainly designed for low-power and portable applications. Hence, many previous studies have been conducted based on metal catalysts, with relatively few (though important) studies conducted using acid acceleration. First, Schlesinger et al. [24] revealed that the hydrolysis reaction was significantly accelerated by the addition of acidic substances. Subsequently, several papers reported fundamental studies on acid-accelerated hydrolysis of SBH. Murugesan et al. [65] evaluated the acceleration effect of various mineral and carboxylic acids in the hydrolysis of solid SBH through a 5 mm^3 reactor.

Although they analyzed the reaction products by various acids and the acceleration effect of hydrolysis, this was in small-scale systems and the effect of temperature was not analyzed. Akdim et al. [66] asserted that acetic acid was a preferable alternative to HCl, as it is environmentally benign and safe. When strong acid catalysts are used, gasified acid or acid-byproducts that are harmful to the environment are generated. Hence, a purification facility is required, reducing the hydrogen storage density of the system. Kim et al. [67] contributed to the field by creating a protocol for hydrogen generation from the acid-accelerated hydrolysis of solid SBH. In addition, Aiello et al. [68], Beaird [69], and Liu [70] studied SBH hydrolysis via vapor without catalyst, including analyses of the reaction products. Their studies demonstrated that hydrogen can be produced through the hydrolysis of solid SBH with vapor at a sufficiently high temperature. Senliang, et al. [71], investigated theoretical support for seawater hydrogen production in coastal areas. The authors focused on the kinetics of $NaBH_4$ hydrolysis catalyzed by phosphotungstic acid, $H_3PW_{12}O_{40}$. Phosphotungstic acid is a kind of polyoxometalate with strong acid properties and it was selected as the active component of the catalyst. However, this solid acid supported by this activated carbon cannot show the advantage of acid-acceleration that this study focused. Several studies have investigated the acid-accelerated hydrolysis of solid SBH with vapor in small-scale systems [29, 59,

72-78]. For example, Lee, C.J. et al. [77] generated hydrogen from solid-state $NaBH_4$ using a HCl solution to circumvent the use of a catalyst. The aim was to address the need for a portable and stable hydrogen supply system for integration with a fuel cell. Their hydrogen supply system successfully provided a stable hydrogen supply to the fuel cell, allowing the 100 W fuel cell to operate reliably with an electric load of 0–6 A. Kwon, S.M. et al [29] developed hydrogen generation system using solid SBH and HCl for acceleration. Since they aimed at hydrogen generation devices for unmanned aerial vehicles, their hydrogen generation system achieved a maximum hydrogen production rate of 9 L/min, 5.1 wt.% gravimetric hydrogen storage density with a weight of 5.5 kg. The operation temperature and pressure of their system is maximum 70 ℃ and 5 bar. However, it is difficult to say that it is for high-power fuel cell application because this system can operate fuel cell of up to 1 kW. Akkus, M.S. et al. [75] revealed that the conversion of SBH according to vapor temperature is not directly proportional, and is maximized at a specific temperature. It would appear that when the vapor temperature increases, the molecule density of the vapor decreases, and an insufficient reaction causes a low conversion of SBH. This indicates that solid SBH needs to react with liquid water to produce a sufficiently high hydrogen flow rate for high-output fuel cell applications. Özkan, et al. [78], combined experimental data with a Box–

Wilson statistical experimental design technique to optimize the reaction temperature. Their experiments were carried out under different operating conditions and HCl concentrations to determine the maximum amount of hydrogen, which they found to be about 3.7 M HCl and 430 K.

1.2.2. Simulation of hydrogen generation system based on hydrolysis of SBH

The hydrolysis of SBH is an exothermic reaction. However, as previously discussed, since most of the hydrogen generation systems by hydrolysis of SBH were conducted with excess water in the low-power system at room temperature, there is almost any change in the temperature of the system, so the issue of heat management is rarely addressed and most hydrogen generation systems using metal catalysts did not even have a thermal management device. When an acid catalyst is used to cause a fast reaction with a small stoichiometric number, the system temperature rises, but since the higher temperature increases the reaction rate, it is not necessary to lower the temperature unless it is a threat to safety. Therefore, it can be seen that the previous study was limited to measuring the temperature [29]. Also, since hydrolysis of $NaBH_4$ for hydrogen generation is a complex process, which is influenced by factors such as catalyst performance, $NaBH_4$ concentration, stabilizer concentration,

reaction temperature, complex kinetics and excess water requirement, the kinetics of $NaBH_4$ hydrolysis reaction is not fully understood [79]. Since research on the reaction mechanism is being conducted on individual catalysts, there is a problem that it cannot be applied to systems using catalysts different from previous studies. In addition, the research method has also experimentally corrected empirical formula of some known mechanisms such as zero-order kinetics, nth order kinetics [80], Langmuir-Hinshelwood Model [42], Michaelis-Menten kinetics model [81], making it difficult to apply them in general. There was an example of an experimental study on the kinetics of pH-catalyzed hydrolysis of SBH [82-84], which is the reaction condition of this study, but the reaction temperature range was up to 80 ℃, which was different from the maximum temperature condition used in this study, up to 200 ℃. Therefore, since the purpose of the simulation in this study is to maintain the target operating temperature, the simulation was performed by predicting the reaction heat based on the hydrogen generation by the experimental results without applying theoretical reaction kinetics.

For the reasons described above, there have been hundreds of studies on the catalyst and hydrogen generation system, but there have been very few papers about simulating hydrolysis of SBH or its system [63, 85-89]. All of the papers about simulation dealt with metal catalysts, and focused on the

conversion of SBH to $NaBO_2$ by hydrolysis. Temperature is not an object to be "managed" but to be "simulated", and it was simply simulating the system temperature change according to the reaction. In most studies, the maximum temperature was below 70 °C, which did not require thermal management. The kinetics are calculated by experiment, and if a thermal management is not introduced, it is difficult to obtain a meaningful result through the simulation, so the study on the simulation seems to be insufficient. In addition, these studies hardly considered scale-up, which seems to be because hydrogen generation based on hydrolysis of SBH was expected to be applied to low-power fuel cell applications.

However, target operation conditions of this study are very harsh. Thermal management system is required to control the temperature inside the high temperature and pressure reactor as desired. In this study, a cooling system using pressurized water as a coolant was constructed, and the temperature was controlled by removing excess heat of reaction from the reactants through a helical coil installed inside the semi-batch reactor. Therefore, modeling of the thermal management system is very important to accurately simulate this hydrogen generation system.

1.3. Objectives and scopes

Hydrolysis using metal catalysts or vapor, which is the existing method, has limitations in generating sufficient hydrogen generation rate that can drive high-power fuel cells. The objectives of this study are to analyze the characteristics of the hydrogen generation system based on SBH hydrolysis that can be used in high-power fuel cell applications and to show its practicality. To this end, in this study, the system was pressurized to 40 bar to perform hydrolysis with solid SBH and liquid water, so that water did not vaporize even at a sufficiently high temperature. In addition, formic acid was used to accelerate the reaction. The outline of this study is as follows.

In Chapter 2, experimental study of hydrogen generation system based on acid-accelerated liquid hydrolysis of solid-state SBH was performed. Experiments on various parameters affecting this hydrogen generation system was conducted and hydrogen generation characteristics such as hydrogen generation rate and the conversion of SBH were analyzed. The analyzed parameters were the reactant temperature, the feed injection rate, the stoichiometric number, the feed concentration. The reaction product composition and its ratio were analyzed as ^{11}B nuclear magnetic resonance (NMR) spectroscopy, and viscosity was measured by rheometer.

In Chapter 3, simulation of hydrogen generation system based on acid-accelerated liquid hydrolysis of solid-state SBH was performed. Thermal management is very important for exothermic reactions carried out under high temperature and pressure as in this study. It is also important to predict the performance limit of the system for stable operation. Dynamic modeling of this hydrogen generation system was performed with Matlab/Simulink. The thermal models of the reactor, cooling system were modeled. Also, the amount of heat generated by hydrolysis of SBH was calculated by hydrogen generation rate which was expressed as a function of feed injection rate and the reaction progress ratio. Based on the simulation, the maximum hydrogen generation capability, which is difficult to confirm through experiments, was analyzed. Also, the design adequacy of the cooling system was analyzed.

In Chapter 4, The operation strategies for the efficient operation of hydrogen generation system in this study were analyzed. First, the feasibility of on-board operation was analyzed to utilize the characteristics of SBH, which has an advantage in transportation. For this purpose, it was analyzed by experiments whether the hydrogen generation rate was proportional to the change of the feed injection rate within a single batch reaction. In addition, through the experimental results of 5% concentration feed in Chapter 2, it was possible to obtain the conversion ≥ 95 % and sufficient hydrogen generation

rate by liquid hydrolysis of solid SBH at elevated temperature and pressure. The operation strategy that can maximize the hydrogen storage density and reduce the use of formic acid while maintaining a high conversion was analyzed. For this purpose, optimal operation strategies were derived by analyzing the hydrogen generation characteristics while performing the reaction by changing feed concentration within a single batch reaction.

In Chapter 5, the overall results of this study are summarized.

Chapter 2. Experimental study of SBH hydrogen generation system

2.1. Introduction

The hydrolysis process of SBH is expressed as Equation 2.1 [24]:

$$NaBH_4 + 2H_2O \rightarrow NaBO_2 + 4H_2 \quad (2.1)$$

Although Equation 2.1 is the ideal reaction, in practice, because of the mass transfer limitation and the vaporization of water during the reaction process, it is difficult to achieve such a high hydrogen capacity, as Equation 2.2 [76]:

$$NaBH_4 + (2 + x)H_2O \rightarrow NaBO_2 \cdot xH_2O + 4H_2, \quad (2.2)$$

where x is the excess of water. The theoretical gravimetric hydrogen storage densities based on water amounts of H_2O (2+x) per 1 mol of SBH are shown in Figure 2.1. As shown in Figure 2.1, the hydrogen storage density decreases significantly as the amount of water injected into the reaction increases. Due to the limitation of the solubility of the reaction product ($NaBO_2$), a system to which a metal catalyst is applied requires a lot of water and thus has a hydrogen storage density of 2-3% (gray area in Figure 2.1: the amount of

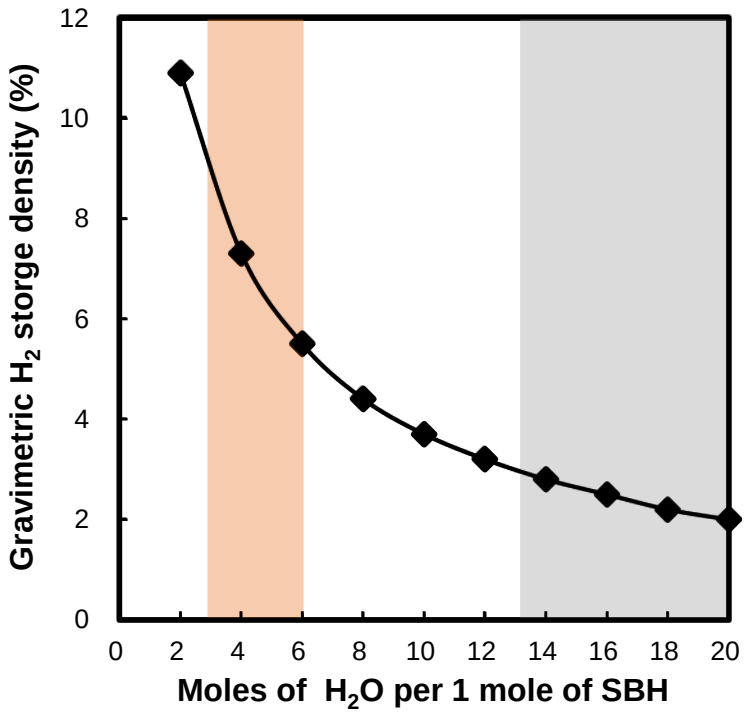

Figure 2.1 Theoretical gravimetric hydrogen storage density (in wt.% H_2) according to moles of H_2O per mole of SBH.

water that the reaction product ($NaBO_2$) can all dissolve in). According to the solubility of $NaBH_4$ and thermodynamics, $NaBH_4$ has a maximum hydrogen density of 7 wt.%. The solubility of $NaBH_4$ and the hydrolysis by-product $NaBO_2$ determine the full amount of $NaBH_4$ and H_2O. As a rule of thumb, the solubility of $NaBH_4$ and $NaBO_2$ depends on the reaction temperature. The amount of water and $NaBH_4$ can be calculated from the following Equation 2.3 and Equation 2.4 [60].

$$\text{Solubility of } NaBH_4 \text{ (g/100 g } H_2O) = -261 + 1.05\,T \quad (2.3)$$

$$\text{Solubility of } NaBO_2 \text{ (g/100 g } H_2O) = -245 + 0.915\,T \quad (2.4)$$

where T is the temperature (K). However, in case of acid-accelerated hydrolysis, the hydrogen storage density can be increased by minimizing the use of water (orange area in Figure 2.1: in acid conditions, the area means that it can react with solid phase SBH). From Equation 2.1 and Equation 2.2, it is evident that water provides half of the hydrogen, which is one of the reasons why hydrolysis is more attractive than thermolysis for hydrogen generation method using SBH.

It was reported that the rate at which SBH self-hydrolysis in water depends on the pH and solution temperature [90]. The rate is empirically represented by Equation 2.5

$$\log(t_{1/2}) = \text{pH} - (0.034\,T - 1.92) \quad (2.5)$$

Where $t_{1/2}$ is the time (min) it takes for one-half of a SBH mole to decompose versus temperature (K) [91]. Although it is difficult to apply Equation 2.5 directly owing to it is not a formula calculated under the same conditions as this study (pH from 7 to 10, reactant temperature from 15 ℃ to 35 ℃), Equation 2.5 shows that the hydrolysis of SBH occurs quickly at high temperature and low pH by addition of acid. Self-hydrolysis is an obstacle in the case of a metal catalyst in which SBH should be prepared in an aqueous solution, but when SBH is prepared in solid state, it is important to accelerate self-hydrolysis.

Through experiments in this chapter, the effect of parameters affecting the performance of acid-accelerated solid-state SBH hydrolysis on the hydrogen production characteristics was analyzed.

2.2. Experimental apparatus of hydrogen generation system

2.2.1. Experimental setup

Figure and schematics of the experimental apparatus of hydrogen generation system in this study (based on the acid-accelerated hydrolysis of solid SBH) are presented in Figure 2.2 and Figure 2.3. The thermal insulated 2.6 L cylindrical pressure vessel was installed as a semi-batch reactor. The perspective CAD view of reactor is as shown in Figure 2.4. The primary thermal insulation was performed with vacuum between the reactor and the outer jacket, and the secondary thermal insulation was performed with an insulation material outside the jacket. Through this double insulation, the reactor is insulated from the outside, and excessive reaction heat is released through the cooling coil. The aqueous formic acid solution, denoted as feed hereinafter was supplied to the reactor through a reciprocating piston pump to achieve a quantitative injection under 40 bar(s) pressure conditions. A helical coil was installed inside the reactor and a buffer tank was installed to maintain target reactant temperature and to prevent reactant overflow and sudden pressure changes. An agitator was installed to ensure uniform composition of the internal reactants, and a back pressure regulator was installed at the outlet of the buffer tank to

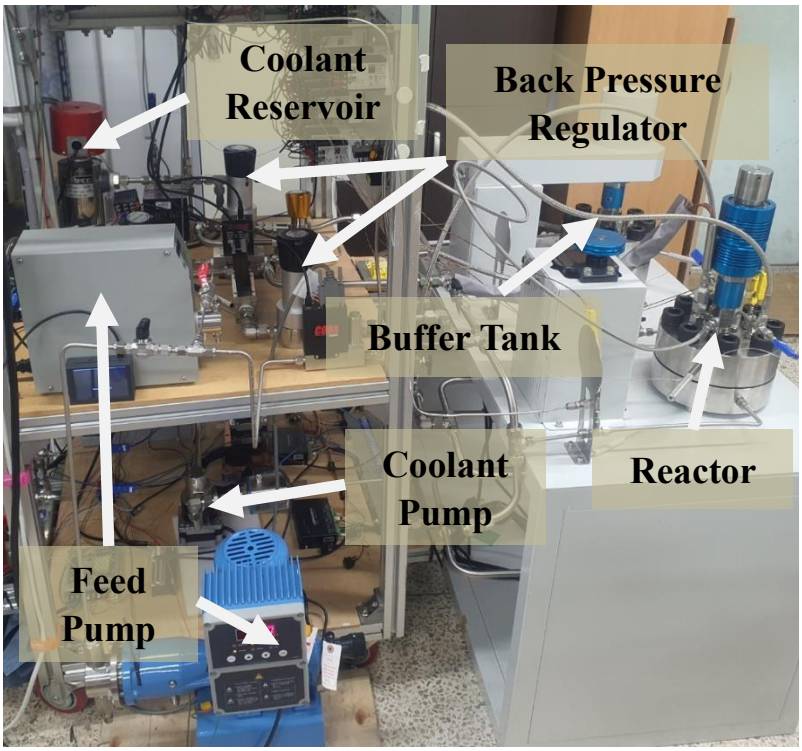

Figure 2.2 Experimental apparatus of hydrogen generation system based on acid-accelerated liquid hydrolysis of solid SBH at elevated temperature and pressure

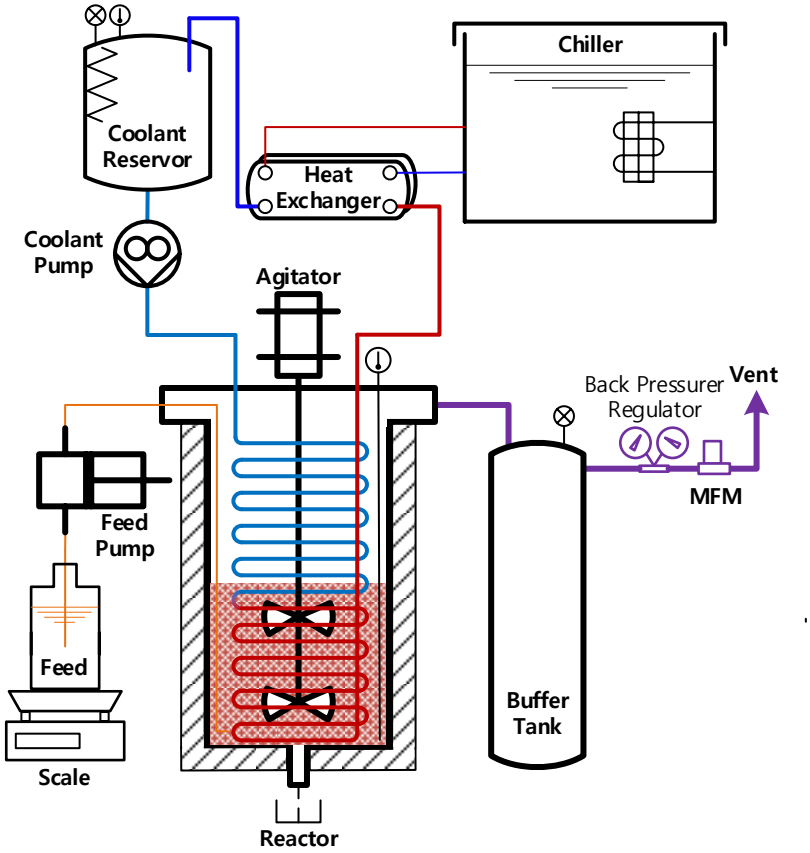

Figure 2.3 Schematic diagram of experimental apparatus

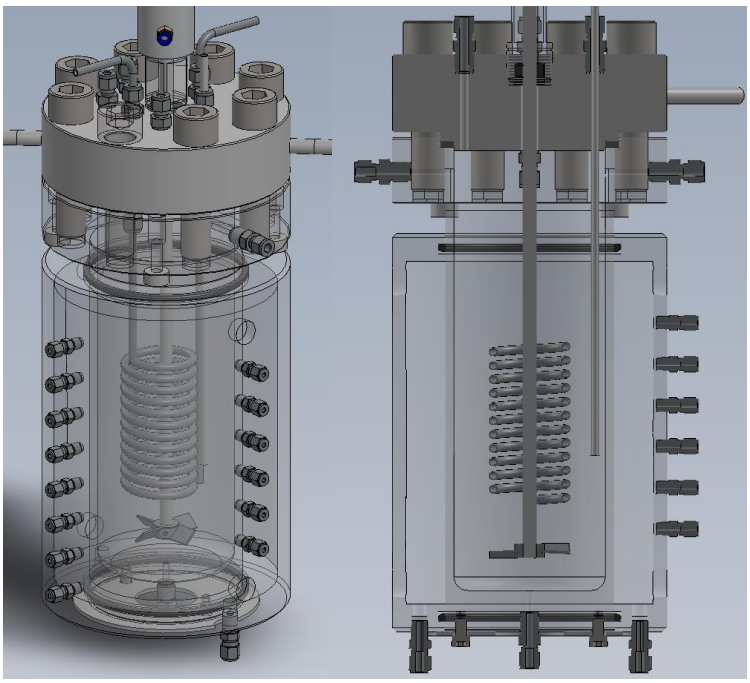

Figure 2.4 CAD perspective view of the reactor (Coil position and shape are approximate and not exact)

maintain the desired pressure inside the reactor and buffer tank. The coolant water circulated through a gear pump. After being heated in the reactor, the temperature of the coolant was reduced by passing through a heat exchanger and a chiller. Moreover, the coolant temperature was adjusted to a desired inlet temperature in the coolant reservoir before entering the reactor. The cooling system was initially pressurized to 7 bar and was designed as a closed system to prevent vaporization due to increases in the coolant outlet temperature. The reactant temperature inside the reactor was measured using 36 thermocouples (4 × 8 point thermocouples), while the coolant temperature was measured at several points in the coolant loop (reactor inter and outlet, 1st fluid of heat exchanger inlet and outlet, 2nd fluid of heat exchanger inlet and coolant reservoir inlet and outlet). The precise location of multipoint thermocouples and cooling coil inside the reactor is shown in Figure 2.5. The pressure of the coolant reservoir was measured to calculate the exact physical properties of the coolant. The reactor pressure was measured by pressure transmitter and maintained at 40 bar by a back pressure regulator. The hydrogen flow rate was measured with a gas mass flow meter (MFM) after the back pressure regulator. Finally, the mass of the feed injection amount was measured with a scale.

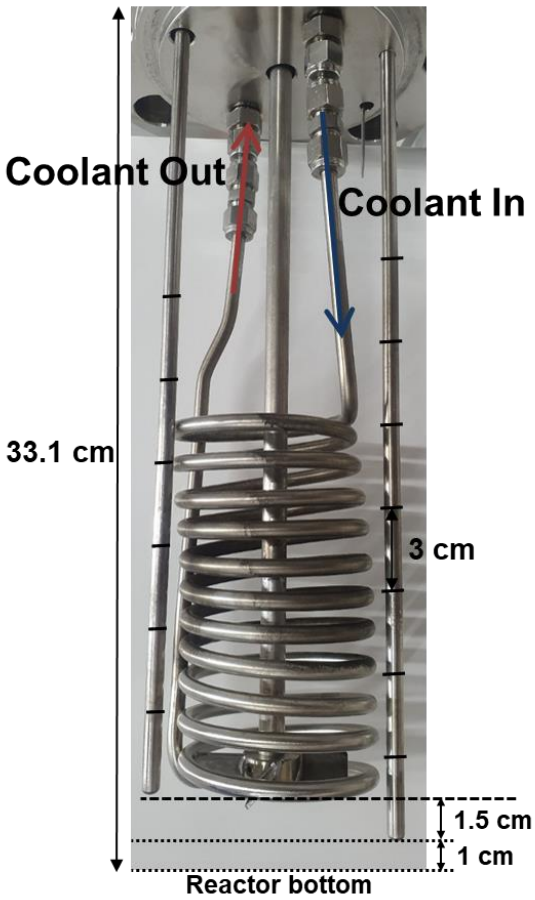

Figure 2.5 Sensing point of multi-point thermocouple and position of cooling coil

2.2.2. Accuracy of measuring devices and uncertainty analysis

The main physical properties measured in the hydrogen generation system in this study were the temperature, mass flow rate, volume flow rate and pressure. The temperature inside the reactor is measured by a K-type thermocouple, and the temperature of the cooling system is measured by a T-type thermocouple. Reactor pressure and coolant pressure were measured with pressure transmitter with the accuracy of 0.5%. the amount of feed injection was measured with two scales having different measuring range. K-type and T-type thermocouple with grounded junction probe was used as the temperature measuring device with an accuracy of 0.4%. Hydrogen flow rate was measured with differential pressure mass flow meter and coolant volumetric flow rate was measured with electromagnetic flow meter; the accuracies of each flow meter are 0.4% and 0.8%, respectively. Table 2.1 summarizes the accuracy of each sensor.

Table 2.1 Accuracies of measuring devices

Sensors	Range	Unit	Accuracy
K-type thermocouple	0 ~ 1200	°C	2.2 °C
T-type thermocouple	-270 ~ 400	°C	1.0 °C
Pressure transmitter	0 ~ 100	bar	0.5%
Differential pressure mass flow meter	0 ~ 500	SLPM	0.4%
Electromagnetic volumetric flow meter	0.05 ~ 25	L/min	0.8%
Scale #1	0 ~ 6000	g	0.01 g
Scale #2	0 ~ 20000	g	0.1 g

2.2.3. Experiment procedure

The reactor was filled with solid SBH (granules, ca 3 mm) and the feed was aqueous formic acid solution. After the reactants were heated to the target temperature by hydrolysis reaction heat, the target reactant temperature was maintained by a cooling system. In consideration of the link with the thermal management system of fuel cell applications and the prevention of local reactant overcooling, the coolant inlet temperature was set to 50 ℃ and the target reactant temperature was maintained by adjusting the coolant mass flow rate.

The experiments were performed by changing the parameters that affecting the hydrogen generation characteristics such as reactant temperature, feed injection rate, feed concentration, stoichiometric number, and SBH charging amount. The parameters of each experiment cases are presented in Table 2.2. The experiments were conducted until hydrogen was no longer generated after injecting feed, in accordance with the specified conditions in each case. The feed injection amount according to experimental condition are presented in Table 2.3.

Table 2.2 Experimental conditions

Parameter	RT#1	RT#2	RT#3	SN#1	SN#2
SBH charging amount (g)	500			500	
Feed injection rate (mL/min)	45			45	
Feed concentration (wt.%)	5			5	
Reactant temperature (°C)	160	180	200	160	180
Stoichiometric number	4.0			4.5	

Parameter	FIR#1	FIR#2	FIR#3	FIR#4	FIR#5
SBH charging amount (g)	250			500	
Feed injection rate (mL/min)	45	75	105	75	105
Feed concentration (wt.%)	5				
Reactant temperature (°C)	200				
Stoichiometric number	4.0				

Parameter	FC#1	FC#2	FC#3
SBH charging amount (g)	500		
Feed injection rate (mL/min)	45		
Feed concentration (wt.%)	2.5		
Reactant temperature (°C)	160	180	200
Stoichiometric number	4.0		

Table 2.3 Feed injection amount by experimental condition (g/100 g SBH)

Feed concentration (%)	Stoichiometric number	
	4.0	4.5
2.5	198	223
5	206	232

2.2.4. Analytical techniques

To analyze the composition of the reaction product, ^{11}B solid nuclear magnetic resonance (NMR) spectroscopy and powder X-ray diffractometer (XRD) were conducted. Furthermore, NMR data were obtained from a 500 MHz Avance III HD Bruker Solid-state NMR and powder XRD data were obtained from SmartLab (Rigaku, Japan).

The viscosity of reaction product was measured to evaluate the ease of reaction product discharge performance owing to the hydrolysis reaction was conducted in the semi-batch reactor. The viscosity of reaction product by temperature was measured with Rheometer (ARES-G2, TA instrument).

2.3. Experimental analysis of factors affecting hydrogen generation characteristics

2.3.1. Effect of the reactant temperature

The effect of reactant temperature was analyzed under the conditions of 500 g SBH charging amount, 45 ml/min feed injection rate, and 4.0 stoichiometric number (RT#1, RT#2, and RT#3 in Table 2.2). Depending on the target reactant temperature, the time taken for the system to reach the target temperature differed. In all the target reactant temperature experiments, the target reactant temperature was maintained after 600 s from the time of feed injection. Therefore, the hydrogen generation characteristic analysis was divided into three sections: from the start of feed injection to 600 s (0–600 s, Section 1), from 600 s to the end of feed injection (600 s–feed end, Section 2), and until no more hydrogen was generated (feed end–experiment end, Section 3).

The experimental results according to reactant temperature are presented in Figure 2.6, Figure 2.7, Figure 2.8, Figure 2.9 and Table 2.4. The experimental results of reactant temperature over time are shown as Figure 2.6. At the beginning of feed injection, the solid SBH and feed were in direct contact, causing a high and rapid increase in reactant temperature. Since the heat transfer

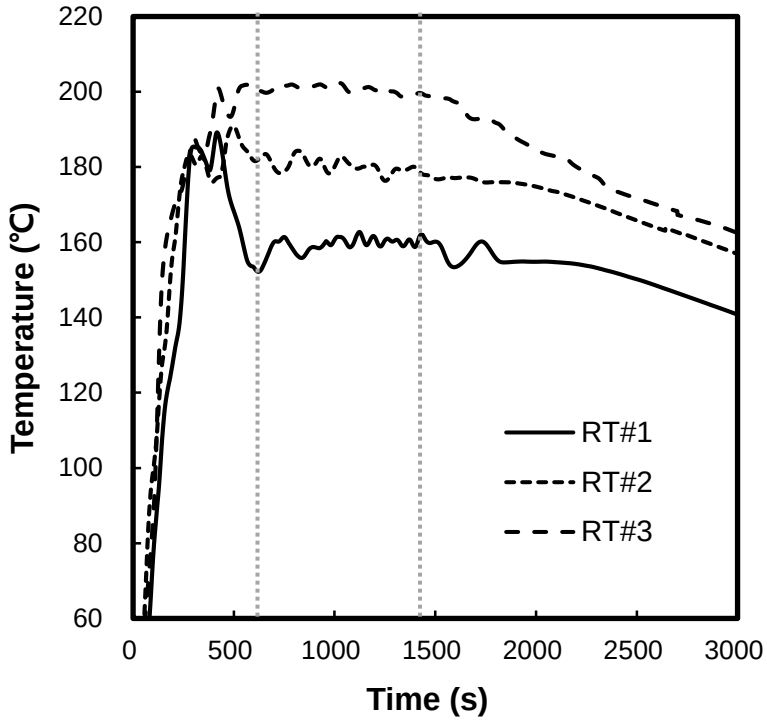

Figure 2.6 Reactant temperature over time in case of RT#1, RT#2, and RT#3

* the Gray vertical dotted lines indicate 600 s and feed end time

coefficient between the granule SBH and the cooling coil was relatively low, it was difficult to perform the desired cooling in this section. However, as shown in Figure 2.6, sufficient cooling was possible to prevent the reactant temperature from significantly exceeding 200 ℃. As the reaction proceeded, the heat transfer coefficient between the reactant and the cooling coil increased so that it could be operated at the target temperature. In this system, the reactant was heated to approximately 180 °C by reaction heat, and then cooled to the target temperature if necessary. As a result, it was possible to operate at the target temperature after 600 s from the start of feeding. After the feed injection was completed, some hydrogen was generated due to the residual reaction.

As shown in Figure 2.7 (a) and Figure 2.8, In Section 1, where there was no significant difference in reactant temperature, there was also no significant difference in the amount of hydrogen generated. However, in Section 2, the reactant temperature and the cumulative hydrogen production were proportional (Figure 2.7 (b)). After completion of the feed, the amount of hydrogen generated through the residual reaction was inversely proportional to the reactant temperature. This is interpreted as the reaction rate being relatively slow when the reactant temperature is low as can be inferred from Equation 2.5. At a reactant temperature of 160 ℃, the final hydrogen generation amount was lower than at 180 and 200 ℃. Notably, comparing the results for 180 and 200 ℃,

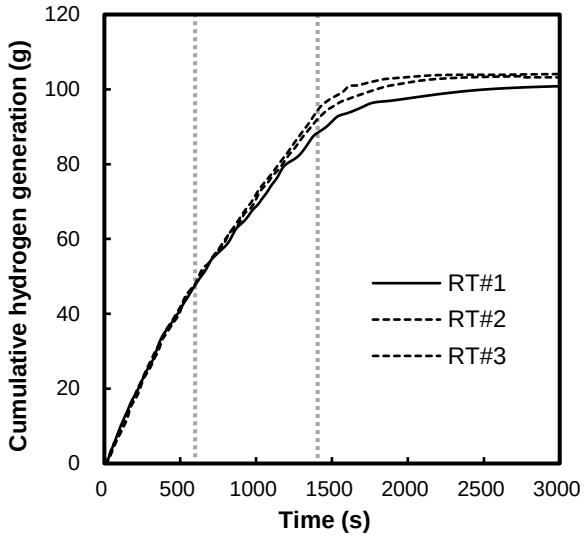

(a)

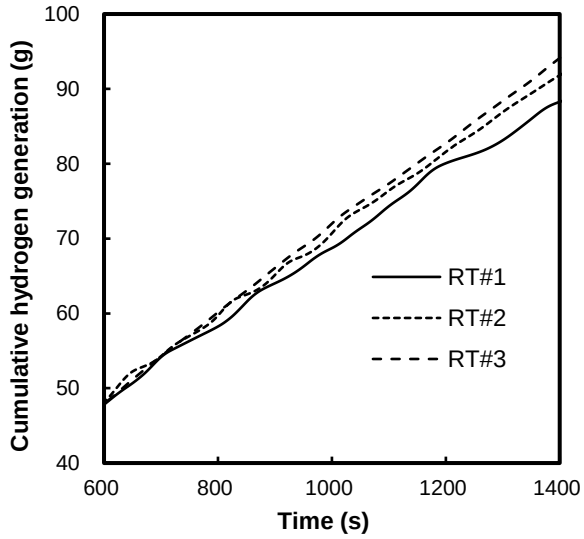

(b)

Figure 2.7 Cumulative hydrogen generation over time in case of RT#1, RT#2, and RT#3 (a) entire experiment (Section 1 ~ Section 3) (b) stable operation section (Section 2)

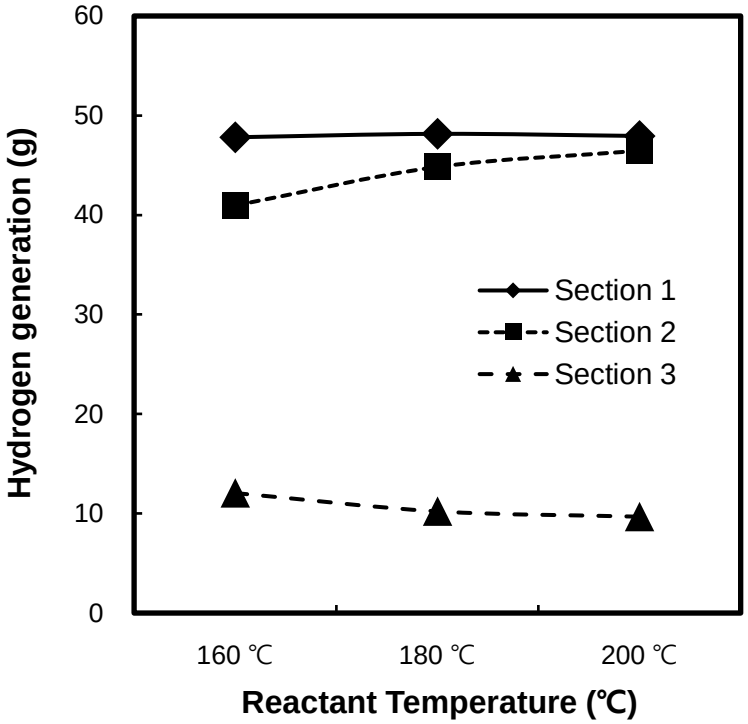

Figure 2.8 Hydrogen generation amount by section in case of RT#1, RT#2, and RT#3

Table 2.4 Hydrogen generation amount according to reactant temperature

Reactant Temperature (℃)	Hydrogen generation amount (g)			
	Section 1	Section 2	Section 3	Total
160	47.81	40.86	12.16	100.83
180	48.16	44.33	10.72	103.21
200	47.94	46.05	9.09	104.08

although hydrogen was generated faster at 200 ℃, the final hydrogen generation amount was not significantly different between them. This indicates that all SBH reacted sufficiently when the reactant temperature was ≥180 ℃ under the 4.0 stoichiometric number condition.

The ^{11}B solid NMR spectroscopy results of the reaction products for experiments RT#1, RT#2, and RT#3 are presented in Figure 2.9. The commonality of a high peak at approximately 1 ppm and a peak at approximately 15 ppm can be observed in Figure 2.9 (a), (b), and (c). This result is the same as the solid NMR result for dried borax powder [92, 93]. A high peak at approximately 1 ppm was tetra-coordinated boron (Bφ_4) and a peak at approximately 15 ppm was tri-coordinated boron (Bφ_3), where φ refers to either O or OH. The peak of approximately 42 ppm, which is only prominent only in Figure 2.9 (a), represented the SBH [94]. The NMR results suggested that the reason for the relatively low hydrogen generation at 160 ℃ reactant temperature was unreacted dissolved SBH and the reaction mechanism does not vary depending on the reaction temperature.

Based on these results, it was revealed that the higher the reactant temperature, the more hydrogen was generated. Although the difference in hydrogen generation between the 180 and 200 ℃ experiments was not significant, hydrogen generation was smaller in the 160 ℃ experiment. If there

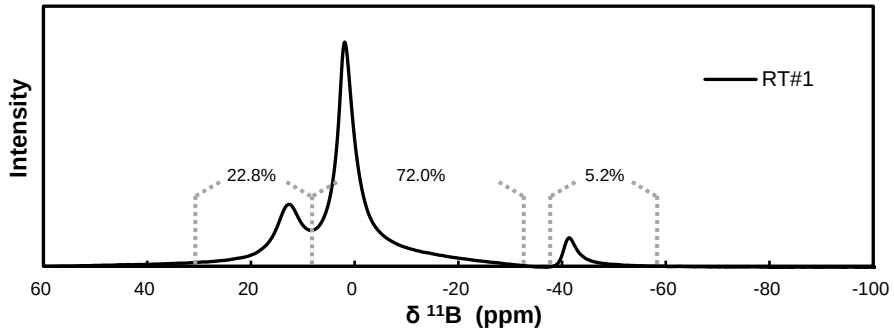

(a)

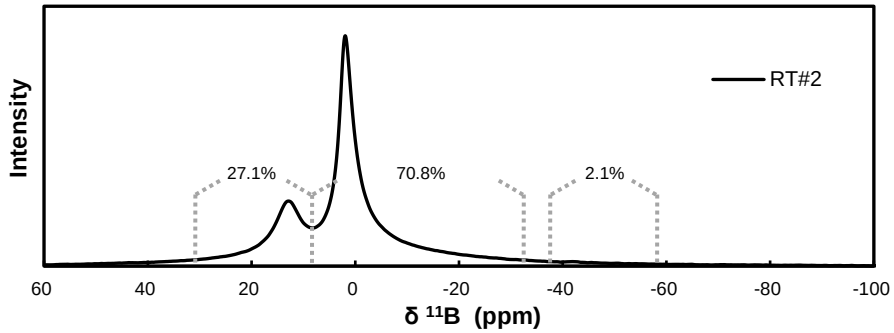

(b)

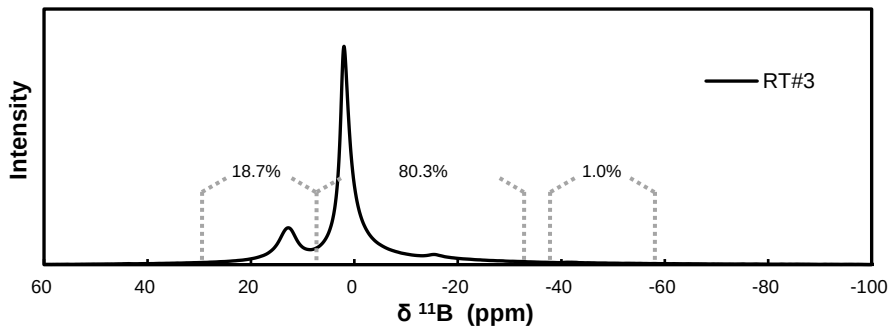

(c)

Figure 2.9 ^{11}B solid NMR spectroscopy results of reaction product in case of (a) RT#1 (b) RT#2 (c) RT#3

were no restrictions to increase in reactant temperature (such as the reactor material or heat dissipation effects), it would only be appropriate to adopt a cooling strategy to prevent overheating.

In addition to ^{11}B NMR, X-ray diffractometer (XRD) was performed to determine the exact composition of the reaction product. The tested reaction product was RT#3, which had the highest hydrogen conversion rate. As shown in Figure 2.10, it was found that the reaction product was present in the form of sodium formate (NaCOOH) due to the combination of the carboxyl group derived from formic acid with sodium of SBH or sodium metaborate hydrate ($NaBO_2 \cdot 2H_2O$) [70].

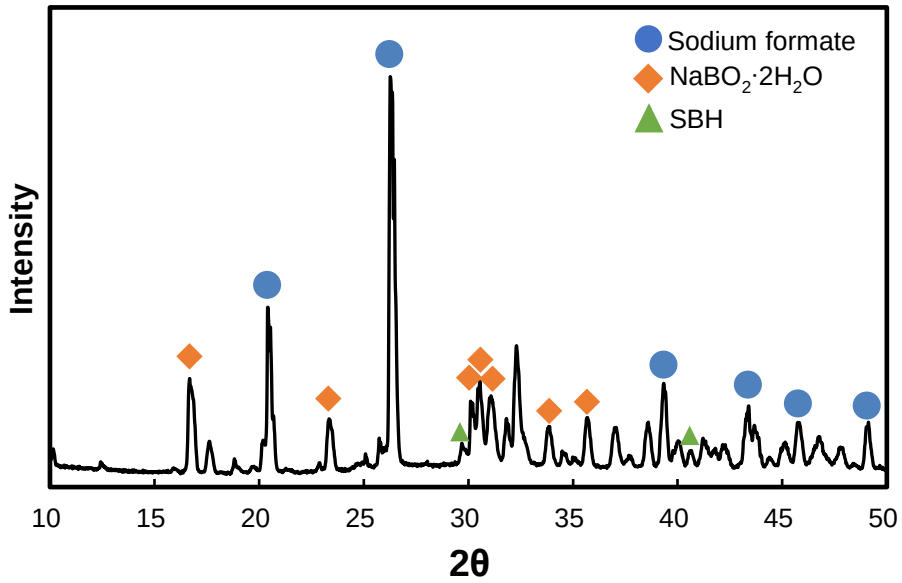

Figure 2.10 X-ray diffractometer result of reaction product of RT#3

2.3.2. Effect of the feed injection rate

The main reason why SBH has been highlighted as a hydrogen storage material is the convenience of transportation and storage. Therefore, since hydrogen generation systems using SBH hydrolysis are mainly on-board, it is essential to control the hydrogen generation rate flexibly to apply it to various fuel cell applications. In this chapter, differences in hydrogen generation rates were analyzed according to the feed injection rate. The effect of feed injection rate was analyzed in the 250 g SBH charging (FIR#1, FIR#2, and FIR#3) and 500 g SBH charging (RT#3, FIR#4, and FIR#5) scenarios, and experiments were conducted on feed injection rates of 45, 75, and 105 mL/min in each charging amount. Since the stoichiometric number conditions were the same, the total amount of feed injected in all cases was the same. Therefore, the higher the feed injection rate, the faster the feed injection was terminated.

The experimental results according to the feed injection rate are displayed in Figure 2.11 and Figure 2.12, where Figure 2.11 is the results for the 250 g SBH charging cases, and Figure 2.12 is the results for the 500 g SBH charging cases. The figure indicates that for both 250 and 500 g SBH charging, the hydrogen generation rate increased as the feed injection rate increased (Figure 2.11 (a), Figure 2.12 (a)). Moreover, since the amount of feed injected was the same, there was no significant difference in total hydrogen generation (Figure

2.11 (b) and Figure 2.12 (b)). However, as shown in Figure 2.11 (a), the difference in hydrogen generation rate between 75 and 105 mL/min was smaller than the difference between 45 and 75 mL/min. However, as shown in Figure 2.12 (a), the difference in hydrogen generation rate between 45, 75, and 105 mL/min was similar. In the case of 250g SBH charging, when the feed injection rate was 105 mL/min, it was impossible to secure sufficient reaction sites to achieve a higher hydrogen generation rate compared to the 75 mL/min feed injection rate. For 500 g SBH charging, it would appear that the difference between the hydrogen generation rate 105 mL/min and 75 mL/min can be made because the reaction site can be sufficiently ensured. However, as displayed in Figure 2.11 (a), after the beginning (approximately 100 s), the 105 mL/min feed injection rate had a higher hydrogen generation rate than at 75 mL/min, which appeared to be because the average pH of the reactants decreased due to an increase in the acidic feed injection amount, promoting hydrogen generation as can be inferred Equation 2.5.

Combining the experimental results according to feed injection rate, when the total feed injection amount was the same, there was no significant difference in conversion when the feed injection rate was increased, although the hydrogen generation flow rate increased. This indicates that it is possible to control the hydrogen generation flow rate by adjusting the feed injection rate. However,

when the initial SBH charge amount was small, the hydrogen generation rate was not sufficiently increased due to a lack of reaction sites at feed injection rates above a certain level. This means that there is an upper limit on the hydrogen generation rate according to the initial SBH charge amount. Therefore, to achieve the target hydrogen generation flow rate, the feed injection rate and the initial SBH charging amount should be considered simultaneously.

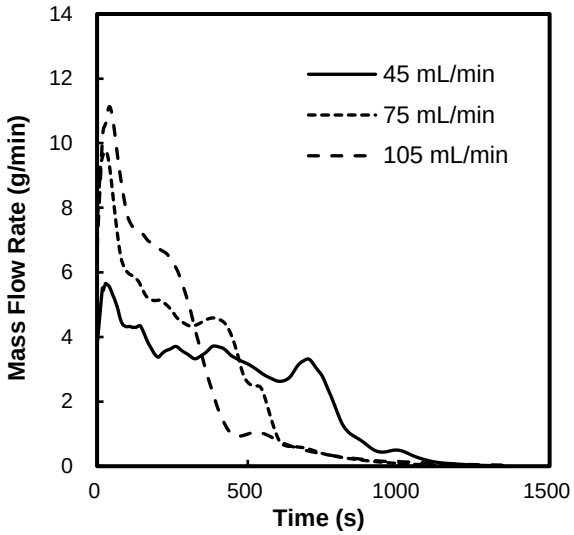

(a)

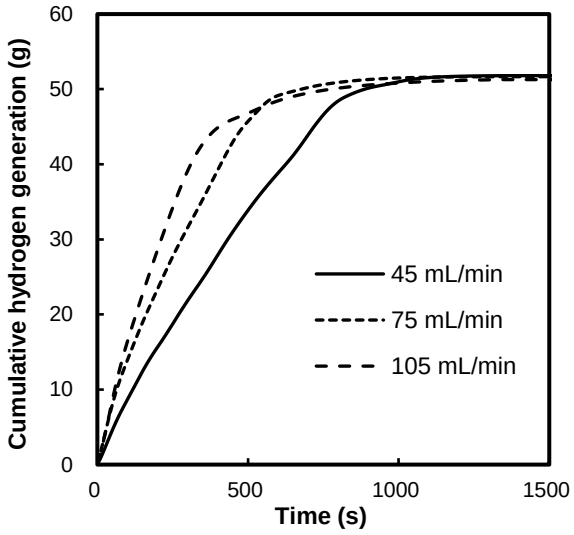

(b)

Figure 2.11 Experimental results according to feed injection rate, in case of 250 g SBH charging (a) hydrogen mass flow rate, (b) cumulative hydrogen generation amount

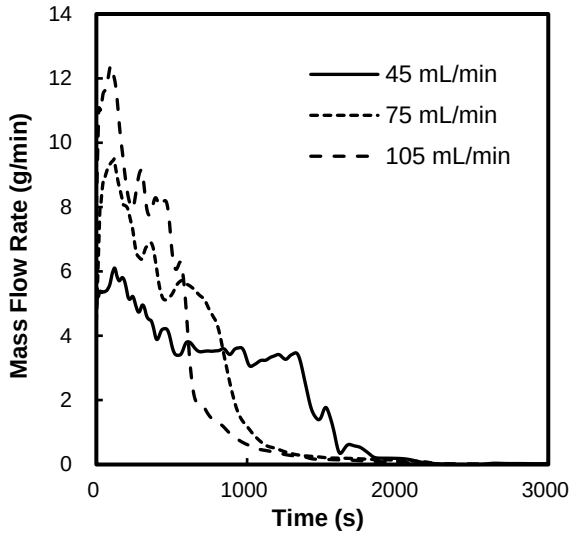

(a)

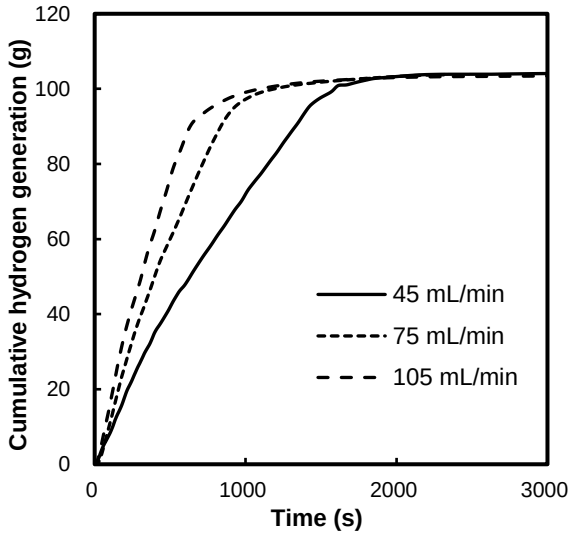

(b)

Figure 2.12 Experimental results according to feed injection rate, in case of 500 g SBH charging (a) hydrogen mass flow rate, (b) cumulative hydrogen generation amount

2.3.3. Effect of the stoichiometric number

If the stoichiometric number increased, the hydrogen storage density of the system decreased as shown in Figure 2.1. In the system under study, when the stoichiometric number was 4.0, the hydrogen storage density (according to Equation 2.2) was 7.0 wt.%, and when the stoichiometric number was 4.5, the hydrogen storage density was 6.4 wt.%. However, if a slight increase in the stoichiometric number could benefit system operation, a higher stoichiometric number may be considered. Table. 2.5 displays the hydrogen generation amount for experiments on stoichiometric numbers 4.0 (RT#1 and RT#2) and 4.5 (SN#1 and SN#2). Cumulative hydrogen generation over time (according to stoichiometric number) is presented in Figure 2.13. The gray vertical and dotted lines in Figure 2.13 indicate the feed end time when stoichiometric number 4.0 and 4.5. When the reactant temperature was 160 ℃, the stoichiometric number of 4.5 produced more hydrogen than 4.0. This is because when the stoichiometric number was 4.5, the pH was relatively reduced as feed was added to promote the reaction. Moreover, as the concentration and viscosity of the reactant reduced, the reaction site increased. For this reason, unreacted dissolved SBH in the case of the stoichiometric number 4.0 reacted, and the amount of hydrogen generation increased. When the reactant temperature was 180 ℃, hydrogen was produced faster due to the same effect as the addition of

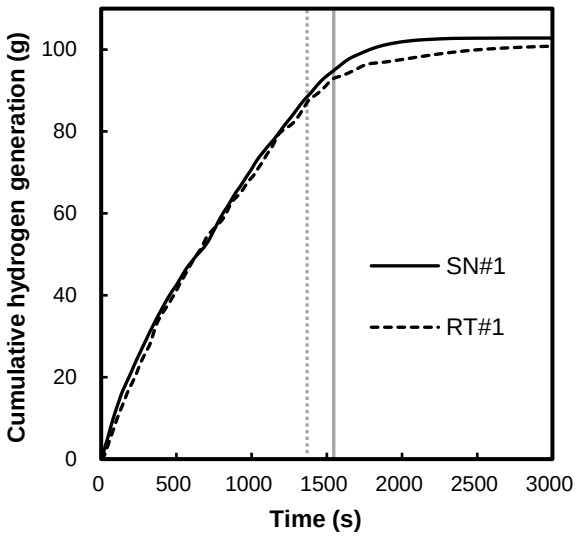

(a)

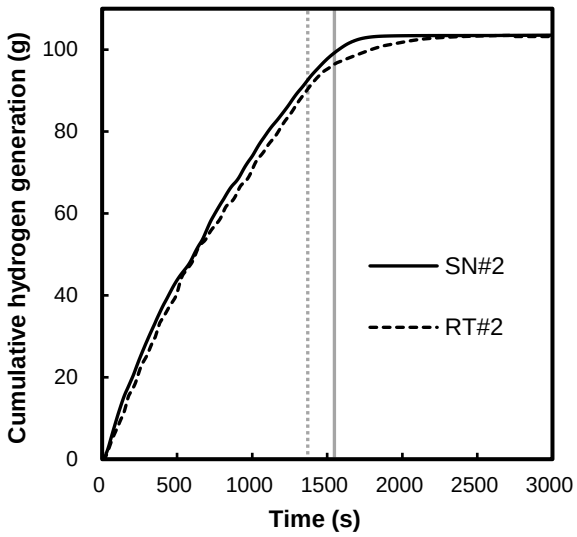

(b)

Figure 2.13 Cumulative hydrogen generation amount overtime according to stoichiometric number (a) 160 ℃ reactant temperature (RT#1, SN#1) (b) 180 ℃ reactant temperature (RT#2, SN#2)

Table 2.5 Hydrogen generation amount according to stoichiometric number

Stoichiometric number	Reactant Temperature (℃)	Hydrogen generation amount (g)			
		Section 1	Section 2	Section 3	Total
4.0	160	47.81	40.96	12.06	100.83
	180	48.16	44.83	10.22	103.21
4.5	160	48.10	47.37	7.36	102.83
	180	49.01	50.74	3.79	103.54

feed at 160 ℃. However, even when the stoichiometric number was 4.0, most of the SBH reacted; hence, the difference in total hydrogen generated was small.

The ^{11}B solid NMR spectroscopy results of experiments SN#1 and SN#2 are presented in Figure 2.14. Comparing Figure 2.9 (a) and Figure 2.14 (a), it can be observed that the peak of approximately 42 ppm (representing SBH) is much lower in Figure 2.14 (a). Based on the NMR results, it can be seen that when the reactant temperature was low, the unreacted dissolved SBH could be reduced by increasing the stoichiometric number. In addition, hydrogen generation also increased. As demonstrated in Figure 2.14 (b), even when the reactant temperature was sufficiently high (180 ℃), the amount of unreacted dissolved SBH was reduced. Furthermore, referring to Figure 2.9 and Figure 2.14, a comparison of the ratio of 15 and 1 ppm peaks reveals that the ratio of the 15 ppm peak was lower in the case of the stoichiometric number 4.5 compared to when the stoichiometric number 4.0. This means that the ratio of tetra-coordinate boron (Bφ_4) increased (more O or OH was combined with one boron molecule), indicating that the reaction product's solubility in water increased and its viscosity decreased.

The rheometer results of experiments RT#1, RT#2, SN#1, and SN#2 are presented in Figure 2.15. All measurements were made at sheer rate 1 /s. In the case of the stoichiometric number of 4.0, the gel phase product was almost solid

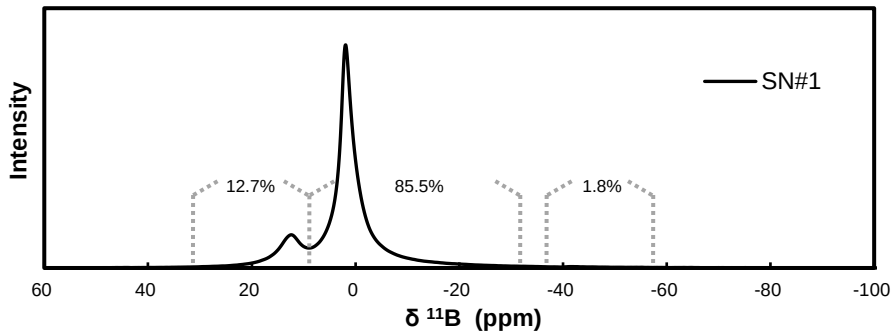

(a)

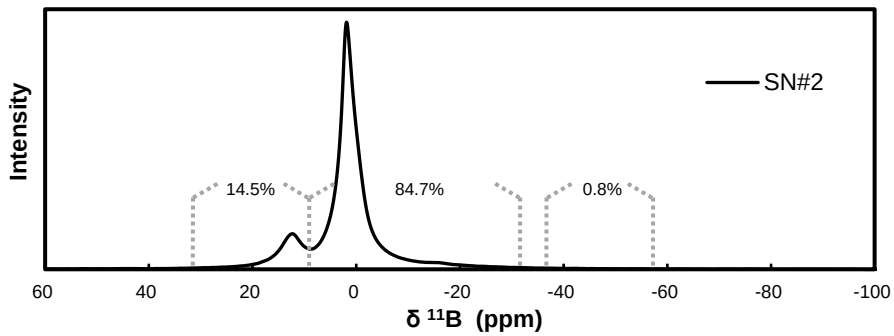

(b)

Figure 2.14 ^{11}B solid NMR spectroscopy results of reaction product in case of (a) SN#1 (b) SN#2

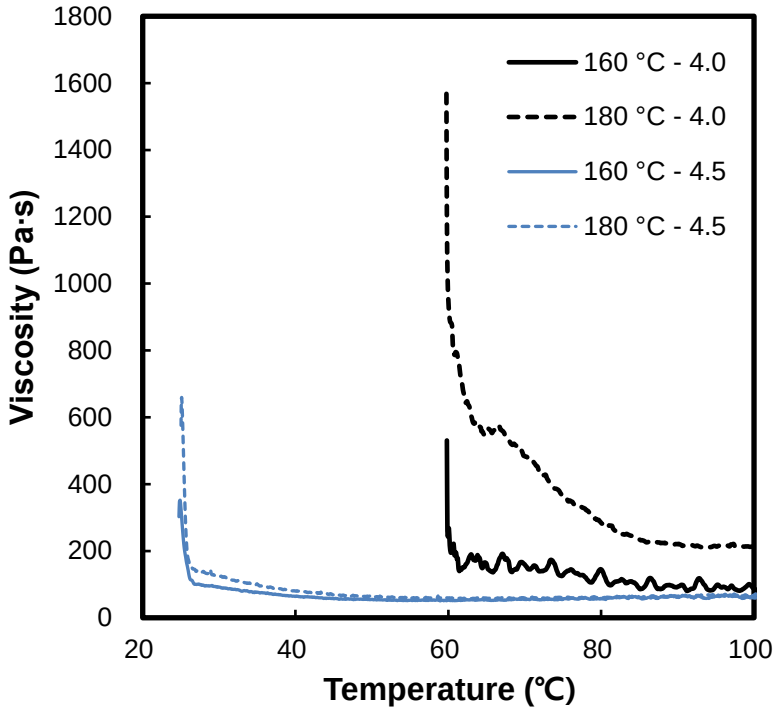

Figure 2.15 Rheometer results of reaction product in case of RT#1, RT#2, SN#1, and SN#2 at sheer rate 1 /s

at a temperature below around 60°C, and the viscosity decreased rapidly as it became solution at a temperature above around 60°C. In the case of a stoichiometric number of 4.5, solutionization proceeded at about 25 ℃. This solution-gel transition is a characteristic that occurs in macromolecular substances like polymer or in high-concentration solutions. In the gel state, components bond together to form a network extending throughout the whole substance and these network gives the material an elasticity which is a solid-like property. As the temperature rises, these bonds gradually weaken and above a certain temperature so called solution-gel transition temperature, these subunits dispersed in the solvent are relatively free to move, they become solution and have liquid-like property. Solution-gel transition temperature of the reaction product seems to be determined by the stoichiometric number. In the case of a stoichiometric number of 4.5, there was no difference in the viscosity after solutionization by reactant temperature, but in the case of the stoichiometric number of 4.0, the reaction product reacted at 160 ℃ was less viscous than the product reacted at 180 ℃. Since the same amount of feed was injected, unreacted dissolved SBH means less reaction product, $NaBO_2$ hydrate. Therefore, it can be seen from the viscosity measurement result that $NaBO_2$ in the hydrated state has a greater viscosity than the SBH aqueous solution. The viscosity measurement results show that when this hydrogen generation system

is practically applied, it is virtually impossible to discharge the reaction product at a temperature below the solution-gel transition temperature. Therefore, if the low stoichiometric number is used to increase the hydrogen storage density, it means that the product must be discharged at a higher temperature. Since the solution-gel transition temperature can be significantly reduced with only a slight increase in the stoichiometric number (4.0 → 4.5), it may be beneficial to consider increasing the stoichiometric number according to the using environment. In particular, because of its high viscosity, the gel-state product is unlikely to be emitted by a valve-controlled outlet even at high differential pressure. Therefore, in order to discharge, the reactant temperature must be at least solution-gel transition temperature or higher.

The hydrogen generation system used in this study conducted SBH hydrolysis at elevated temperature and pressure in a semi-batch reactor. Therefore, the reaction product had to be discharged after the reaction was completed. The hydrolysis reaction product of SBH has a lower viscosity as the temperature and stoichiometric number increase. Accordingly, if a high-temperature product cannot be handled (depending on the using environment of the application), it is necessary to lower the viscosity and solution-gel transition temperature of the reaction product by performing hydrolysis at a higher stoichiometric number.

2.3.4. Effect of the feed concentration

The less acid is used, the higher the hydrogen storage density and the lower the fuel price. In addition, the ease of operation of the system increases as the proportion of acid that must be handled with care is reduced. As can be inferred from Equation 2.3, if the temperature is high enough, a sufficient reaction rate can be obtained even at a relatively high pH. Therefore, it is necessary to derive the optimal acid concentration by analyzing the hydrogen production characteristics according to the acid concentration.

To confirm the effect of the acid concentration of the feed, the experiments were performed by changing the reactant temperature with a 2.5% formic acid solution (FC#1, FC#2, and FC#3 in Table 2.2). This is because, as shown in Equation 2.3, the hydrolysis of SBH is affected by the reactant temperature and pH, so changing reactant temperature for analyzing the effect of feed concentration were determined that the system behavior according to the reactant temperature could be changed due to the effect of the pH increased due to the relatively small amount of acid input. Therefore, experiments FC#1, FC#2, and FC#3 were analyzed together with RT#1, RT#2, and RT#3.

As in the experiment according to the reactant temperature in Chapter 2.3.1, the hydrogen generation characteristic analysis was divided into three sections: from the start of feed injection to 600 s (0–600 s, Section 1), from 600

s to the end of feed injection (600 s–feed end, Section 2), and until no more hydrogen was generated (feed end–experiment end, Section 3).

The experimental results according to reactant temperature in case of 2.5% acid concentration feed are presented in Figure 2.16, Figure 2.17, Figure 2.18 and Table 2.6. The experimental results of reactant temperature over time are shown as Figure 2.16. Even with the feed concentration of 2.5%, there was no significant difference in the initial temperature increase pattern, and after rising to a high temperature, the target temperature was reached and maintained. The time required to achieve the target temperature of 160 ℃ was similar to the case of the feed concentration of 5%. As shown in Figure 2.17 and Figure 2.18, at the beginning, there was no significant difference between the acid concentration of 5% case and 2.5% case. Since there is no basic reaction product, it seems that sufficient protons are provided for the reaction even at an acid concentration of 2.5%, resulting in a sufficient reaction. However, after 400 s, the 2.5% concentration experiments showed lower hydrogen generation than the 5% concentration experiments. As the amount of reaction product increases, the reaction rate decreased as the pH of the reactant were higher than in the case of 5% concentration. It can also be confirmed that the difference in the amount of hydrogen generated gradually increases at all reactant temperatures. At all reactant temperatures, it can be seen that the difference of

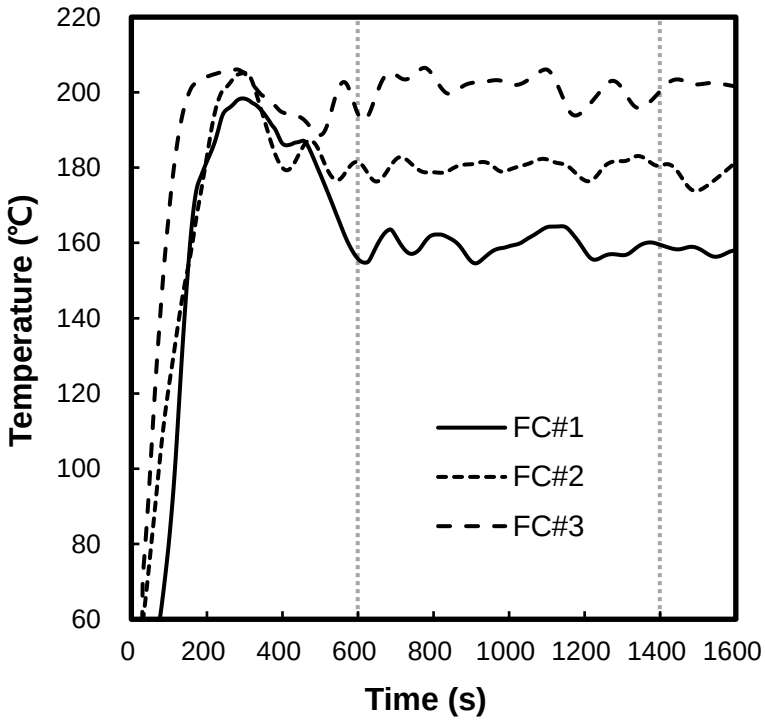

Figure 2.16 Reactant temperature over time in case of FC#1, FC#2, and FC#3

* the Gray vertical dotted lines indicate 600 s and feed end time

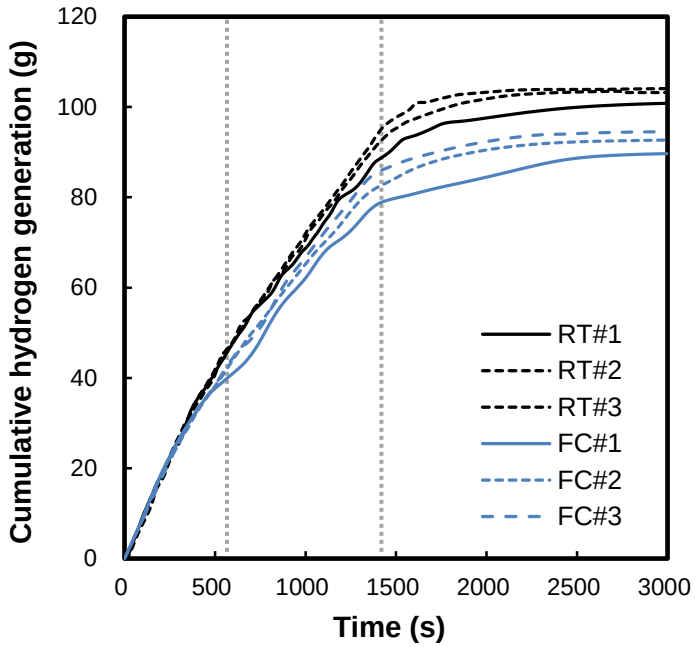

(a)

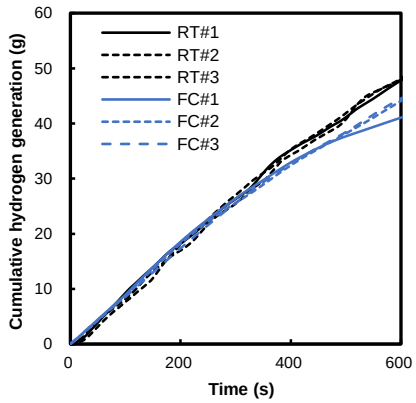

(b)

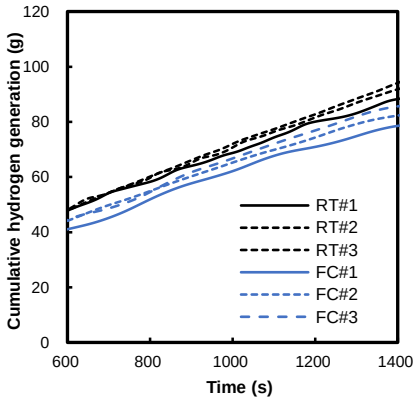

(c)

Figure 2.17 Cumulative hydrogen generation over time in case of FC#1, FC#2, and FC#3 (a) entire experiment (Section 1 ~ Section 3) (b) initial section (Section 1) (c) stable operation section (Section 2)

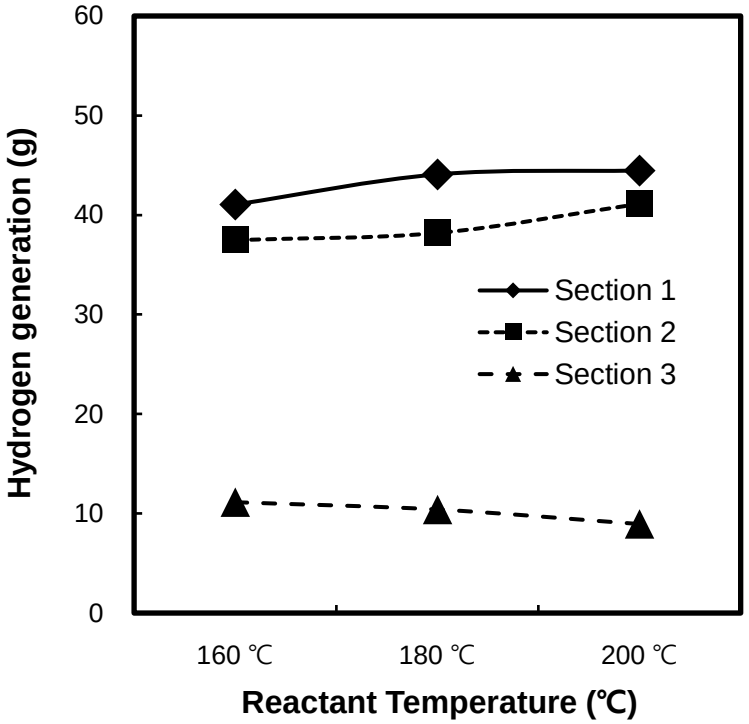

Figure 2.18 Hydrogen generation amount by section in case of FC#1, FC#2, and FC#3

Table 2.6 Hydrogen generation amount according to reactant temperature in case of 2.5 % feed concentration

Reactant Temperature (℃)	Hydrogen generation amount (g)			
	Section 1	Section 2	Section 3	Total
160	41.05	37.48	11.14	89.67
180	44.08	38.19	10.40	92.67
200	44.47	41.12	8.94	94.53

hydrogen generation amount between the 2.5% concentration and the 5% concentration gradually increased, which also seems to be due to the increase in the reactant pH at low acid concentration.

In the case of acid concentration of 5%, there was no significant difference in hydrogen generation amount between 180 ℃ and 200 ℃, but there was a difference in hydrogen production between 180 ℃ and 200 ℃ in the case of acid concentration of 2.5%. This is interpreted as the following reasons. In the case of the 5% acid concentration, a sufficient reaction is possible at a reactant temperature of 180 ℃ or higher, and thus a difference between 180 ℃ and 200 ℃ is not significant. However, in the case of a 2.5% acid concentration, a sufficient reaction does not occur due to a pH increase triggered by an acid shortage, so the effect of promoting the reaction by reactant temperature was shown at 180 ℃ or higher.

Also, noteworthy, as shown in Figure 2.19, in the case of the 2.5% acid concentration experiment, unreacted agglomerated SBH was commonly observed after the end of reaction in all experimental cases. This unreacted agglomerated SBH was not observed at an acid concentration of 5%. This seems that as the pH increased as the reaction progresses, the feed could not penetrate and the reaction did not occur any more on the surface of unreacted agglomerated SBH. A similar amount (about 50 g) of unreacted agglomerated

Figure 2.19 Example of the unreacted agglomerated SBH after experiment

SBH was observed at all reactant temperatures. This indicates that when the acid concentration was 5%, all SBH participated in the reaction but little SBH did not react when the reactant temperature was low, but when the acid concentration was 2.5%, about 10% of the SBH did not even participate in the reaction. Therefore, in the experiments FC#1, FC#2, FC#3, feed corresponding to the stoichiometric number of 4.0 was injected, but the reaction was performed under approximately the conditions of 4.5 stoichiometric number. In fact, the viscosity of the reaction product was similar to the previous 4.5 stoichiometric number experiment (SN#1, SN#2).

The ^{11}B solid NMR spectroscopy results of reaction product FC#1, FC#2, and FC#3 are shown in Figure 2.20. It can be seen that the lower the reactant temperature, the greater the dissolved residual SBH in the reaction product. And compared with the ^{11}B solid NMR spectroscopy results of 5% concentration feed experiments in Figure 2.9, it can be seen that the proportion of tri-coordinated boron (Bφ_3) is smaller. This means that SBH reacted with more water, which is similar to the result of Figure 2.14, which is actually similar to the product when it is performed with a higher stoichiometric number. Also, the unreacted dissolved SBH was observed even at high reactant temperature, unlike the 5% experimental result or the stoichiometric number 4.5 experiment. In summary the ^{11}B solid NMR results, when using the 2.5% concentration feed,

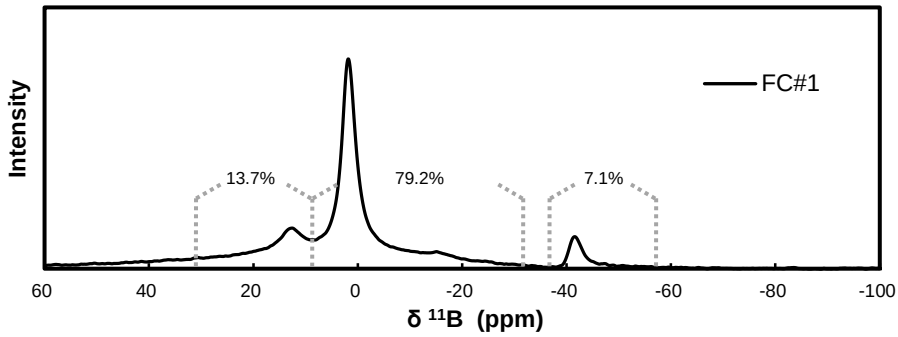

(a)

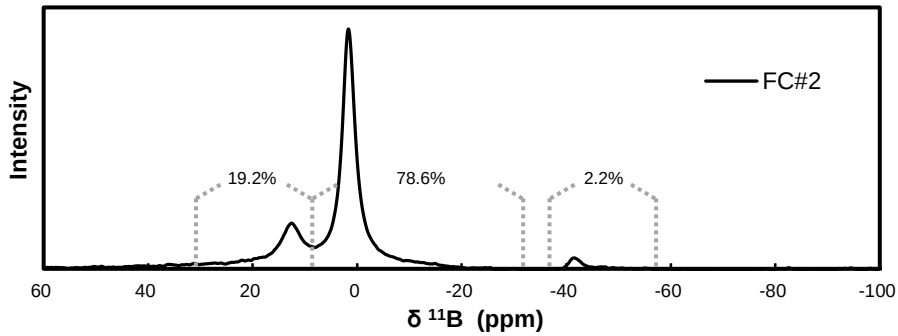

(b)

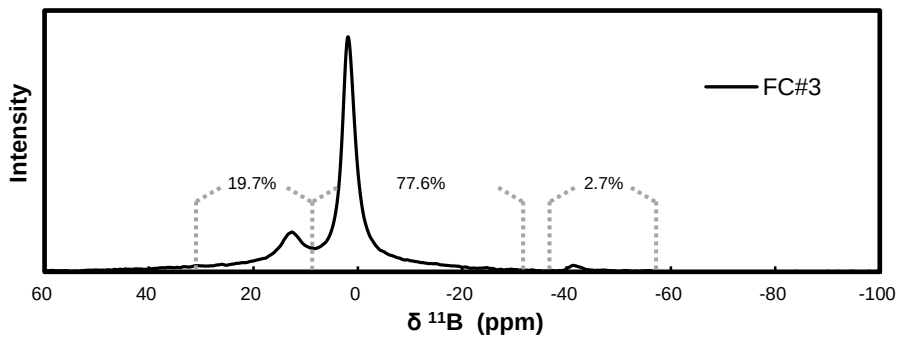

(c)

Figure 2.20 ^{11}B solid NMR spectroscopy results of reaction product in case of (a) FC#1 (b) FC#2 (c) FC#3

about 10% of solid SBH does not participate in the reaction, and the SBH that participated in the reaction showed a lower conversion despite the fact that it reacted with a stoichiometric number of higher than 4.0.

This means that an additional feed is required for a complete reaction, and in this case, the hydrogen storage density is rather decreased. Therefore, the original purpose of increasing the hydrogen storage density cannot be achieved.

In conclusion, it was found that it is inappropriate to use a 2.5% acid concentration feed in a single batch reaction. However, since hydrogen generation rate and reactant temperature rise tendency is similar to 5% acid concentration at the initial stage of the reaction, there seems to be room for improvement through additional operation strategies. This were dealt with in Chapter 4.

2.3.5. Hydrogen conversion of the liquid hydrolysis of solid SBH

According to Equation 2.3, the theoretical amount of hydrogen generated by this system is 21.22 g H_2 per 100 g of SBH. The conversions of experiments are shown in Table. 2.6. In all cases of 5% acid concentration, the conversion was >95%, which was mostly affected by the temperature of the reactant. In study of Akkus, M.S. [75], where the hydrolysis reaction of vapor and solid SBH was conducted, the conversion decreased above a certain temperature. This seems to be because when the vapor temperature increases at atmospheric pressure, the decrease in vapor density reduces the number of reaction sites. In this study, we were able to overcome this limitation by increasing the system pressure and by performing a hydrolysis reaction with liquid water. Furthermore, compared to other studies on the acid-accelerated hydrolysis of SBH aqueous solution, there was no basic stabilizer and a higher conversion was obtained at a low reactant temperature due to a direct reaction being possible.

However, in case of 2.5% acid concentration of feed, at all reactant temperatures, much lower conversions (<90%) were shown than for the 5% acid concentration. In particular, about 50 g of unreacted agglomerated SBH that did not participate in the reaction was commonly observed after the reaction. Therefore, it is not appropriate to lower the acid concentration to 2.5%

in order to improve the hydrogen storage density.

When the feed injection rate was different, the conversion was similar if the total feed injection amount was the same. Moreover, the additional feed compensated for low conversion at low reactant temperatures.

Table 2.7 Hydrogen generation amount and conversion of experiments

Ex. number	Hydrogen generation (g)	Conversion (%)
RT#1	100.83	95.0
RT#2	103.49	97.5
RT#3	104.08	98.1
FIR#1	51.80	97.6
FIR#2	51.67	97.4
FIR#3	51.53	97.1
FIR#4	103.74	97.8
FIR#5	103.42	97.5
SN#1	102.83	96.9
SN#2	103.54	97.6
FC#1	89.67	84.5
FC#2	92.67	87.4
FC#3	94.54	89.1

2.4. Summary

In this chapter, the parameters affecting the hydrogen generation characteristics of a hydrogen generation system based on acid-accelerated liquid hydrolysis of solid-state SBH were analyzed. Experiments were performed by pressurizing the reactor to 40 bar to cause a hydrolysis reaction with liquid water at reaction temperatures of up to 200 ℃. The following conclusions can be drawn:

(1) Reaction temperature and hydrogen production tended to be proportional. The amount of hydrogen generated at reactant temperatures between 180 and 200 ℃ did not exhibit any significant differences. However, the results between 160 and 180 ℃ exhibited a greater difference. Based on the ^{11}B NMR spectroscopy results, the difference in the amount of hydrogen generated was due to unreacted dissolved SBH, and there was no significant difference in the composition of the reaction product.

(2) For on-board applications, it is necessary to have flexible control of the hydrogen generation rate. It was revealed that when the feed injection rate increased, the hydrogen generation rate also increased. However, there was an upper limit depending on the initial SBH charging amount. This indicates that

for the desired hydrogen generation rate, the feed injection rate and SBH charging amount must be considered simultaneously.

(3) An increase in stoichiometric number resulted in a decrease in hydrogen storage density. However, since the amount of unreacted dissolved SBH when the reaction was performed at low temperatures and the viscosity of the product are reduced. Also, the solution-gel transition temperature was significantly reduced with a slight increase in the stoichiometric number, and since the gel-state product had very high viscosity, it is practically impossible to discharge the product below the solution-gel transition temperature. The strategy of increasing stoichiometric number could be selected for applications where it is difficult to discharge the reaction product or increase the reaction temperature.

(4) To increase the hydrogen storage density of the hydrogen storage system applied in this study, it is necessary to reduce the amount of acid used. The reduction in acid use can be even more dramatic, especially if the water used for hydrolysis is obtained from fuel cells. To compare with the 5% acid concentration experiments, a reaction temperature of 160, 180, and 200 ℃ was performed with the 2.5% acid concentration feed. At the beginning of the reaction, there was a similar tendency to the case of the 5% acid concentration, but as the reaction progressed, the hydrogen generation amount gradually

decreased. This seems to be because the reaction rate decreased as the pH of the reactants increased due to the low acid concentration. Also, about 50 grams of unreacted agglomerated SBH that did not participate in the reaction was observed at all reactant temperatures. Therefore, it is not appropriate to perform the reaction with only a 2.5% acid concentration feed. However, at the beginning, even with a 2.5% acid concentration feed, sufficient hydrogen generation and reactant temperature rise were shown, so there is a possibility to improve the hydrogen storage density through an appropriate operation strategy.

(5) In all cases of 5% acid concentration, the conversion of SBH was >95%, suggesting that it could be beneficial to pressurize the system to cause a hydrolysis reaction with liquid water at high temperatures. The conversion was most affected by the temperature of the reactant, while additional feed could compensate for the low conversion at lower reactant temperatures.

Chapter 3. Thermal simulation of SBH hydrogen generation system

3.1. Introduction

As mentioned in Chapter 1, the kinetics of SBH hydrolysis reaction is not fully understood. Also, since the kinetics are different depending on the catalyst used, there is a limit to the study on the simulation. In addition, since most of the studies have been conducted on low-power systems, the need for research in areas where it is advantageous to check through simulations such as maximum performance evaluation and thermal management is low. However, when a hydrogen generation system based on hydrolysis of SBH is applied to high-power fuel cell applications, there are important details that cannot be confirmed only through experiments. Equation 3.1 is the general hydrolysis reaction of SBH.

$$NaBH_4 + 2H_2O \rightarrow NaBO_2 + 4H_2 + \Delta H \quad (3.1)$$

Where ΔH is the standard enthalpy change of formation expressed in kJ. The ΔH can be expressed as Equation 3.2.

$$\Delta H = \sum \Delta H_{reactant} - \sum \Delta H_{product} \quad (3.2)$$

$\sum \Delta H_{reactant}$ is the sum of the standard enthalpies of formation of the reactants expressed in kJ/mol; $\sum \Delta H_{product}$ is the sum of the standard enthalpies of formation of the products expressed in kJ/mol. The enthalpy of formation is the enthalpy of the hypothetical reaction required to form the species from its constituent elements in their standard states at standard pressure. ΔH is positive if a reaction adds energy to a system, i.e., is endothermic, and negative if a reaction subtracts energy from a system, i.e., is exothermic. Calculation of ΔH is expressed as Equation 3.3 based on the knowledge that the enthalpy of SBH formation is −188.6 kJ/mol, the enthalpy of $NaBO_2$ formation is −977 kJ/mol, the enthalpy of H_2O formation is −285.8 kJ/mol, and that the enthalpy of H_2 formation is zero, because this is already the most elementary form [95].

$$\begin{aligned} \Delta H &= (1 \times (-977) + 4 \times 0) - \left(1 \times (-188.6) + 2 \times (-285.8)\right) \\ &= -216.8 \text{ kJ} \end{aligned} \tag{3.3}$$

As can be seen from Equation 3.3, SBH hydrolysis is an exothermic reaction that emits a lot of heat to the environment. Therefore, when a large amount of hydrogen is generated for high-power applications, a huge amount of heat is generated in the system, and it becomes very important to remove excess reaction heat for stable operation.

In this chapter, simulation of the SBH hydrogen generation system focused on thermal management essential for high flow rate hydrogen generation was performed, and the simulation was validated through experimental results, and the system behavior at extreme operation, which is difficult to confirm through experiments, was evaluated. The kinetics of SBH hydrolysis under experimental conditions of this study were derived from the hydrogen generation rate experimental results. Thermal modeling of the cooling system components was also performed.

3.2. Model description

3.2.1. Hydrolysis reaction modeling

The dynamic behavior of the reactor is modelled by a set of differential equations derived from mass and energy balances on the reactant mixture. It also considers heat transfers between the utility fluid circulating inside the helical coil, the helical coil wall and the reactant mixture.

For this system, the model has been established using the following assumptions:

i) The reactor is perfectly mixed with homogeneous temperature and concentrations in the reaction mixture

ii) Feeding of the reactive is performed without volume contraction.

iii) The reactions are carried out in a pseudo-homogeneous phase

iv) The physicochemical properties of each component of the reaction mixture are constant in the considered range of temperature, and the physical properties of the reaction mixture are revalued at each computation step as functions of temperature.

v) The kinetic laws of the chemical reactions are function of the feed injection rate and the reaction progress ratio.

Since it is a reaction of injecting a liquid feed into solid SBH, it cannot be regarded as completely homogeneous in the beginning, but it is assumed that it is homogeneous in the model.

If the kinetics of hydrolysis of SBH follow the Arrhenius law, the reaction rate can be expressed as Equation 3.4.

$$r = k_0 e^{-E_a/RT_r} \prod_{i=1}^{nc} {C_i}^{\alpha_i} \tag{3.4}$$

where k_0 is the Arrhenius coefficient, R is ideal gas constant, C_i is the concentration of component i, α_i is partial order of component i. However, the kinetics of hydrolysis of SBH have not yet been clearly understood, and it varies depending on the catalyst used and the experimental conditions. Therefore, in this study, the reaction rate equation was derived from the hydrogen generation rate based on the reaction of Equation 3.5.

$$NaBH_4 + (2 + x)H_2O \rightarrow NaBO_2 \cdot xH_2O + 4H_2, \tag{3.5}$$

As confirmed in Chapter 2, since most SBH reacts at a sufficiently high reaction temperature (180 ℃) or higher, in this case, the amount of hydrogen generated can be defined as a function of the feed injection rate and the reaction progress ratio. The reaction progress ratio (γ) is defined as the amount of feed injected after the start of the reaction compared to the total amount of injected feed (Equation 3.6).

$$\gamma = \frac{\int f dt}{m_{0,\mathrm{SBH}} F} \tag{3.6}$$

where $\dot{m}_f$ is the feed injection rate, $m_{0,\mathrm{SBH}}$ is the initial SBH charging amount, f is the feed injection rate, F is the feed injection amount per 1 g SBH determined by the experimental conditions. Therefore, the reaction rate is expressed as the Equation 3.7.

$$r = f'(f, \gamma) \tag{3.7}$$

In this study, the goal is not to know the exact reaction rate of the reaction, but to analyze the reaction through the hydrogen generation rate, so the reaction rate can be expressed as a function of the amount of hydrogen produced, so it can be shown as Equation 3.8. The reaction rate function is derived from the experimental results.

$$\dot{m}_{H2} = g(r) = f(f, \gamma) \tag{3.8}$$

As shown in Equation 3.3, when SBH is hydrolyzed, the heat of reaction is 216.8 kJ/mol, which generates 43.2 kJ of heat per mol of hydrogen. Therefore, the reaction heat release of the system is determined as in Equation 3.9.

$$\dot{Q}_{\mathrm{reac}} = \frac{\Delta \mathrm{H}}{4 M_{\mathrm{H2}}} \dot{m}_{\mathrm{H2}} = 21.43\ \dot{m}_{\mathrm{H2}} \tag{3.9}$$

From Equation 3.5, the molar balance of the reaction components is as shown in Equation 3.10.

$$\frac{dn_{\mathrm{H2}}}{dt} = -4\frac{dn_{\mathrm{SBH}}}{dt} = -\frac{4}{2+x}\frac{dn_{\mathrm{feed}}}{dt} = \frac{4}{x}\frac{dn_{\mathrm{prod}}}{dt} \tag{3.10}$$

The molar balance and the mass change rate of component x have a relationship as shown in Equation 3.11.

$$\frac{dn_x}{dt} = \frac{\dot{m}_x}{M_x} \tag{3.11}$$

Therefore, the mass change rate of SBH and reaction product can be expressed as Equation 3.12.

$$\begin{aligned} \dot{m}_{\mathrm{SBH}} &= -\frac{M_{\mathrm{SBH}}}{4M_{\mathrm{H2}}}\dot{m}_{\mathrm{H2}} \\ \dot{m}_{\mathrm{prod}} &= \frac{M_{\mathrm{prod}}}{4M_{\mathrm{H2}}}\dot{m}_{\mathrm{H2}} \\ \dot{m}_{\mathrm{feed}} &= f - \frac{(2+x)M_{feed}}{4M_{\mathrm{H2}}}\dot{m}_{\mathrm{H2}} \end{aligned} \tag{3.12}$$

The key variables in simulation are the mass and physical properties of the reactant inside the reactor. The reactant is a substance in the reactor at a specific time and is defined as the sum of unreacted SBH, feed residue, and product. That is, it means a reaction component excluding the generated gaseous hydrogen. The mass change rate and mass at time t of the reactant in reactor are shown in Equation 3.13

$$\begin{aligned} \dot{m}_r &= \dot{m}_{\mathrm{SBH}} + \dot{m}_{\mathrm{feed}} + \dot{m}_{\mathrm{prod}} \\ m_r(t) &= \int_0^t \dot{m}_r\, dt = \int_0^t \left(\dot{m}_{\mathrm{SBH}} + \dot{m}_{\mathrm{feed}} + \dot{m}_{\mathrm{prod}}\right) dt \\ m_r(t) &= m_{0,\mathrm{SBH}} + \int_0^t f\, dt - \int_0^t \dot{m}_{\mathrm{H2}}\, dt \end{aligned} \tag{3.13}$$

The physical property x of the reactant in reactor when t seconds have passed since the start of feed injection $x_r(t)$ can be expressed as Equation 3.14.

$$x_r(t) = \frac{x_{\mathrm{SBH}} \left(m_{0,\mathrm{SBH}} + \int_0^t \dot{m}_{\mathrm{SBH}}\, dt \right) + x_{\mathrm{prod}} \int_0^t \dot{m}_{\mathrm{prod}}\, dt}{m_{0,\mathrm{SBH}} + \int_0^t f\, dt - \int_0^t \dot{m}_{\mathrm{H2}}\, dt} \qquad (3.14)$$

x_{SBH} is the physical property x of SBH and x_{prod} is the physical property of reaction product. x can be specific heat, density, thermal conductivity, etc. The physical properties of particular interest in this study are specific heat and thermal conductivity. The specific heat is corelated using the univariate polynomial functions as a function of temperature, as expressed Equation 3.15 [96].

$$Cp(T) = \alpha + \beta T + \gamma T^2 + \delta T^3 + \varepsilon T^4 \qquad (3.15)$$

where α, β, γ, δ, and ε are substance-dependent constants, obtained from dedicated tables, and T is absolute temperature, expressed in K [97]. The specific heat value of reactant component as seen in Figure 3.1. As shown in Figure 3.1, It can be seen that the specific heat values of SBH and $NaBO_2$ under the main reaction temperature conditions do not change significantly. Therefore, in this simulation, the specific heat values of SBH and $NaBO_2$ were treated as constants. The physical properties of H_2O and hydrogen were calculated by Refprop 9.1 [98].

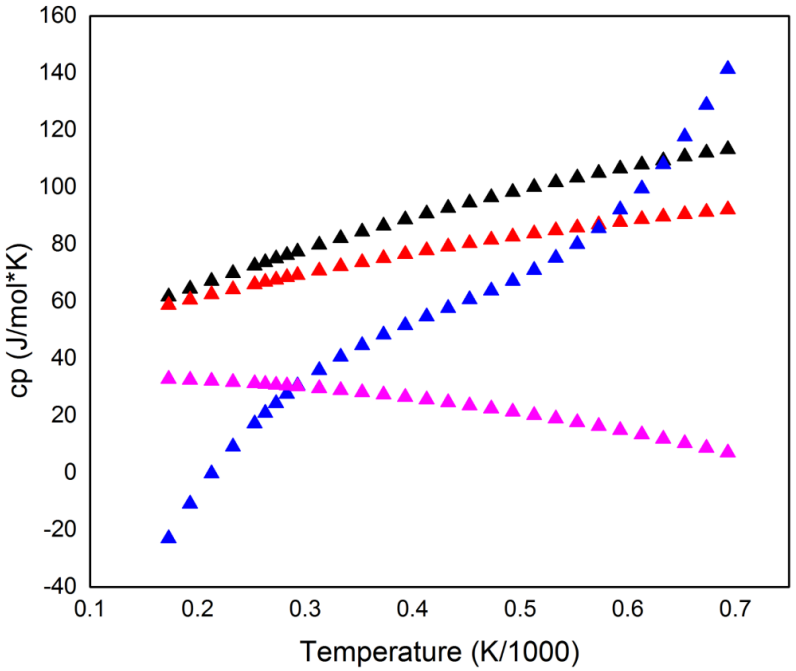

Figure 3.1 Specific heat value with temperature change of reaction component

* Black : SBH, red : $NaBO_2$, blue : H_2O, magenta : H_2

The energy balance for the reaction components is expressed as the following differential equation (Equation 3.16).

$$m_r(t) \cdot Cp_r(t) \frac{dT_r}{dt} = \dot{Q}_{\text{reac}} - \dot{Q}_c - \dot{Q}_w - \dot{Q}_f \quad (3.16)$$

where $\dot{Q}_c$ is heat release by helical cooling coil, $\dot{Q}_w$ is heat release by reactor wall and $\dot{Q}_f$ is the heat required to heat up the feed to the react.

The hydrogen generation system was modeled through the mass and energy balance equations implemented through the above equations.

The method described above is to model hydrolysis of SBH indirectly through experimental results. As described above, the purpose of this study is not to identify the reaction mechanism of SBH hydrolysis, but to analyze the hydrogen generation characteristics, so there is little need to directly analyze the reaction kinetics.

However, for more academic analysis, the reaction kinetics of acid-accelerated hydrolysis of SBH under the operating conditions of this SBH hydrogen generation system were analyzed through an Arrhenius equation. In addition, since the Arrhenius equation assumes a homogeneous reaction, if the experimental results follow the Arrhenius equation, the homogeneity of the reaction after the beginning stage (refer to Figure 2.6) mentioned in Chapter 2 can be indirectly shown.

Analysis through the Arrhenius equation was performed through

experiments at 5% acid concentration, which showed a sufficient conversion rate (RT#1, RT#2, RT#3 in Chapter 2).

Considering the reaction of this hydrogen generation system in which solid-phase SBH reacts with liquid-phase feed, Equation 3.4 can be written as Equation 3.17.

$$r = k_0 e^{-E_a/RT_r}[feed] \tag{3.17}$$

which $[feed]$ is concentration of feed. It was assumed that the hydrolysis reaction of SBH accelerated by formic acid was the 1st order reaction. This referenced research results that the hydrolysis reaction using the same carboxylic acid, acetic acid, was the 1st order reaction [66]. Also, since the feed is continuously supplied, it is assumed that the concentration of the feed is constant. With this assumption, it becomes difficult to accurately obtain k_0 in Equation 3.17, but the activation energy E_a of the reaction can be accurately calculated. In order to accurately obtain k_0, a batch reactor for identifying the reaction mechanism should be used, not a semi-batch reactor.

In the experimental results at 600s ~ 1400s, which are homogeneously reacted areas in experiment RT#1, RT#2, and RT#3 in chapter 2 (Figure 2.6), as shown in Figure 2.7, the cumulative hydrogen generation amount of each experiment is similar at 600s, but the accumulated hydrogen generation at 1400s is differ due to the difference in reaction rate according to the reactant

temperature. Arrhenius plot is derived from this reaction rate difference, and the activation energy can be known through the slope of Arrhenius plot.

Figure 3.2 shows the cumulative hydrogen generation amount converted into mol in the homogeneous reaction condition of RT#1, RT#2, RT#3 and the result of linear interpolation. An Arrhenius plot can be created by taking the log on the slope of each linear interpolation line in Figure 3.2. Through this method, the Arrhenius plot of the 5% acid concentration experiment (RT#1, RT#2, RT#3) is shown in Figure 3.3.

Through the derived Arrhenius plot, it was found that the activation energy of the hydrolysis reaction of SBH catalyzed by formic acid under high temperature and pressure in this study was 5.29 kJ/mol. This was lower than the activation energy data (7.5 ~ 8.8 kJ/mol) of the experiment performed under acetic acid at normal pressure and similar to the activation energy data (4.9 ~ 6.2 kJ/mol) of the experiment performed under HCl.[99] Considering that HCl is a stronger and more dangerous acid than formic acid, the method of this study has advantages. Also, since the Arrhenius plot as shown in Figure 3.3 follows the Arrhenius equation exactly as the R-squared value is 0.998, it can be seen that the hydrolysis reaction occurs homogeneously after 600s of the reaction.

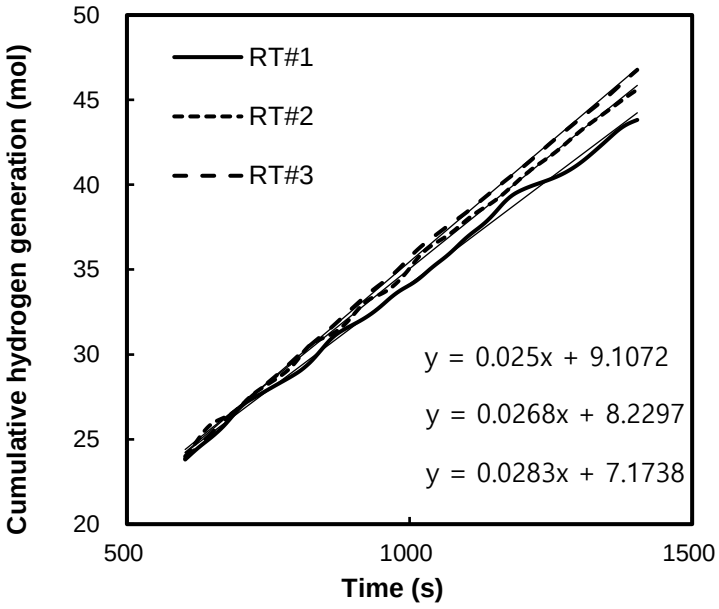

Figure 3.2 Cumulative hydrogen generation (mol) of experiments RT#1, RT#2, and RT#3 in homogeneous condition

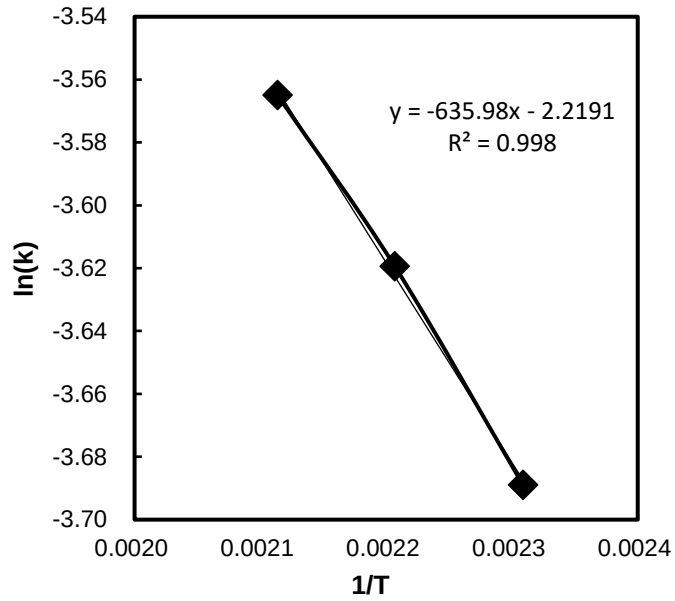

Figure 3.3 Arrehnius plot of 5% acid concentration experiment (RT#1, RT#2, RT#3)

3.2.2. Heat transfer modeling of cooling system

The hydrogen generation system in this study removes excess heat of reaction with the helical cooling coil installed inside the reactor. The numerical model was developed to predict the heat transfer in the helical cooling coil vertically installed in the reactor. Convection heat transfer in the tube, conduction through the tube wall, and convection heat transfer to the reactant in the reactor were considered as the dominant heat transfer modes. The shape and dimension symbols of the reactor and helical cooling coil are shown in Figure 3.4. The biggest difference between a general helical coil heat exchanger or a commercial batch reactor and hydrogen generation system in this study is that the internal heat exchange area and heat transfer coefficient of component are continuously changed as the reaction progresses. The volume occupied by the reactants in the reactor can be expressed as Equation 3.18.

$$V_r(t) = \frac{\pi}{4} {D_{rin}}^2 h_r(t) - \frac{\pi}{4} {d_{cout}}^2 \frac{\sqrt{p^2 + \pi^2 {D_c}^2}}{p} (h_r(t) - h_{cs}) \qquad (3.18)$$

where h_{cs} is distance between reactor bottom and coil. The volume of the reactant is expressed as Equation 3.19 based on a function of the mass of the reactant in Equation 3.13 and the density in Equation 3.14.

$$V_r(t) = \frac{m_r(t)}{\rho_r(t)} = \frac{m_{0,\mathrm{SBH}} + \int_0^t f \, dt - \int_0^t \dot{m}_{\mathrm{H2}} \, dt}{\rho_r(t)} \qquad (3.19)$$

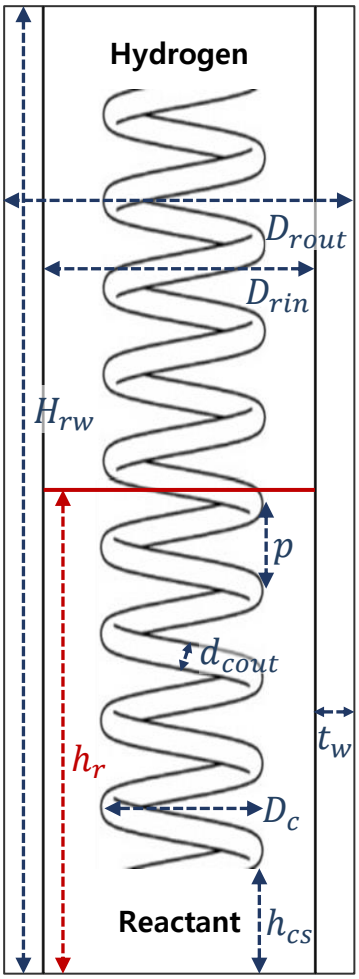

Figure 3.4 The shape and dimension symbols of the reactor and helical cooling coil

The height of the reactant inside the reactor at the time t after the feed injection can be expressed as Equation 3.20.

$$h_r(t) = \frac{\frac{4\left(m_{0,\mathrm{SBH}} + \int_0^t f\,dt - \int_0^t \dot{m}_{\mathrm{H2}}\,dt\right)}{\pi\rho_r(t)} - {d_{cout}}^2\frac{\sqrt{p^2+\pi^2{D_c}^2}}{p}h_{cs}}{{D_{rin}}^2 - {d_{cout}}^2\frac{\sqrt{p^2+\pi^2{D_c}^2}}{p}} \quad (3.20)$$

As shown in Equation 3.20 and Figure 3.4, the heat transfer through the outer coil must be calculated by dividing the region of 40 bar hydrogen and the region of the reactant.

The thermal model of vertical helical coil was conducted as one helically coiled tube divided into several small control volumes. Each control volume is composed from a portion of tube defined as a model parameter as shown in Figure 3.5. The model equations were formulated from the mass, energy and momentum balances applied to each system in each selected control volume. The energy balance of coolant, tube, and reactant are expressed as Equation 3.21 and 3.22, where T_c is helical coil tube temperature of each control volume.

$$\dot{m}_c Cp_c \frac{1}{R_c}\frac{\partial T_f}{\partial \theta} + \dot{m}_c g \sin\phi = -U_i\left(T_f - T_c\right)\frac{4}{d_i} \quad (3.21)$$

$$\dot{Q}_c = U_o d_o (T_c - T_r) = U_i d_i \left(T_f - T_c\right) \quad (3.22)$$

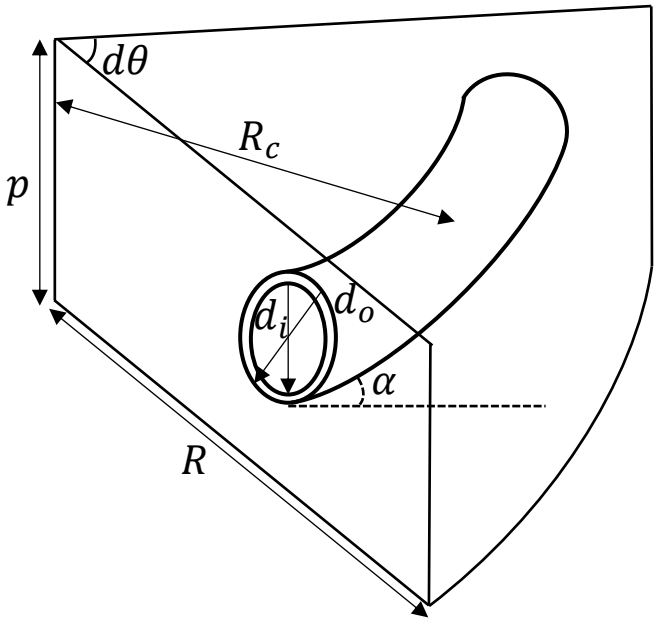

Figure 3.5 Control volume of the reactor and vertically helical coil

The inner overall heat transfer coefficient U_i and the outer overall heat transfer coefficient U_o are determined according to Equation 3.23.

$$U_i = \frac{1}{\frac{1}{h_i} + \frac{d_{cin} \ln \frac{d_{cin} + d_{cout}}{2d_{cin}}}{2k_c}}, \quad U_o = \frac{1}{\frac{1}{h_o} + \frac{d_{cout} \ln \frac{2d_{cout}}{d_{cin} + d_{cout}}}{2k_c}} \tag{3.23}$$

In this system, the effect of gravity is negligible because the pitch of the coil and the diameter of the coil tube are small. Therefore, if the heat transfer coefficient considering the effect of the coil shape is applied, the control volume can be set based on the straight shape as shown in Figure 3.6. Since the coolant is injected at the top of reactor, it passes through the region where the external fluid is hydrogen and exits from reactor after passing through the region where the external fluid is the reactant. The energy balance of the hydrogen region as Equation 3.24 can be used to obtain the coolant temperature at the boundary between the hydrogen region and the reactant region, T_{fif}.

$$\dot{m}_f Cp_f (T_{i+1} - T_i) = U_{H2} \frac{A_{H2}}{n} (T_r - T_i), T_n = T_{fif} \tag{3.24}$$

The cooling water outlet temperature, T_{fout} can be obtained by Equation 3.25 of the energy balance of the reactant region.

$$\dot{m}_f Cp_f (T_{j+1} - T_j) = U_r \frac{A_r}{n} (T_r - T_j), T_m = T_{fout} \tag{3.25}$$

The amount of heat transfer through the helical cooling coil is as Equation 3.26.

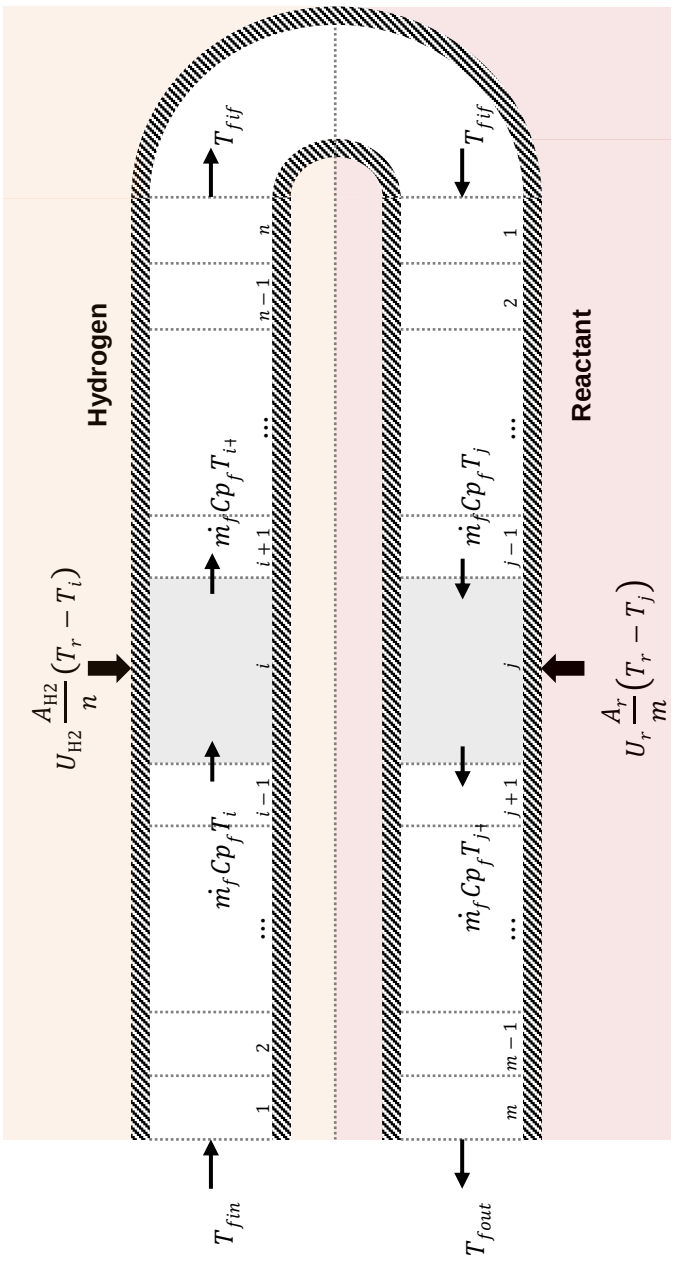

Figure 3.6 The schemetic diagram of heat transfer in helical cooling coil

$$\dot{Q}_c = \dot{m}_f Cp_f \left(T_{fout} - T_{fin}\right) \tag{3.26}$$

In order to determine the amount of heat transfer through the helical cooing coil through the above equations, it is necessary to calculate the overall heat transfer coefficient of the helical coil, and for this, the Nusselt number must be calculated. Several correlations found in technical literature were used in the developed model to obtain the inner convection heat transfer coefficient and friction factor, as well as the outer convection heat transfer coefficients. The correlations were formulated as a function of the dimensionless numbers commonly used in convection heat transfer processes to data reduction. The Nusselt, Reynolds, Prandtl, Rayleigh and Grashof numbers are calculated from Equation 3.27-3.31.

$$\mathrm{Nu}_x = \frac{h \cdot x}{k} \tag{3.27}$$

$$\mathrm{Re}_x = \frac{\rho \cdot v \cdot x}{\mu} \tag{3.28}$$

$$\mathrm{Pr} = \frac{Cp \cdot \mu}{k} \tag{3.29}$$

$$\mathrm{Ra}_x = \mathrm{Gr}_x \cdot \mathrm{Pr} \tag{3.30}$$

$$\mathrm{Gr}_x = \frac{g\beta(T_c - T_r) \cdot x^3}{v^2} \tag{3.31}$$

where h is convection heat transfer coefficient, k is thermal conductivity, v is velocity of fluid, μ is dynamic viscosity, Cp is specific heat, g is

gravitational acceleration due to Earth, β is the coefficient of thermal expansion, υ is the kinematic viscosity, and x is the characteristic length.

Based on the Reynolds number, the inner convection heat transfer coefficient of the water flowing into the tube is determined from the inner Nusselt number. The single-phase inner heat transfer correlations available in this system are summarized in Table 3.1. In most experiments, the cooling were conducted in laminar flow region, so the correlations of Schmidt [100] and Manlapaz and Churchill [101], which can obtain relatively accurate results in the laminar flow region, was selected to calculate the inner heat transfer coefficient of helical cooling coil. In addition, calculations for various other correlations were also performed, and an appropriate correlation was selected. The inner convection heat transfer correlation used in this simulation is as follows. In the laminar flow region, Nusselt numbers are given by Equation 3.32 and Equation 3.33.

$$\mathrm{Nu}_i = 3.65 + 0.08[1 + 0.8(d/D)^{0.9}]\mathrm{Re}^{[0.5+0.2903(d/D)^{0.194}]}\mathrm{Pr}^{\frac{1}{3}} \qquad (3.32)$$

$$\mathrm{Nu}_i = \left[\left(\frac{48}{11} + \frac{51/11}{(1 + 1342/\mathrm{PrHe}^2)^2}\right)^3 + 1.816\left(\frac{\mathrm{He}}{1 + 1.15/\mathrm{Pr}}\right)^{1.5}\right]^{1/3} \qquad (3.33)$$

The definition of dimensionless number in Equation 3.32 is as Equation 3.34.; He is twist number of the helical cooling coil and Dn is the Dean number.

Table 3.1 Correlations and conditions used in inner convection heat transfer coefficient calculation

Reference	Correlation	Conditions
Mori and Nakayama [103]	$\left(\frac{\mathrm{Nu_C}}{\mathrm{Nu_S}}\right)_1 = 0.1979\frac{\mathrm{Dn}^{0.5}}{x};\ \mathrm{Nu_S} = 4.11; x = \frac{2}{11}\left(1+\sqrt{1+\frac{77}{4}\frac{1}{\mathrm{Pr}^2}}\right)$	Constant heat flux; For laminar region
	$\left(\frac{\mathrm{Nu_C}}{\mathrm{Nu_S}}\right)_2 = \left(\frac{\mathrm{Nu_C}}{\mathrm{Nu_S}}\right)_1 \frac{1}{1+\frac{37.05}{x}\left\{\frac{1}{40}-\frac{17}{120}x+\left(\frac{1}{10x}+\frac{13}{30}\right)\frac{1}{10\mathrm{Pr}}\right\}\mathrm{Dn}^{-0.5}}$	
	$\mathrm{Nu}\cdot\mathrm{Pr}^{-0.4} = \frac{1}{41}\mathrm{Re}^{\frac{5}{6}}(d/D)^{\frac{1}{12}}\left\{1+\frac{0.098}{[\mathrm{Re}(d/D)^2]^{\frac{1}{6}}}\right\}$	For turbulent region
Schmidt [100]	$\mathrm{Nu} = 3.65 + 0.08[1+0.8(d/D)^{0.9}]\mathrm{Re}^{[0.5+0.2903(d/D)^{0.194}]}\mathrm{Pr}^{\frac{1}{3}}$	Constant wall T For laminar region
	$\mathrm{Nu} = 0.023\left[1+14.8(1+d/D)(d/D)^{\frac{1}{3}}\right]\mathrm{Re}^{[0.8-0.22(d/D)^{0.1}]}\mathrm{Pr}^{\frac{1}{3}}$	For transient region
	$\mathrm{Nu} = 0.023[1+3.6(1-d/D)(d/D)^{0.8}]\mathrm{Re}^{0.8}\mathrm{Pr}^{\frac{1}{3}}$	For turbulent region

Table 3.1 Correlations and conditions used in inner convection heat transfer coefficient calculation (continue)

Reference	Correlation	Conditions
Xin and Ebadian [104]	$\mathrm{Nu} = (2.153 + 0.318\mathrm{Dn}^{0.643})\mathrm{Pr}^{0.177}$	$20 < \mathrm{Dn} < 2000$
	$\mathrm{Nu} = 0.00619\mathrm{Re}^{0.92}\mathrm{Pr}^{0.4}\left(1 + 3.455\frac{d}{D}\right)$	$5000 < \mathrm{Re} < 100000$
Petukhov [102]	$\mathrm{Nu} = \frac{\left(\frac{\zeta}{8}\right)\mathrm{Re}\cdot\mathrm{Pr}}{1.07 + 12.7\sqrt{\frac{\zeta}{8}}(\mathrm{Pr}^{2/3} - 1)}$	$10^4 \le \mathrm{Re} < 5 \times 10^6$
	$\zeta = (1.82\ln\mathrm{Re} - 1.64)^{-2}$	$0.5 \le \mathrm{Pr} < 2000$
Cioncolini and Santini [105]	$\mathrm{Nu} = \frac{(f/2)\mathrm{Re}\cdot\mathrm{Pr}}{1.07 + 12.7\sqrt{f/2}(\mathrm{Pr}^{0.677} - 1)}[1 + 0.059\mathrm{Re}^{0.34}(d/D)^{0.68}]\left(\frac{\mu_b}{\mu_w}\right)^{0.11}$	Constant heat flux; For turbulent region
	$f = (1.58\ln\mathrm{Re} - 3.28)^{-2}$	

Table 3.1 Correlations and conditions used in inner convection heat transfer coefficient calculation (continue)

Reference	Correlation		Conditions
Manlapaz and Churchill [101]	$\mathrm{Nu} = \left[\left(\frac{48}{11} + \frac{51/11}{(1+1342/\mathrm{PrHe}^2)^2}\right)^3 + 1.816\left(\frac{\mathrm{He}}{1+1.15/\mathrm{Pr}}\right)^{1.5}\right]^{1/3}$ $\mathrm{He} = \frac{\mathrm{Dn}}{\left[1+\left(\frac{p}{\pi D}\right)^2\right]^{0.5}}, \mathrm{Dn} = \mathrm{Re}\left(\frac{d}{D}\right)^{0.5}$		Constant heat flux; For laminar region
Pawar and Vivek [106]	$\mathrm{Nu} = 0.0472\mathrm{Dn}^{0.8346}\mathrm{Pr}^{0.4}$	$586 < \mathrm{Dn} < 4773$ $3.83 < \mathrm{Pr} < 7.3$	Constant wall temperature; Based on avg. liquid and avg. wall temperature
Pimenta amd Campos [107]	$\mathrm{Nu} = (0.5\mathrm{Dn}^{0.481} - 0.465)\mathrm{Pr}^{0.367}$	$91 < \mathrm{Re} < 6293$ $10 < \mathrm{Pr} < 353$	Constant wall temperature; Base on LMTD method

$$\mathrm{He} = \frac{\mathrm{Dn}}{\left[1 + \left(\frac{p}{\pi D_c}\right)^2\right]^{0.5}}, \mathrm{Dn} = \mathrm{Re}\left(\frac{d_{cin}}{D_c}\right)^{0.5} \tag{3.34}$$

In the turbulent flow region, Nusselt numbers are given by Equation 3.35 [102].

$$\mathrm{Nu}_i = \frac{\left(\frac{\zeta}{8}\right)\mathrm{Re}\cdot\mathrm{Pr}}{1.07 + 12.7\sqrt{\frac{\zeta}{8}}\left(\mathrm{Pr}^{2/3} - 1\right)} \tag{3.35}$$

$$\zeta = (1.82\ln\mathrm{Re} - 1.64)^{-2}, 22000 < \mathrm{Re}$$

The critical Re number transitions from the laminar flow region to the transition region is defined by Equation 3.36.

$$\mathrm{Re}_{cri} = 2300\left[1 + 8.6\left(\frac{d_{cin}}{D_c}\right)^{0.45}\right] \tag{3.36}$$

The Nu number in the transition region is as Equation 3.37.

$$\mathrm{Nu}_i = C\cdot\mathrm{Nu}_{i,\mathrm{Re}=\mathrm{Re}_{cri}} + (1-C)\cdot\mathrm{Nu}_{i,\mathrm{Re}=20000}$$
$$C = \frac{22000 - \mathrm{Re}}{22000 - \mathrm{Re}_{cri}} \tag{3.37}$$

Regarding the helical cooling coil outer heat transfer process, it is difficult to derive an accurate relational expression because the flow outside the coil is affected by many more variables than inside the coil, such as the type of material, the shape of the reactor, and the flow pattern of reactant. In order to calculate the outer natural convection heat transfer coefficient, many studies have been conducted and empirical formulas have been derived. Table 3.2

summarizes the correlations between the results of some studies conducted in areas similar to the conditions of this study. The calculation of the outer natural convection heat transfer coefficient of helical cooling coil is important to analyze the coil wall temperature and detailed heat flux. However, the internal heat transfer amount and the external heat transfer amount of the coil must have the same value due to the energy balance, and since this study focuses on heat dissipation through the coil, the objective can be achieved by accurately modeling the inside of the helical cooling coil.

Table 3.2 Correlations and conditions used in outer convection heat transfer coefficient calculation

Reference	Correlation		Conditions, Characteristic length
Fernandez-Seara et al. [108]	$\mathrm{Nu} = 0.4998\mathrm{Ra}_{do}{}^{0.2633}$	$4.67 \times 10^6 \leq \mathrm{Ra}_{do} < 3.54 \times 10^7$	Coil tube outer diameter
Churchill and Chu [109]	$\mathrm{Nu} = 0.36 + \frac{0.4998\mathrm{Ra}_{do}{}^{0.25}}{\left[1 + \left(\frac{0.559}{\mathrm{Pr}}\right)^{9/16}\right]^{4/9}}$	$\mathrm{Ra}_{do} < 10^9$	Coil tube outer diameter
	$\mathrm{Nu} = \left\{0.6 + 0.387\left[\frac{\mathrm{Ra}_{do}}{\left[1 + \left(\frac{0.559}{\mathrm{Pr}}\right)^{9/16}\right]^{16/9}}\right]^{1/6}\right\}^2$	$\mathrm{Ra}_{do} \geq 10^9$	
Ali [110]	$\mathrm{Nu} = 0.685\mathrm{Ra}_L{}^{0.295}$	$3 \times 10^{12} \leq \mathrm{Ra}_L < 8 \times 10^{14}$	Coil tube length
	$\mathrm{Nu} = 0.00044\mathrm{Ra}_L{}^{0.516}$	$6 \times 10^{11} \leq \mathrm{Ra}_L < 10^{14}$	
	$\mathrm{Nu} = 0.257\mathrm{Ra}_H{}^{0.323}$	$6 \times 10^8 \leq \mathrm{Ra}_H < 3 \times 10^{11}$	Coil height

Table 3.2 Correlations and conditions used in outer convection heat transfer coefficient calculation (continue)

Reference	Correlation	Conditions, Characteristic length
Ali [111]	$\mathrm{Nu} = 0.0000253\mathrm{Ra}_L^{0.739}(d/D)^{1.313}$ $10^{12} \le \mathrm{Ra}_L < 10^{14}$ $\mathrm{Nu} = 0.00001535\mathrm{Ra}_L^{0.671}(d/D)^{0.702}$ $7 \times 10^{12} \le \mathrm{Ra}_L < 8 \times 10^{14}$	Coil tube length
Xin and Ebadian [112]	$\mathrm{Nu} = 0.29\mathrm{Ra}_{do}^{0.293}$ $4 \times 10^{13} \le \mathrm{Ra}_{do} < 10^{15}$	Coil tube outer diameter
Rahul et al. [113]	$\mathrm{Nu} = 0.5186\mathrm{Re}^{0.595}\left(\frac{p}{D}\right)^{0.875}$	coiled tube surfaces in across-flow of air
Moawed [114]	$\mathrm{Nu} = 0.0345\mathrm{Re}^{0.48}\left(\frac{d}{D}\right)^{0.914}\left(\frac{p}{D}\right)^{0.281}$	The forced convection from outside surfaces of helical coiled tubes

Table 3.2 Correlations and conditions used in outer convection heat transfer coefficient calculation (continue)

Reference	Correlation		Conditions, Characteristic length
Kharat [115]	$\mathrm{Nu} = 0.0265\mathrm{Re}^{0.835}\mathrm{Pr}^{0.3}\left(\frac{d_o - d_i}{D}\right)^{-0.097}$		flow between concentric helical coils
Prabhanjan et al. [116]	$\mathrm{Nu} = 0.009759\mathrm{Ra}_L{}^{0.3972}$	$5 \times 10^{14} \leq \mathrm{Ra}_L < 3 \times 10^{15}$	Coil tube length
	$\mathrm{Nu} = 0.0749\mathrm{Ra}_H{}^{0.3421}$	$9 \times 10^9 \leq \mathrm{Ra}_H < 4 \times 10^{11}$	Coil height

3.3. Results and discussion

3.3.1. Simulation validation

The SBH hydrogen generation system in this study was modeled by inputting the geometric shape and material properties of the reactor and cooling devices. The simulation was conducted by inputting the hydrogen generation rate, coolant inlet temperature, and coolant mass flow rate, and the derived reactant temperature and coolant outlet temperature were compared with experimental values to verify the simulation. For validation of this simulation, two experiments (SV#1, SV#2) as shown in Table 3.3 were used. The hydrogen generation rate, coolant inlet temperature, and coolant mass flow rate of the experiment are shown in Figure 3.7 and Figure 3.8.

The coolant outlet temperature of the simulation and the experiment as shown in Figure 3.9 and Figure 3.10 was compared to check whether the cooling system was properly modeled and whether it showed an appropriate response to the change in the coolant mass flow rate. Overall, the simulation results followed the experimental results well as shown in Figure 3.9 and Figure 3.10. In particular, it showed the effectiveness of cooling system modeling by responding appropriately to changes in coolant mass flow rate. The main error

Table 3.3 Experimental conditions for simulation validation

Parameter	SV#1	SV#2
SBH charging amount (g)	500	500
Feed injection rate (mL/min)	45	75
Feed concentration (wt.%)	5	5
Reactant temperature (°C)	200	Above 180
Stoichiometric number	4.0	4.0

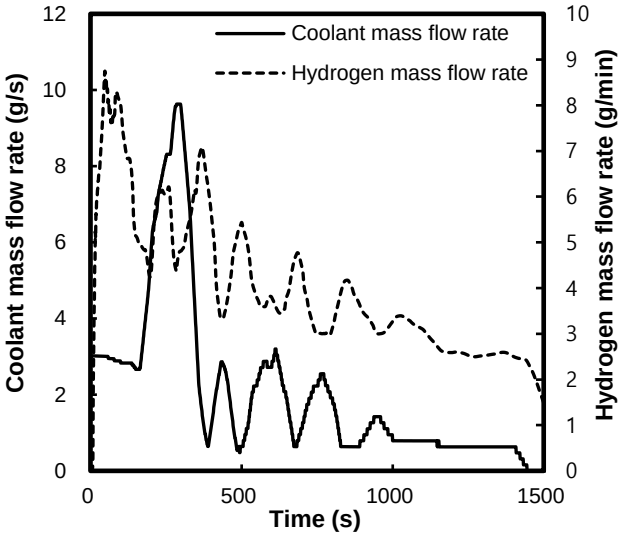

(a)

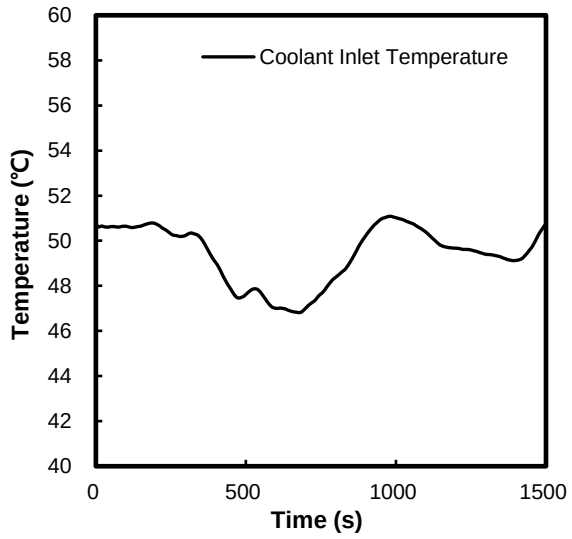

(b)

Figure 3.7 Experimental data of SV#1 inputed in the simulation (a) coolant and hydrogen mass flow rate, (b) coolant inlet temperature

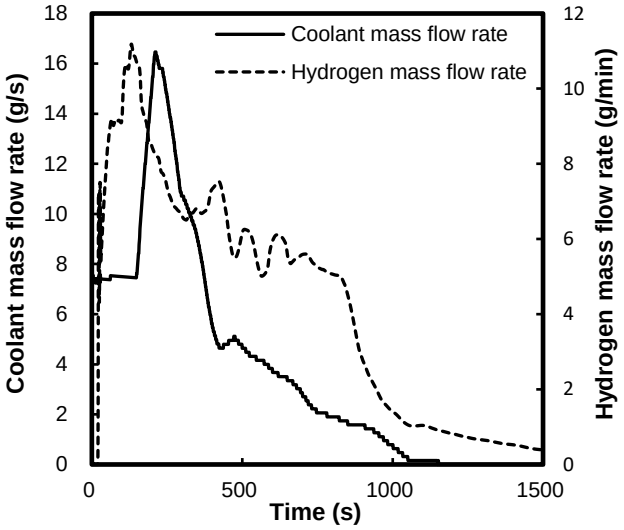

(a)

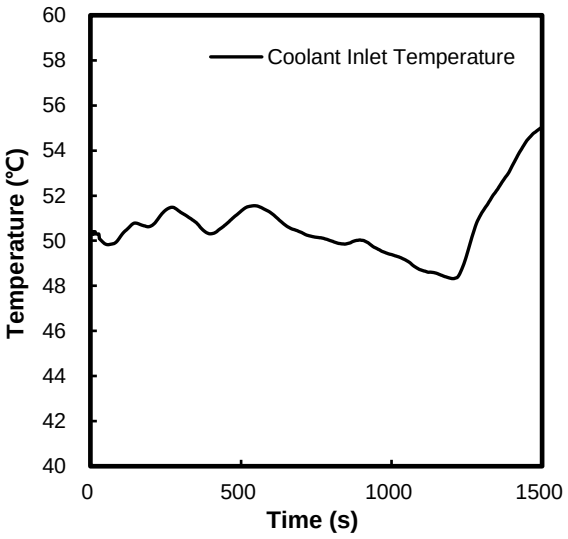

(b)

Figure 3.8 Experimental data of SV#2 inputed in the simulation (a) coolant and hydrogen mass flow rate, (b) coolant inlet temperature

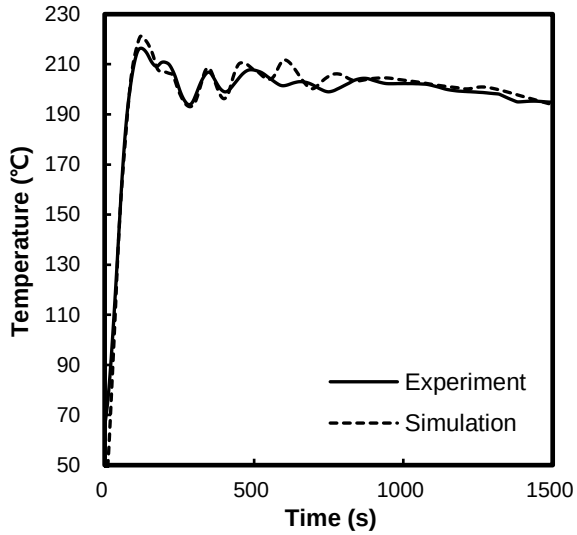

(a)

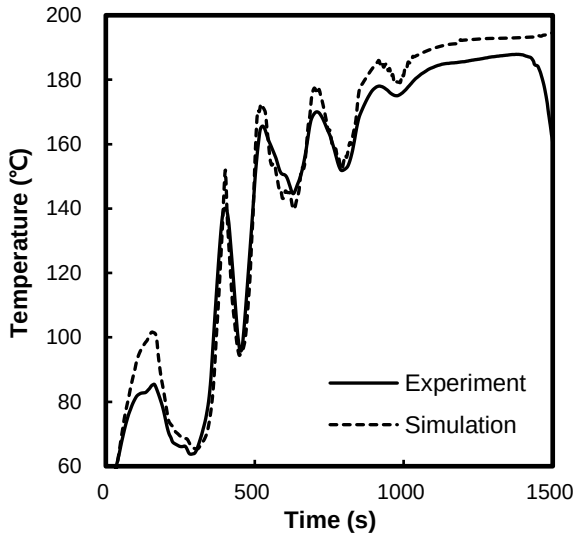

(b)

Figure 3.9 Experiment and simulation comparison of SV#1 (a) reactant temperature, (b) coolant outlet temperature

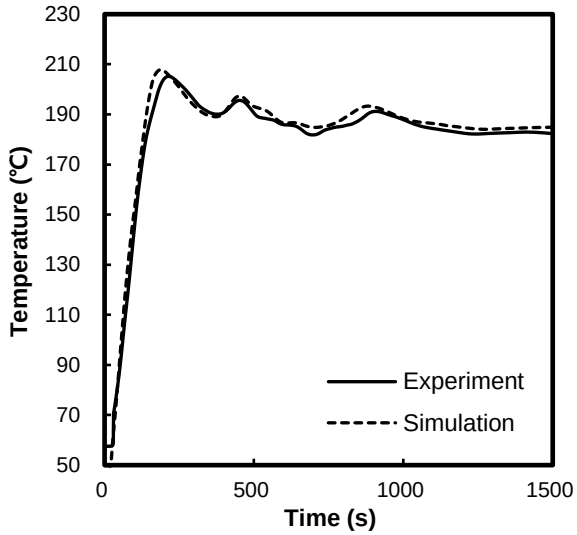

(a)

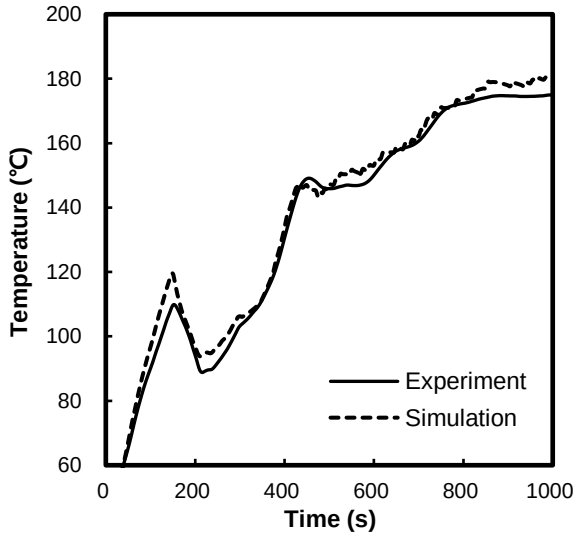

(b)

Figure 3.10 Experiment and simulation comparison of SV#2 (a) reactant temperature, (b) coolant outlet temperature

occurred at the beginning of the reaction and when the coolant mass flow rate was low as shown in Figure 3.11. The cause of these error can be analyzed as follows.

i) In this simulation, it is assumed that the reactant is homogeneous, but in the initial stage of the reaction, there is inevitable non-homogeneity in the reactant despite stirring. Although the overall temperature of the reactant rises, if the SBH in contact with the cooling coil does not react, the temperature and thermal conductivity of that part are relatively low, so the heat transfer amount is reduced, which makes the experimental value of the coolant outlet temperature smaller than the simulation value.

ii) In case of the low coolant mass flow rate, the flow of coolant is very slow, so even if it is well insulated, the time to reach the coolant outlet temperature measurement point from the inside of the reactor is long, and it led to lose heat from coolant. This can be explained that the experimental value of the coolant outlet temperature is smaller than the simulation value when the coolant mass flow rate is low. In particular, the smaller the coolant mass flow rate, the higher the coolant outlet temperature, so the heat dissipation amount to the surroundings increases. For the same reason, when the input coolant mass flow rate is 0, the coolant outlet temperature may not be given a meaning. In the simulation, the minimum flow rate was

set to prevent the occurrence of singularity points divided by 0.

The reactant temperature also confirmed that the simulation results followed the experimental values well. Based on these results, the validity of the simulation of the SBH hydrogen generation system performed in this study was confirmed.

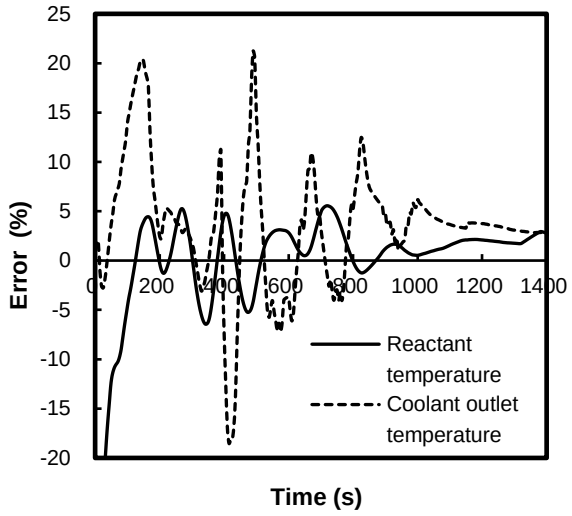

(a)

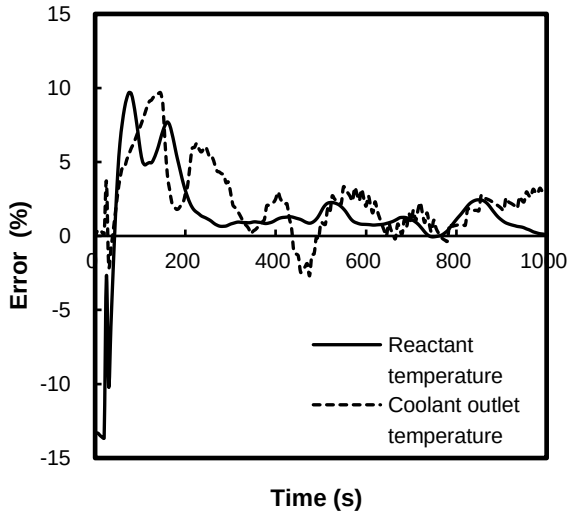

(b)

Figure 3.11 Error between experiment and simulation of the reactant temperature and coolant outlet temperature (a) SV#1 (b) SV#2

3.3.2. Limit hydrogen generation ability evaluation

For optimal design of hydrogen generation system, it is necessary to evaluate the maximum hydrogen generation rate that can be generated in a single reactor. Since it is dangerous to confirm the maximum hydrogen generation rate through experiments, the limit hydrogen generation ability was evaluated through simulation.

The experimental results of the hydrogen generation rate according to the feed injection rate in Chapter 2 as normalized time according to the reaction progress ratio was shown in Figure 3.12 (a). The normalized time N_t represents the reaction progress ratio as the reaction progress time t expressed based on the total feed injection time t_{TF} as shown Equation 3.38.

$$N_t = \frac{t}{t_{TF}} \tag{3.38}$$

The result of converting the result of Figure 3.12 (a) into hydrogen generation rate per 1 mL/min of feed injection rate is shown in Figure 3.12 (b). From results of Figure 3.12 (b), it was found that there was no significant difference in the hydrogen generation rate per 1 mL/min according to the feed injection rate. Therefore, in the simulation, the hydrogen generation rate was expressed as a function of the feed injection rate and the reaction progress ratio. The hydrogen generation rate per 1 mL/min of feed injection rate over normalized time applied to the simulation was set to the average value of the

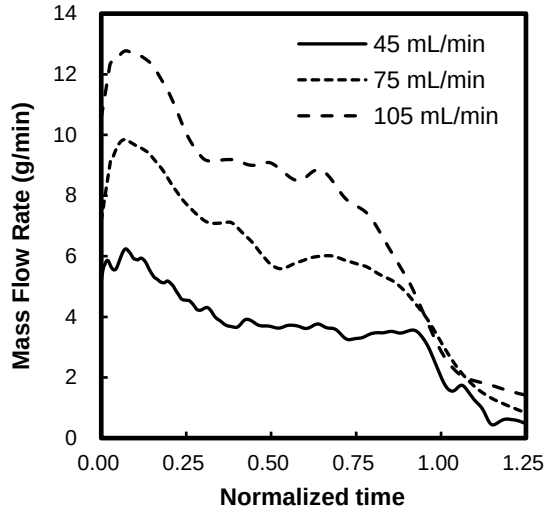

(a)

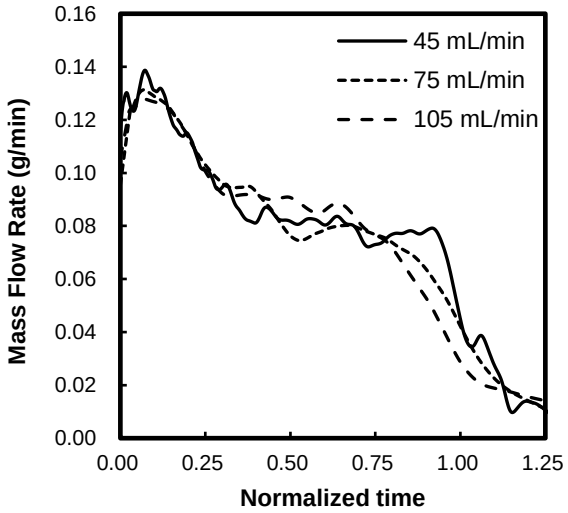

(b)

Figure 3.12 Experimental results of (a) hydrogen generation rate according to feed injection rate over normalized time (b) hydrogen generation rate per 1 mL/min feed injection over normalized time

results in Figure 3.12 (b), and the value is shown in Figure 3.13.

For the evaluation of limit hydrogen generation ability, the cases that the initial SBH charging amount was 1 kg and the feed injection rate was 150 mL/min, 175 mL/min, 200 mL/min were simulated. It was assumed that the coolant inlet temperature was kept constant at 50 °C, and the limiting performance of the helical cooling coil used in this study was evaluated by measuring the reactant temperature while changing the coolant mass flow rate. For each feed injection rate, the simulation results of the reactant temperature and heat release rate by the cooling coil when changing the coolant mass flow rate were shown in Figure 3.14, Figure 3.15, and Figure 3.16. As a result of the simulation, it was confirmed that the maximum coolant mass flow rate of the helical cooling coil installed in the hydrogen generation system was actually about 50 g/s, given that there was no significant difference in the reactant temperature and heat release rate between the coolant mass flow rate of 100 g/s and 50 g/s. In the simulation results of the reactant temperature (Figure 3.14 (b), Figure 3.15 (b), and Figure 3.16 (b)), the maximum temperature in case of 200 mL/min feed injection rate was recorded at 220 °C even when the cooling system was continuously operated at maximum coolant mass flow rate. Considering the safety and local high temperature caused by non-uniformity of reaction, the maximum output through this hydrogen generation system is about

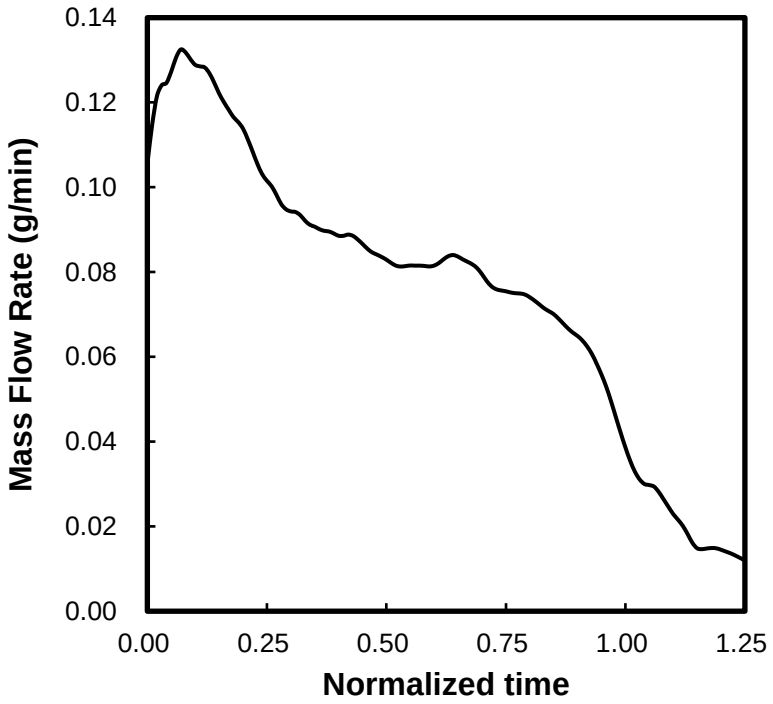

Figure 3.13 Hydrogen generation rate per 1 mL/min feed injection rate over normalized time applied to the simulation

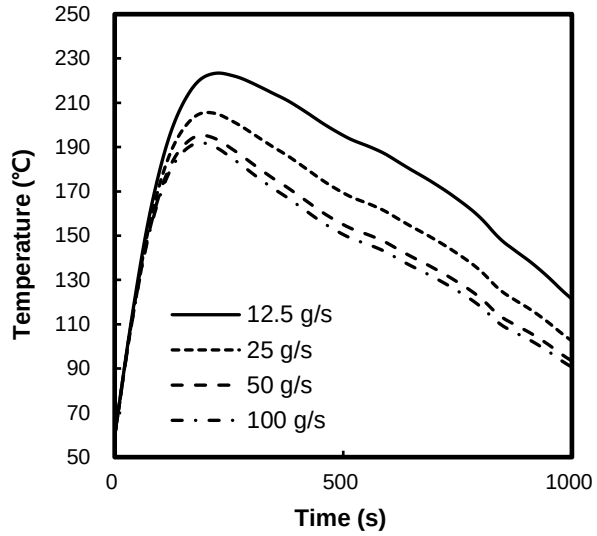

(a)

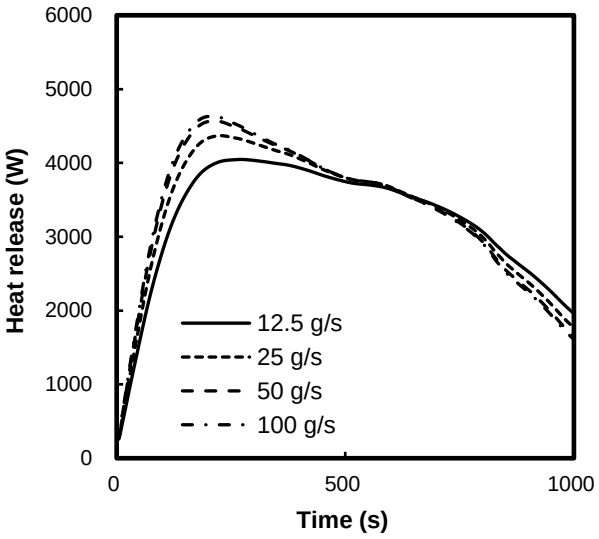

(b)

Figure 3.14 Simulation results in case of 150 mL/min feed injection rate (a) the reactant temperature (b) the heat release by the cooling coil

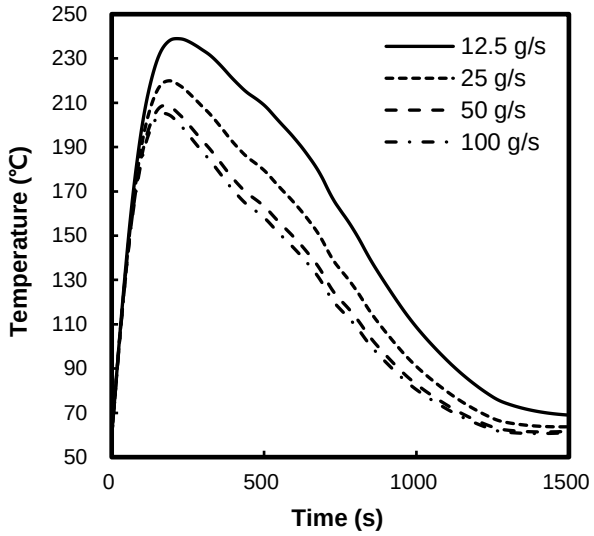

(a)

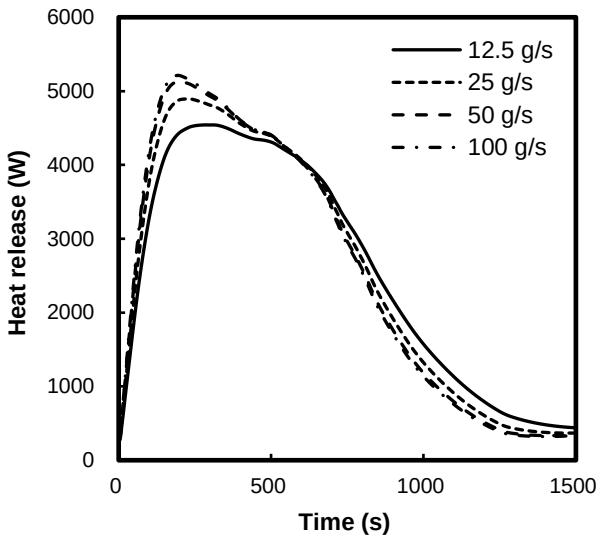

(b)

Figure 3.15 Simulation results in case of 175 mL/min feed injection rate (a) the reactant temperature (b) the heat release by the cooling coil

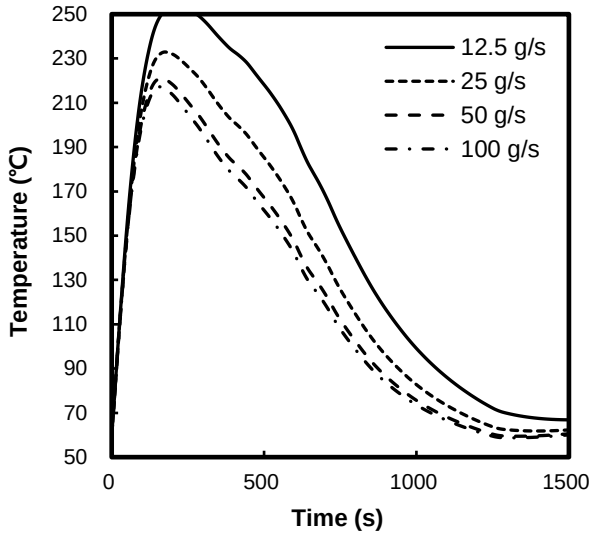

(a)

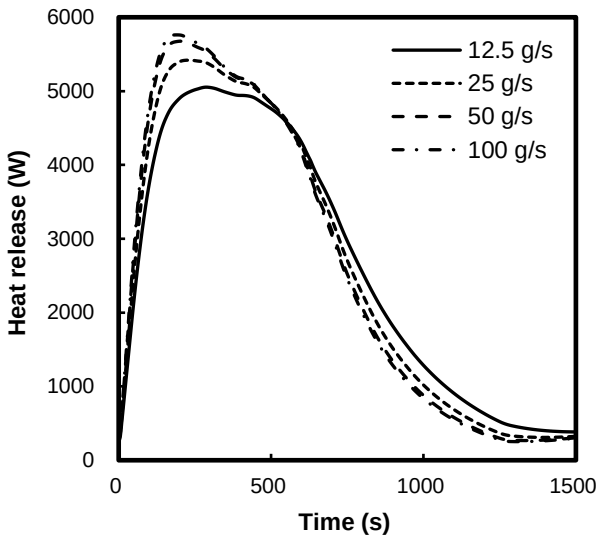

(b)

Figure 3.16 Simulation results in case of 200 mL/min feed injection rate (a) the reactant temperature (b) the heat release by the cooling coil

175 mL/min feed injection rate.

To simulate the actual limiting power operation, the system behavior was analyzed when the feed injection rate was 150, 175, and 200 mL/min. The coolant mass flow rate was proportionally controlled based on the target reactant temperature (180 °C). The reactant temperature and coolant mass flow rate are shown in Figure 3.17, and the coolant outlet temperature and heat release by the cooling coil are shown in Figure 3.18. As previously confirmed, stable operation was possible up to the feed injection rate of 175 mL/min. Considering that the optimal operating conditions of a typical fuel cell are a voltage of 0.6 V and a current density of 1.2 A/cm^2, the fuel cell output power according to the hydrogen flow rate is expressed as Equation 3.39.

$$P = 0.6\frac{2F}{M_{\mathrm{H2}}}\dot{m}_{\mathrm{H2}} \tag{3.39}$$

which P is fuel cell power, F is Faraday constant and $\dot{m}_{\mathrm{H2}}$ is the hydrogen flow rate and the unit is g/s. When the maximum feed injection rate of this hydrogen production system is 175 mL/min, the hydrogen generation rate is 0.22 g/s, which means that a fuel cell of about 12 kW can be operated. Considering that the volume of the reactor used in this study is about 3.2 L, it seems that it is possible to operate high-power fuel cell applications sufficiently by introducing a larger reactor or by connecting several reactors in parallel. Also, the simulation results when the upper limit of the coolant flow rate is

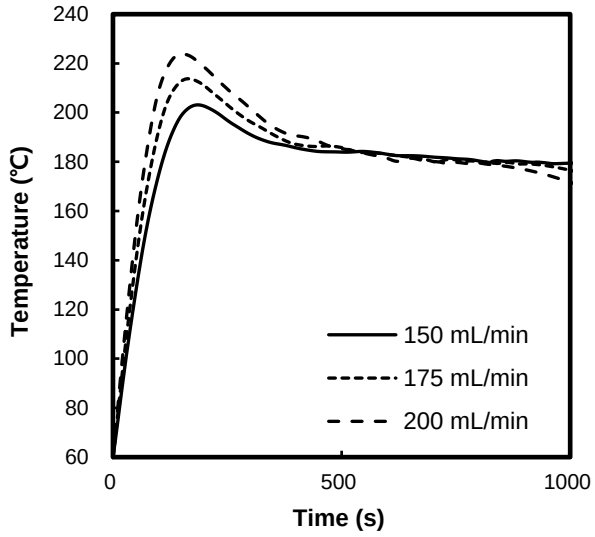

(a)

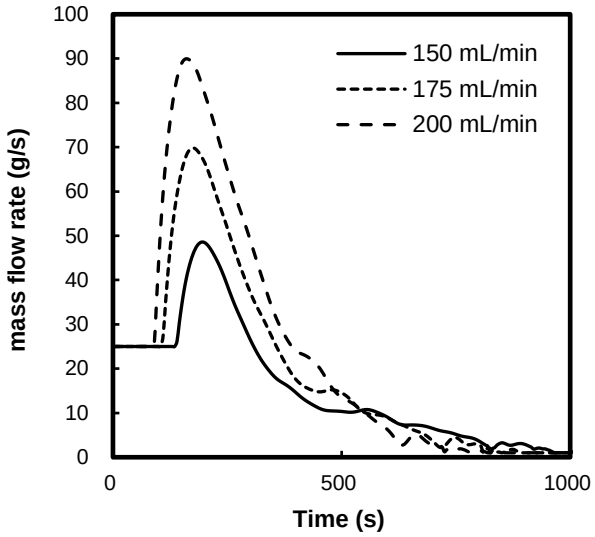

(b)

Figure 3.17 Simulation results when controlling the coolant mass flow rate proportionally (a) the reactant temperature (b) the coolant mass flow rate

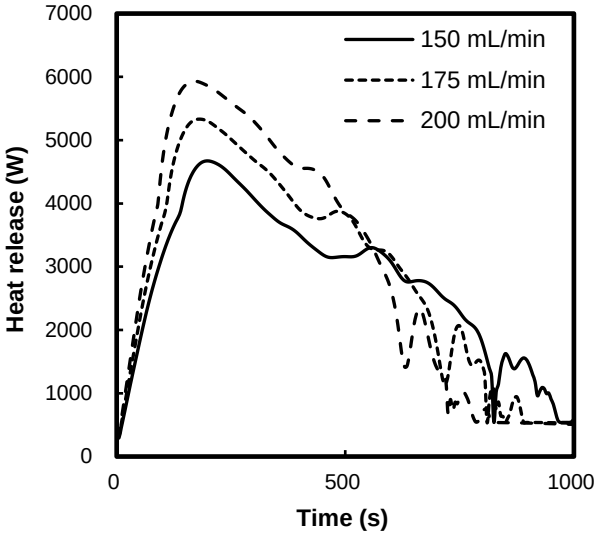

(a)

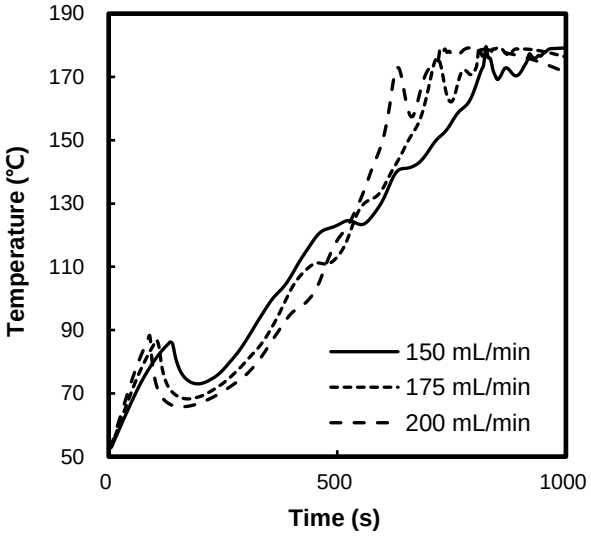

(b)

Figure 3.18 Simulation results when controlling the coolant mass flow rate proportionally (a) the heat release by the cooling coil (b) the coolant outlet temperature

limited to 50 g/s under the same conditions are shown in Figure 3.19 and Figure 3.20. As previously evaluated, even if the coolant flow rate is 50 g/s or more, there is no significant difference in cooling performance, so there is no significant difference in the maximum reactant temperature. Considering the pump power and pressure drop, it seems appropriate to set the maximum coolant flow rate to 50 g/s.

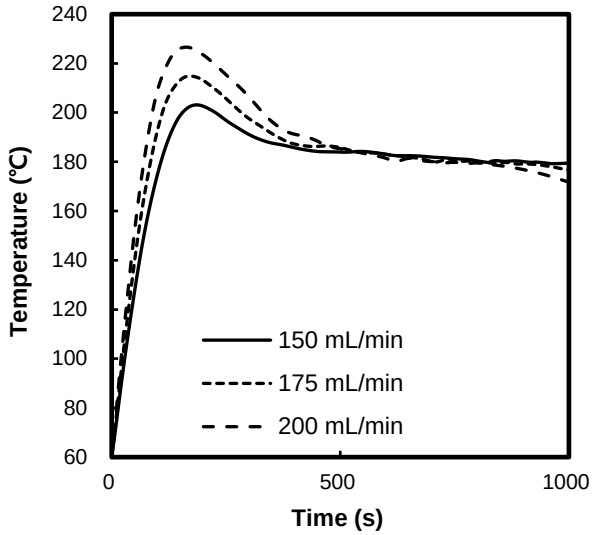

(a)

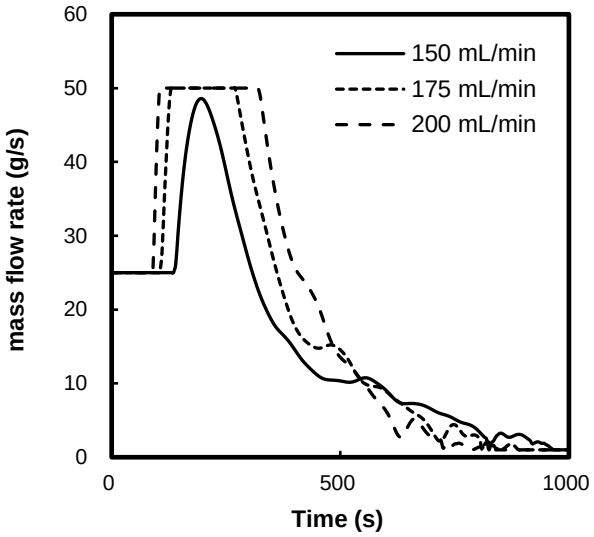

(b)

Figure 3.19 Simulation results when controlling the coolant mass flow rate proportionally (50 g/s maximum coolant mass flow rate) (a) the reactant temperature (b) the coolant mass flow rate

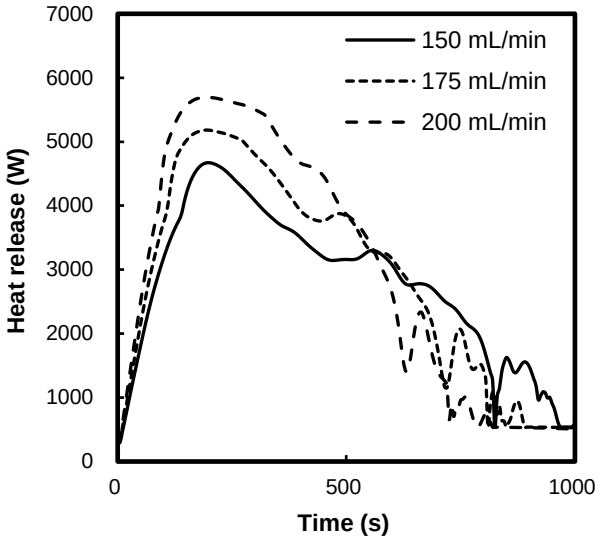

(a)

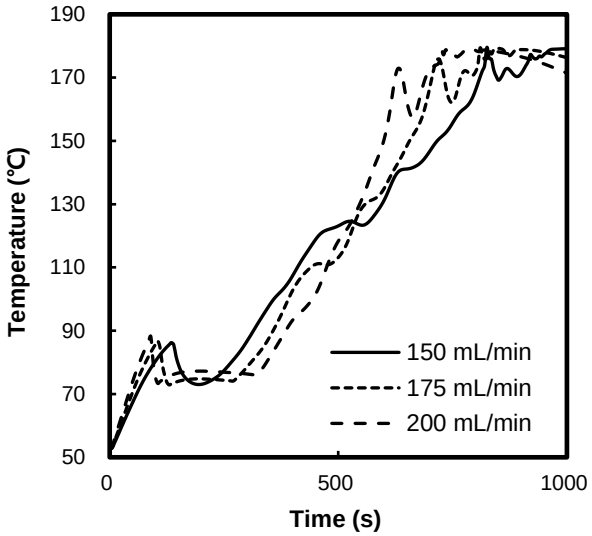

(b)

Figure 3.20 Simulation results when controlling the coolant mass flow rate proportionally (50 g/s maximum coolant mass flow rate) (a) the heat release by the cooling coil (b) the coolant outlet temperature

3.4. Summary

In this chapter, the reaction and thermal management simulation of the SBH hydrogen generation system of this study was performed. A heat transfer model was prepared to consider the reactant properties and heat transfer area that change as the reaction progressed, and the hydrolysis reaction was modeled through the hydrogen generation rate according to the feed injection rate and the reaction progress ratio calculated based on the experimental results. The simulation was validated by comparing the reactant temperature and the coolant outlet temperature with the experimental values when the cooling water flow rate, hydrogen generation rate, and coolant inlet temperature were taken as input values. The reactant temperature was simulated with an error of 5% or less except for the initial stage of the reaction where non-homogeneous reaction was observed.

Since the validity of the simulation was confirmed, the limit hydrogen generation ability of hydrogen generation system in this study, which is difficult to confirm by experiment, was evaluated. When the feed injection rate was 150, 175, and 200 mL/min, the maximum effective coolant flow rate of the cooling coil was evaluated to be approximately 50 g/s. Base on the simulation result of the reactant temperature with proportional control of the coolant mass flow rate,

stable operation was possible up to the feed injection rate of 175 mL/min, which can operate about 12 kW of fuel cell applications. Considering that the volume of the reactor used in this study is about 3.2 L, it seems that it is possible to operate high-power fuel cell applications sufficiently by introducing a larger reactor or by connecting several reactors in parallel.

Chapter 4. Operation strategy of SBH hydrogen generation system

4.1. Introduction

In Chapter 2, the effect of various parameters on the performance of the hydrogen generation system based on acid-accelerated liquid hydrolysis of solid-state SBH was analyzed. As a result of experiments of Chapter 2, it was shown that the hydrolysis of SBH performed at high temperature and high pressure reacted more than 95% in condition of the stoichiometric number 4 or higher and 5% formic acid solution.

Since the value of SBH as a hydrogen storage material is in terms of ease of transportation and storage, the SBH hydrogen generation system should be designed as an 'on-board' system. Also, it is important to achieve a high hydrogen storage density. To this end, in this chapter, the improvement of the operation strategy of the SBH hydrogen generation system was studied through the following two experiments.

i) It was confirmed whether the flexibility in hydrogen generation rate could be obtained by changing the feed injection rate within a single batch

reaction.

In order to be used as an 'on-board' system, it should be possible to control the hydrogen generation according to the hydrogen demand of fuel cell applications. Otherwise, a relatively large volume of buffer tank is required. In addition, the internal pressure of the buffer tank cannot be higher than the reactor pressure because installing a separate compression equipment increases the weight and cost of the system and reduces the energy efficiency. In Chapter 2, It was confirmed that the hydrogen generation rate was changed by the change of the feed injection rate. In addition, it was checked whether the hydrogen generation rate was changed when the feed injection rate was changed within a single batch reaction.

ii) It was confirmed whether the hydrogen storage density could be increased while obtaining a high conversion rate by changing the feed concentration within a single batch reaction.

The amount of formic acid using should be minimized for reasons such as increased feed cost, safety management issues, and decreased hydrogen storage density. In particular, if water generated from a fuel cell is used as a feed, the effect of the concentration of formic acid on the hydrogen storage density of the system may be greater. As described in Chapter 2, a sufficient conversion could not be obtained with a 2.5% concentration of formic acid solution.

However, considering that hydrolysis of SBH reacts better at lower pH, it can be explained that the lower conversion is because the pH increased as the amount of basic product gradually increased. Considering that a sufficient reaction occurred even when 2.5% formic acid solution was used at the initial stage of the reaction, it seems that the amount of formic acid consumed per batch reaction can be reduced through a strategy of injecting a low concentration formic acid solution at the initial stage of the reaction and a high concentration formic acid solution at the later part of reaction.

To sum up, in this chapter, the operability of the 'on-board' hydrogen generation system based on hydrolysis of SBH was evaluated, and an operation strategy for maximizing the hydrogen storage density was derived.

4.2. Experimental condition

Experiments to evaluate the feasibility of 'on-board' operation were performed by changing the feed injection rate according to the reaction progress ratio. In addition, experiments to minimize the amount of formal acid used were performed by changing the concentration of injected feed according to the reaction progress ratio. Variables were changed based on reaction progress ratio of 25%, 50%, 75%, and 100%, and specific experimental conditions are shown in Table 4.1. Experiments were performed on other parameters under the conditions of the SBH charge amount of 500 g, and the stoichiometric number of 4.0. The reactant temperature was set to between 180 ℃ and 200 ℃ in order to minimize the vibration of the hydrogen generation rate. This is because, as a result of Chapter 2, in the case of the stoichiometric number 4.0, using 5% feed condition, there was no significant difference in the conversion at the reactant temperature of 180 ℃ and 200 ℃.

If the hydrogen generation rate increases or decreases according to the increase or decrease of the feed injection rate, it can be evaluated that the 'on-board' operation is possible. To confirm this, the hydrogen production flow rate was confirmed by changing the feed injection rate of 45 mL/min and 75 mL/min according to the reaction progress. SBH was charged with 500 g and the

Table 4.1 Experiments conditions for 'on-board' operability evaluation and optimization of hydrogen storage density

Ex. number	Feed condition	Reaction progress ratio			
		25 %	50 %	75 %	100 %
OB#1	Concentration (%)	5			
	Injection rate (mL/min)	45		75	
OB#2	Concentration (%)	5			
	Injection rate (mL/min)	75			45
OB#3	Concentration (%)	5			
	Injection rate (mL/min)	45	75		45
HD#1	Concentration (%)	2.5	5		
	Injection rate (mL/min)	45			
HD#2	Concentration (%)	2.5		5	
	Injection rate (mL/min)	45			
HD#3	Concentration (%)	2.5			5
	Injection rate (mL/min)	45			

reaction started with injection at 45 mL/min so that there was no effect due to lack of reaction site.

In Chapter 2, it was confirmed that it was difficult to achieve a sufficient reaction with a 2.5% concentration of formic acid solution. However, at the initial stage of reaction, there was no significant difference in the reaction pattern of the 2.5% and 5% acid concentration of feed, the initial 25%, 50%, and 75% reaction progress ratio were injected with a solution of 2.5%, and then a 5% solution was injected to confirm an increase in the conversion.

4.3. Experimental results and discussion

4.3.1. 'On-board' operability evaluation

Through experiments OB#1, OB#2, and OB#3, it was evaluated whether flexible hydrogen generation rate change for on-board operation is possible. The hydrogen generation rate of an experiment in which entire batch reaction was conducted at the feed injection rate of 45 mL/min and 75 mL/min was set as a reference. And the hydrogen generation rate was measured while changing the feed injection rates of 45 mL/min and 75 mL/min according to the reaction progress in one batch reaction. Experiment OB#1 confirmed the system response according to the increase in feed injection rate, OB#2 the system response according to the decrease in feed injection rate, and OB#3 the system response according to multiple feed injection rate changes.

The hydrogen generation rate and hydrogen generation amount of OB#1, OB#2, and OB#3 were shown in Figure 4.1, Figure 4.2, and Figure 4.3. Since the reaction time varies according to the feed injection rate, a normalized time was introduced for comparison according to the reaction progress. The normalized time N_t represents the reaction progress as the reaction progress time t expressed based on the total feed injection time t_{TF} as shown

Equation 4.1.

$$N_t = \frac{t}{t_{TF}} \tag{4.1}$$

As a hydrogen generation rate result of experiment OB#1 in Figure 4.1 (a), it can be confirmed that the hydrogen generation rate, which followed the 45 mL/min reference, was increased with the 75 mL/min reference after the feed injection rate change point (gray dotted line). The graph of the cumulative hydrogen generation in Figure 4.1 (b) also followed the 45 mL/min reference, but it was seen that it increased more rapidly as the feed injection rate increased.

In the result of experiment OB#2 in Figure 4.2, it was also seen that the hydrogen production decreased according to the decrease of the feed injection rate. In Figure 4.2 (a), undershoot and overshoot were observed at the hydrogen flow rate after normalized time 0.75. This seems to be because the coolant mass flow rate did not decrease as much as the reaction heat decreases, resulting in supercooling of the reactant temperature, the hydrogen generation rate decreased more than the reference, and as the temperature recovers, the hydrogen generation rate became larger than the reference. This phenomenon can be improved by preemptively adjusting the coolant mass flow rate according to the change in the feed injection rate since the feed injection rate is a variable that can be directly adjusted. Based on the results of experiment OB#3, it was confirmed that it is possible to change the feed injection rate

multiple times within one batch reaction. As can be seen from the graph of Figure 4.3 (b), it was confirmed that the cumulative hydrogen generation amount had almost the same slope as each reference graph according to the feed injection rate (red dotted line).

According to the results of experiments OB#1, OB#2, and OB#3, about 0.1 normalized time was consumed for the response of hydrogen generation as the feed injection rate was changed, which is about 100 to 120 seconds. The larger the initial SBH filling amount, the longer the total feed injection time, so it seems that it is possible to change the feed injection rate for multiple times within a single batch reaction. Based on these results, it is judged that the on-board operation of this hydrogen generation system is sufficiently possible. This seems to be able to provide a flexible operation strategy even in a system that introduces multiple reactors rather than a single reactor.

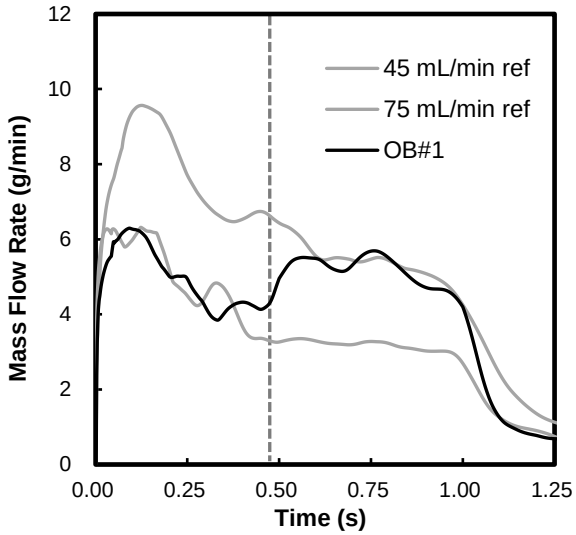

(a)

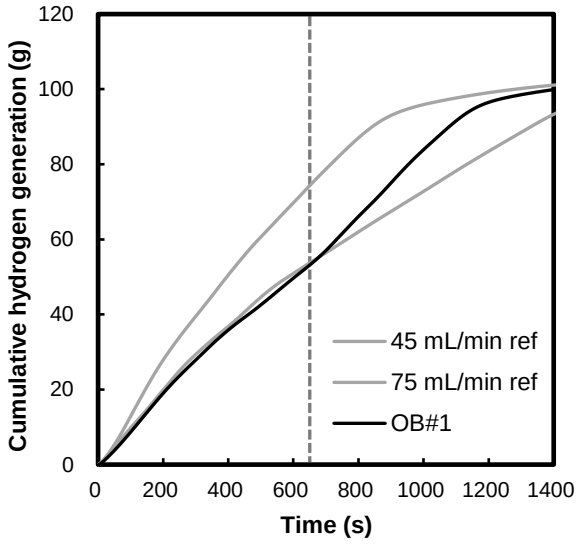

(b)

Figure 4.1 Experimenet result of OB#1 (a) hydrogen mass flow rate over normalized time (b) cumulative hydrogen generation amount over reaction time

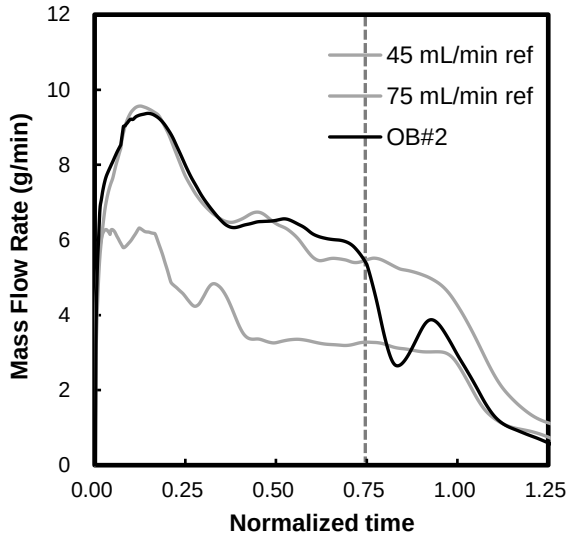

(a)

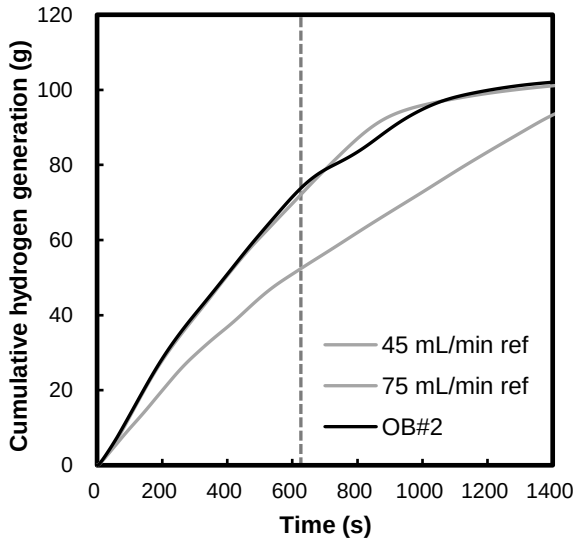

(b)

Figure 4.2 Experimenet result of OB#2 (a) hydrogen mass flow rate over normalized time (b) cumulative hydrogen generation amount over reaction time

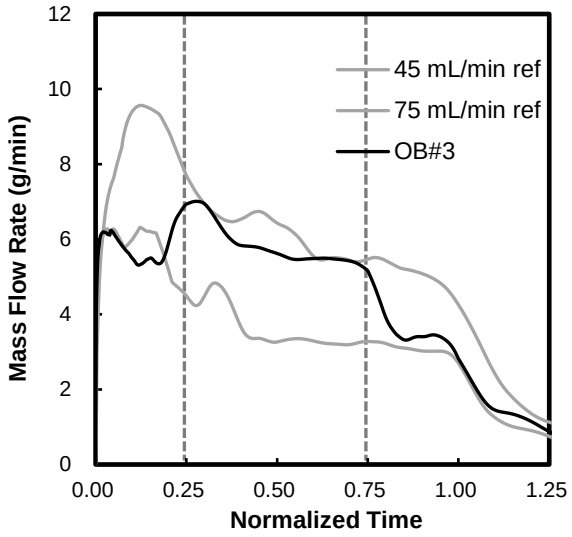

(a)

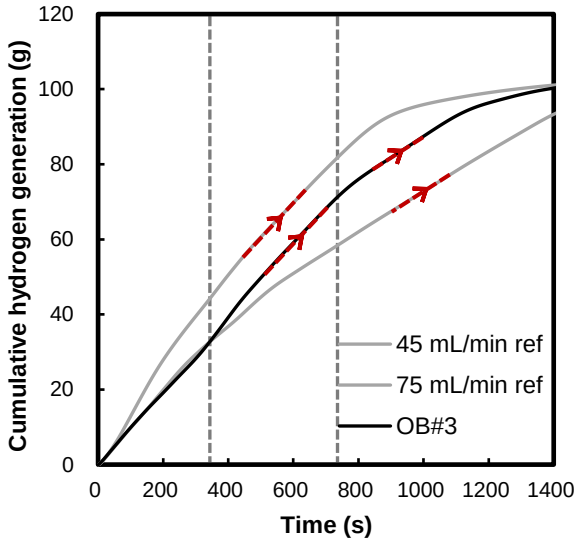

(b)

Figure 4.3 Experimenet result of OB#3 (a) hydrogen mass flow rate over normalized time (b) cumulative hydrogen generation amount over reaction time

4.3.2. Maximize hydrogen storage density

In Chapter 2, even if 2.5% concentration feed is used, it was confirmed that the hydrogen generation amount was similar to the results of the 5% concentration feed test at the initial stage of the reaction. Therefore, the reaction was started with 2.5% concentration feed, and after a certain reaction progress ratio, 5% concentration feed was used to verify whether the conversion corresponding to the experiment using 5% concentration feed was shown.

The hydrogen generation rate and cumulative hydrogen generation amount of experiments HD#1, HD#2, and HD#3 are shown in Figure 4.4, Figure 4.5, and Figure 4.6 and Table 4.2. Initially, the hydrogen generation rate results followed the results of the 2.5% concentration reference experiment, and as 5% concentration feed was injected, generally the hydrogen generation rate was higher than that of the 2.5% concentration reference. Summarizing the experimental results, the cumulative hydrogen generation amount increased as the 5% feed injection ratio increased. However, even in the case of HD#1, which used 2.5% concentration feed the least, it showed less hydrogen generation amount than the case of using only 5% concentration feed. Also, the improvement of the hydrogen storage density, which was the original purpose, could not be obtained. As the ratio of 2.5% concentration feed injection increased, the hydrogen storage density decreased slightly.

Table 4.2 Experimental results of HD#1, HD#2, HD#3

Ex. number	5% ref	HD#1	HD#2	HD#3	2.5% ref
Hydrogen generation (g)	104.03	102.86	99.24	97.60	94.18
Conversion (%)	98.1	97.0	93.5	92.0	88.8
Hydrogen storage density (wt.%)	6.7	6.7	6.5	6.4	6.3
Hydrogen storage density excluding water (wt.%)	16.3	16.6	16.5	16.7	16.6
Unreacted agglomerated SBH (g)	0	~5	~15	~30	~50

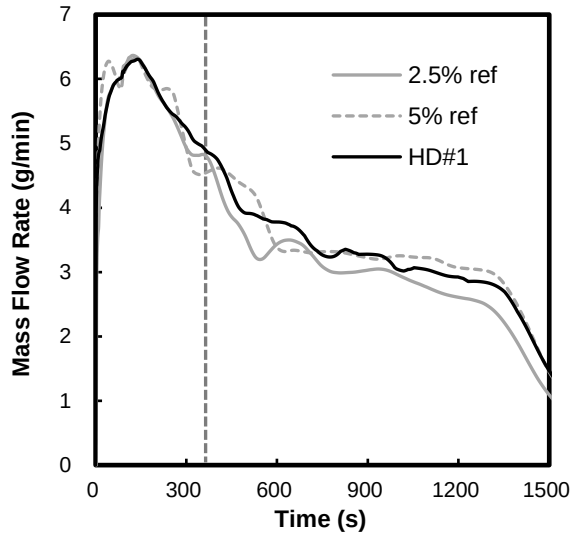

(a)

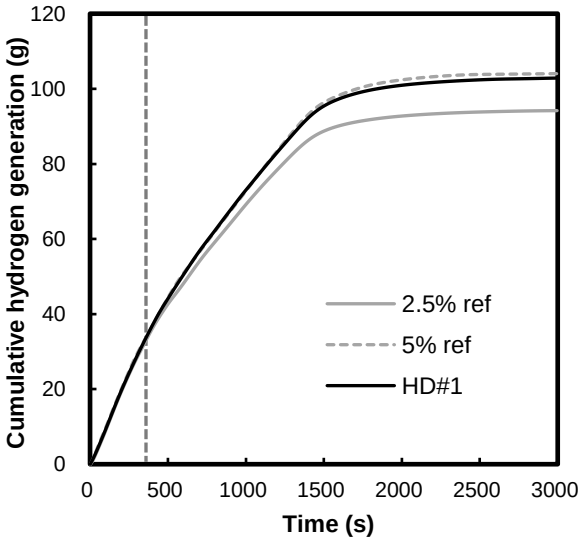

(b)

Figure 4.4 Experimenet result of HD#1 (a) hydrogen mass flow rate over time (b) cumulative hydrogen generation amount over time

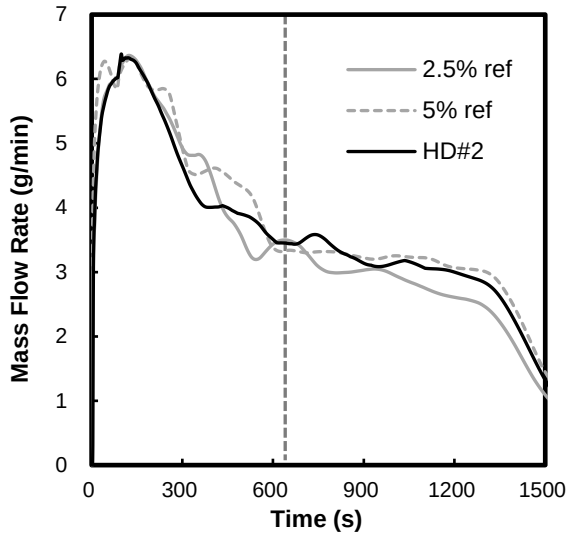

(a)

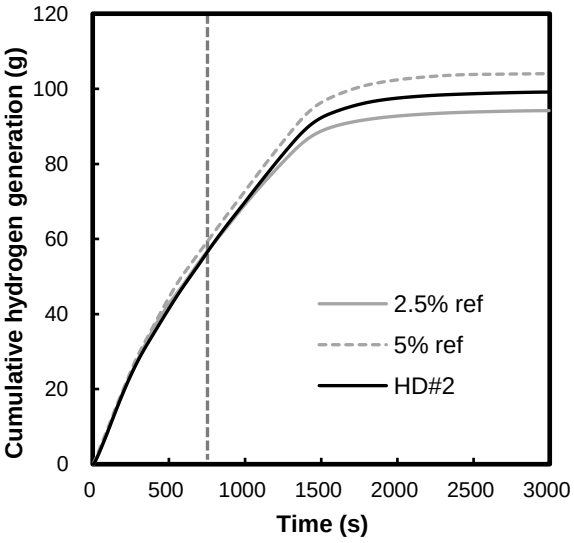

(b)

Figure 4.5 Experimenet result of HD#2 (a) hydrogen mass flow rate over time (b) cumulative hydrogen generation amount over time

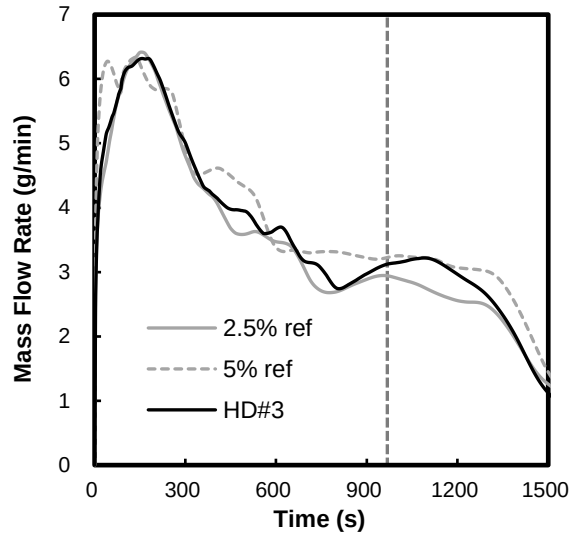

(a)

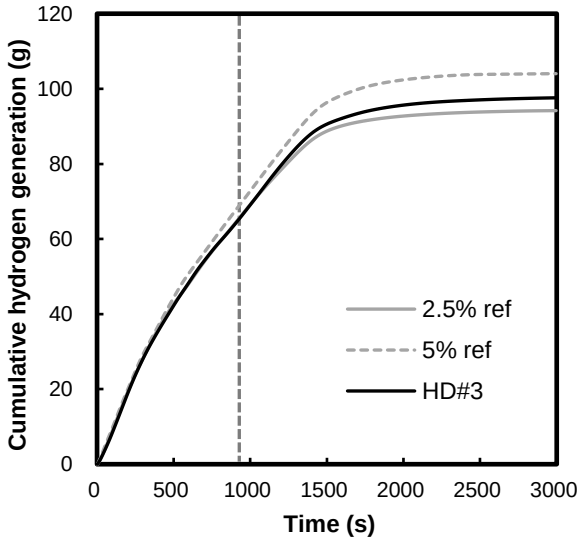

(b)

Figure 4.6 Experimenet result of HD#3 (a) hydrogen mass flow rate over time (b) cumulative hydrogen generation amount over time

The ^{11}B solid NMR spectroscopy results of experiments HD#1, HD#2, and HD#3 are shown in Figure 4.7. As the 2.5% concentration feed increased, the proportion of unreacted dissolved SBH in the product increased. As the 2.5% concentration feed increased, the proportion of unreacted dissolved SBH in the reaction product increased and the proportion of tri-coordinated boron decreased. This seems to be because as the 2.5% concentration feed injection rate increased, the amount of unreacted agglomerated SBH increased and the SBH participating in the reaction decreased, resulting in a relatively high stoichiometric number reaction.

Pictures of unreacted agglomerated SBH observed after the experiments are shown in Figure 4.8. The unreacted agglomerated SBH observed when using 2.5% concentration feed decreased as the 5% concentration feed injection ratio increased. In the case of HD#1, about 5g of unreacted agglomerated SBH was observed, but this is often observed even when 5% concentration feed is used for reasons such as incomplete stirring. This unreacted agglomerated SBH seems to be improved by additionally injecting 5% concentration feed, but in this case, it seems to be meaningless because the effect of increasing the hydrogen storage density is eliminated.

However, if the operation of the hydrogen production system is focused on reducing the cost of feed, or if the water used for the hydrolysis reaction is

the water generated from fuel cell, the amount of formic acid used may be more important. The formic acid usage of experiments HD#1, HD#2, and HD#3 was 87.5%, 75%, and 62.5% compared to the formic acid usage of the 5% concentration reference experiment, showing a much greater difference than the difference in conversion rates. As can be seen in Table 4.2, in the case of the calculated hydrogen storage density excluding water, the order was HD#3 > HD#1 > 2.5% reference > HD#2 > 5% reference. The condition in which excessive unreacted agglomerated SBH occurs is inappropriate to use in actual operation. However, injecting 2.5% concentration feed during the initial 25% reaction progress ratio, such as HD#1, seems to be an operation strategy worth considering in practical usage of SBH hydrogen generation system.

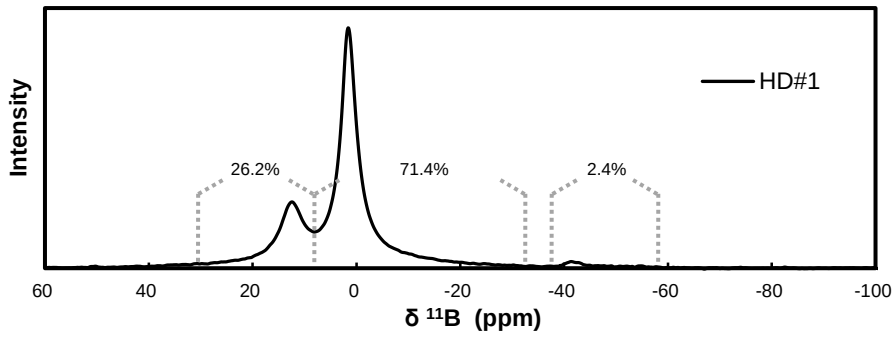

(a)

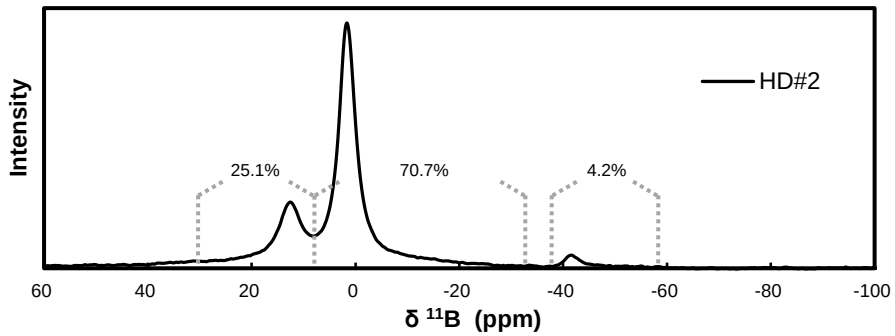

(b)

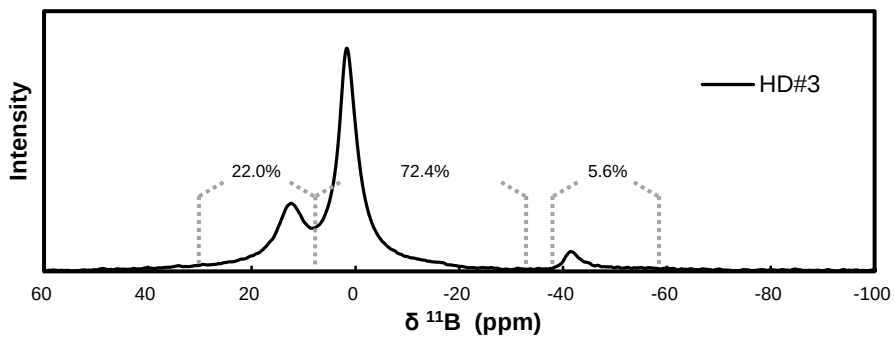

(c)

Figure 4.7 ^{11}B solid NMR spectroscopy results of reaction product in case of (a) HD#1 (b) HD#2 (c) HD#3

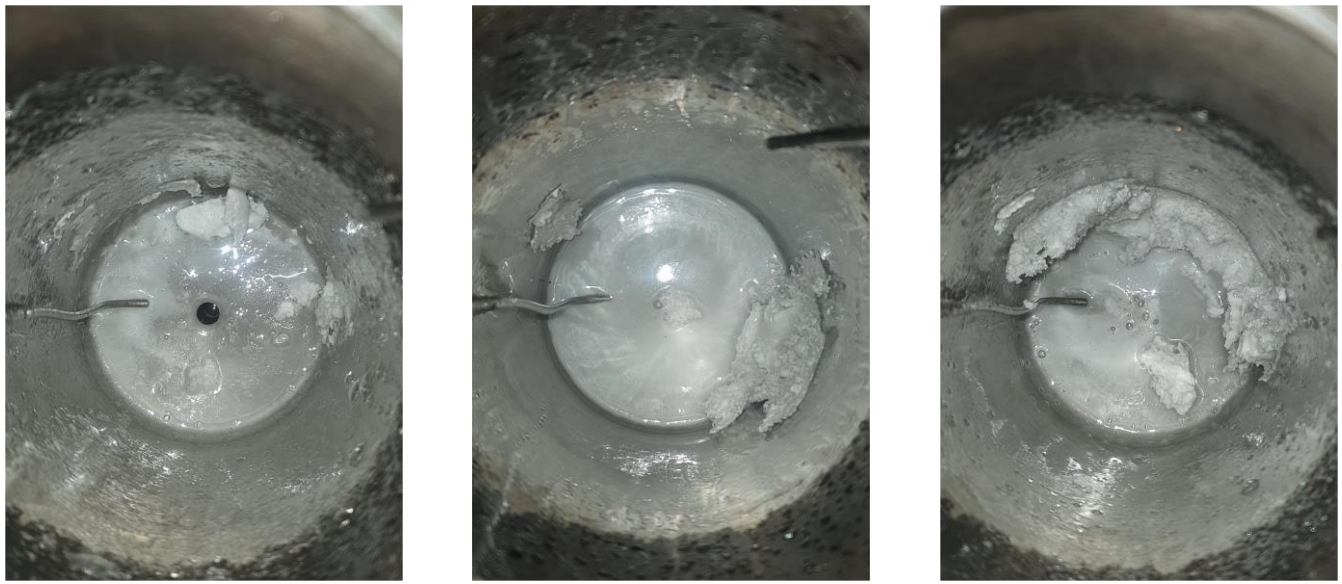

(a) (b) (c)

Figure 4.8 Picture of the unreacted agglomerated SBH after experiment (a) HD#1, (b) HD#2, (c) HD#3

4.4. Summary

In this chapter, operation strategy for on-board operation feasibility and hydrogen storage density improvement of SBH hydrogen generation system based on liquid hydrolysis of SBH.

To utilize the characteristics of SBH, which has a great advantage in transportation compared to other hydrogen storage methods, hydrogen production by SBH is expected to be carried out at the place of hydrogen demand. Therefore, the SBH-based hydrogen generation system must have a flexible hydrogen generation rate. This is also important to reduce the volume, weight, and cost of the entire system by reducing the size of the buffer tank. For on-board operation feasibility evaluation, it was confirmed by experiments how hydrogen generation rate responds by changing the feed injection rate within a single batch reaction. Based on the reference experiment conducted at a constant feed injection rate of 45 mL/min and 75 mL/min in a single batch reaction, the experiments in which the feed injection rate was changed according to the reaction progress ratio was compared. As a result, it was confirmed that when the feed injection rate was changed in a single batch reaction, the hydrogen generation rate followed the changed feed injection rate reference experimental result. In addition, the time it took for the hydrogen

generation rate to respond according to the change in the feed injection rate was about 100 seconds. Thus, it was confirmed that if the entire batch reaction time is secured by sufficient SBH charging amount, it is possible to change the feed injection rate multiple times. Through the experimental results, it was shown that the SBH hydrogen generation system in this study can flexibly control the hydrogen generation rate and can be used as an on-board hydrogen generation system.

To improve the hydrogen storage density and reduce the fuel cost of the hydrogen generation system in this study, it is necessary to reduce the amount of formic acid used. As a result of the experiment using 2.5% acid concentration feed in Chapter 2, the hydrogen generation tendency was similar to that of 5% acid concentration feed at the initial stage of the reaction. Therefore, the experiments were conducted using a 2.5% concentration feed at the initial of the reaction and a 5% concentration feed thereafter to confirm whether it was possible to reduce the amount of acid used. Based on the reference experiment conducted at a constant feed concentration of 2.5% and 5% in a single batch reaction, the experiments in which the feed concentration was changed according to the reaction progress ratio was compared. As a result of the experiments, the experiment using the least 2.5% concentration feed also showed less hydrogen generation amount than the experiment using only 5%

concentration feed, and the amount of hydrogen generation was inversely proportional to the 2.5% concentration feed using ratio. The unreacted agglomerated SBH observed in the experiments using 2.5% concentration feed in Chapter 2 increased in proportion to the 2.5% concentration feed usage ratio. In addition, as the 2.5% concentration feed usage ratio increased, the hydrogen storage density decreased, and in all cases, the hydrogen storage density was lower than that of the experiment using only 5% concentration feed. Therefore, it was not possible to improve the hydrogen storage density through the use of 2.5% concentration feed. However, the hydrogen storage density excluding water were higher in the experiment using the initial 75% (16.7%) and 25% (16.6%) of the 2.5% concentration feed than the experiment using only the 5% concentration feed (16.3%). The hydrogen storage density excluding water may have meaning because the water used in the feed can utilize fuel cell generation water or its cost is very low. In the case of experiments using 2.5% concentration feed during initial 25% reaction progress ratio, the conversion rate was about 1% lower than that of the experiment using only 5% concentration feed, but the usage of formic acid could be reduced by 12.5%, and the unreacted agglomerated SBH was about 5g. Therefore, in some cases, it is possible to consider applying 2.5% concentration feed to the initial 25% reaction progress ratio.

Chapter 5. Concluding remarks

Development of hydrogen storage and transportation technology is essential to expand the use of fuel cell applications necessary to revitalize the hydrogen society to reduce greenhouse gas emissions. In this study, the parameters affecting hydrogen generation performance, reaction and thermal management simulation, and operation strategies of the hydrogen generation system that produces high hydrogen generation rate required for high-power fuel cell applications through acid-accelerated hydrolysis of SBH, a solid-state hydrogen storage material, were analyzed.

In Chapter 2, The characteristics of the SBH hydrogen generation system were analyzed by experiments according to various parameters such as the feed injection rate, reactant temperature, stoichiometric number, and acid concentration of feed. In addition, ^{11}B solid NMR spectroscopy and viscosity measurement by rheometer were conducted to analyze the composition and properties of the reaction product. In experimental cases of 5% feed concentration, the conversion of SBH was ≥95%, and a maximum of 6.71 wt.% gravimetric hydrogen storage density was achieved. The experimental results indicated that it is possible to control the hydrogen generation rate through adjusting the feed injection rate. In addition, as a result of experiments

according to the reactant temperature, it was observed that the lower the reactant temperature, the less hydrogen produced, and the greater the unreacted dissolved SBH. Moreover, when the stoichiometric number increased, the gravimetric hydrogen storage density decreased. However, increased stoichiometric number reduced the viscosity of the reaction product and the amount of unreacted dissolved SBH observed when the reaction was conducted at low reactant temperatures. As a result of the viscosity measurement by rheometer, the reaction product showed gel-solution transition characteristics which has gel and solution state depending on their temperature, suggesting that discharging of the reaction product is virtually impossible at a temperature below the gel-solution transition temperature. Since the gel-solution transition temperature can be significantly lowered by injecting a little additional feed, it is possible to consider increasing the stoichiometric number for practical purposes.

In Chapter 3, The reaction and thermal management simulation of the SBH hydrogen generation system, which has been neglected so far, was performed. Since the hydrogen generation system using SBH has been studied for low-power fuel cell applications, there has been no needs for thermal management simulation. However, since the hydrolysis of SBH is the exothermic reaction and the reaction heat cannot be neglected for high hydrogen generation rate,

thermal management is important in hydrogen generation system for high-power fuel cell applications. Therefore, reaction and thermal management modeling were performed to confirm such as evaluate the maximum operation capability that were difficult to confirm through experiments. The simulation was validated through the experimental results and showed relatively high accuracy. In particular, except for the initial stage of reaction when the reactant was not homogeneous, the reactant temperature was simulated with an error of 5% or less, which means that it is possible to analyze the thermal behavior of the system through this simulation. Base on the simulation result of the reactant temperature, stable operation was possible up to the feed injection rate of 175 mL/min, which can operate about 12 kW of fuel cell applications. Therefore, it is possible to operate high-power fuel cell applications sufficiently by introducing a larger reactor or by connecting several reactors in parallel.

In Chapter 4, The operation strategy for more efficient utilization of this hydrogen generation system was analyzed. First, considering the transportability of SBH, the hydrogen generation system using SBH is likely to be installed in the hydrogen demanding place, so the on-board operation feasibility of hydrogen generation system in this study should be evaluated. If hydrogen generation can be flexibly controlled within a single batch reaction, the buffer tank capacity can be reduced, which can increase the hydrogen

storage density of the entire system. As a result of conducting experiments by changing the feed injection rate within a single batch reaction, the hydrogen generation rate was also increased or decreased according to the increase or decrease of the feed injection rate. The time the system responds to the feed injection rate was about 100 s, and it was confirmed that it is possible to change the hydrogen generation rate multiple times within a single batch reaction if there is sufficient reaction time. Based on this result, it was shown that on-board operation of the hydrogen generation system in this study is possible. In addition, it was evaluated whether it was possible to improve the hydrogen storage density by reducing acid usage. As a result of the experiment according to the acid concentration of feed in Chapter 2, based on the similar tendency of hydrogen generation rate of 2.5% concentration feed and 5% concentration feed at the initial stage of the reaction, a certain ratio of the reaction was conducted with 2.5% concentration feed and the rest stage of the reaction was conducted with 5% concentration feed to maximize hydrogen generation and reduce acid usage. As a result of experiments, even when 2.5% concentration feed was used in the smallest proportion, the conversion and hydrogen storage density were lower than when only 5% concentration feed was used, and the unreacted agglomerated SBH observed when using 2.5% concentration feed was increased as the ratio of 2.5% concentration feed usage increased. However,

when replacing water used for feed with the water generated by fuel cell, using 2.5% concentration feed during the initial 25% reaction progress ratio showed a 1% lower conversion than proceeding with 5% concentration feed, but acid usage can be reduced by 12.5% so it can be considered to reduce fuel cost.

In this study, the hydrogen generation system for high-power fuel cell applications based on hydrolysis of solid-state SBH at high temperature and pressure was introduced and its effectiveness was verified. Through hydrogen generation system of this study, it is expected that the scope of hydrogen applications will be extended to contribute to the revitalization of the hydrogen society in response to fuel cell applications that cannot use high-pressure hydrogen gas or liquefied hydrogen storage methods, and need long-term safe storage of hydrogen.

Reference

[1] Sartbaeva, A., V.L. Kuznetsov, S.A. Wells, and P.P. Edwards, "Hydrogen nexus in a sustainable energy future." *Energy & Environmental Science*, 2008. 1(1).

[2] Dawood, F., M. Anda, and G.M. Shafiullah, "Hydrogen production for energy: An overview." *International Journal of Hydrogen Energy*, 2020. 45(7): p. 3847-3869.

[3] Cigolotti, V., M. Genovese, and P. Fragiacomo, "Comprehensive Review on Fuel Cell Technology for Stationary Applications as Sustainable and Efficient Poly-Generation Energy Systems." *Energies*, 2021. 14(16): p. 4963.

[4] Arzac, G.M., A. Fernández, A. Justo, B. Sarmiento, M.A. Jiménez, and M.M. Jiménez, "Optimized hydrogen generation in a semicontinuous sodium borohydride hydrolysis reactor for a 60W-scale fuel cell stack." *Journal of Power Sources*, 2011. 196(9): p. 4388-4395.

[5] Kim, H., T.H. Oh, and S. Kwon, "Simple catalyst bed sizing of a NaBH4 hydrogen generator with fast startup for small unmanned aerial vehicles." *International Journal of Hydrogen Energy*, 2016. 41(2): p. 1018-1026.

[6] Endo, N., K. Goshome, M. Tetsuhiko, Y. Segawa, E. Shimoda, and T. Nozu, "Thermal management and power saving operations for improved energy efficiency within a renewable hydrogen energy system utilizing metal hydride hydrogen storage." *International Journal of Hydrogen Energy*, 2021. 46(1): p. 262-271.

[7] Sharaf, O.Z. and M.F. Orhan, "An overview of fuel cell technology: Fundamentals and applications." *Renewable and Sustainable Energy Reviews*, 2014. 32: p. 810-853.

[8] Zheng, J., X. Liu, P. Xu, P. Liu, Y. Zhao, and J. Yang, "Development of high pressure gaseous hydrogen storage technologies." *International Journal of Hydrogen Energy*, 2012. 37(1): p. 1048-1057.

[9] Klell, M., "Thermodynamics of gaseous and liquid hydrogen storage." in *International Hydrogen Energy Congress and Exhibition*. 2007. .

[10] Zhang, F., P. Zhao, M. Niu, and J. Maddy, "The survey of key technologies in hydrogen energy storage." *International Journal of Hydrogen Energy*, 2016. 41(33): p. 14535-14552.

[11] Di Profio, P., S. Arca, F. Rossi, and M. Filipponi, "Comparison of hydrogen hydrates with existing hydrogen storage technologies: Energetic and economic evaluations." *International Journal of Hydrogen Energy*, 2009. 34(22): p. 9173-9180.

[12] Folkson, R., "6 - Hydrogen as an energy vector for transportation vehicles**J.W. Sheffield and K.B. Martin, formerly of Missouri University of Science and Technology, United States, contributed to first edition", in Alternative Fuels and Advanced Vehicle Technologies for Improved Environmental Performance (Second Edition), R. Folkson and S. Sapsford, Editors. 2022, Woodhead Publishing. p. 151-171.

[13] De-León Almaraz, S. and C. Azzaro-Pantel, "Chapter 4 - Design and Optimization of Hydrogen Supply Chains for a Sustainable Future", in Hydrogen Economy, A. Scipioni, A. Manzardo, and J. Ren, Editors. 2017, Academic Press. p. 85-120.

[14] Lang, C., Y. Jia, and X. Yao, "Recent advances in liquid-phase chemical hydrogen storage." *Energy Storage Materials*, 2020. 26: p. 290-312.

[15] Demirci, U.B., O. Akdim, J. Andrieux, J. Hannauer, R. Chamoun, and P. Miele, "Sodium Borohydride Hydrolysis as Hydrogen Generator: Issues, State of the Art and Applicability Upstream from a Fuel Cell." *Fuel Cells*, 2010. 10(3): p. 335-350.

[16] Santos, D.M.F. and C.A.C. Sequeira, "Sodium borohydride as a fuel for the future." *Renewable and Sustainable Energy Reviews*, 2011. 15(8): p. 3980-4001.

[17] Wee, J.-H., K.-Y. Lee, and S.H. Kim, "Sodium borohydride as the hydrogen supplier for proton exchange membrane fuel cell systems." *Fuel Processing Technology*, 2006. 87(9): p. 811-819.

[18] Muir, S.S. and X. Yao, "Progress in sodium borohydride as a hydrogen storage material: Development of hydrolysis catalysts and reaction systems." *International Journal of Hydrogen Energy*, 2011. 36(10): p. 5983-5997.

[19] Singh, R., "Reversible chemical hydrogen storage in borohydrides via thermolysis and hydrolysis: Recent advances, challenges, and perspectives." *International Journal of Hydrogen Energy*, 2022. 47(62): p. 26549-26573.

[20] Jubert Tomasso, C., A.L. Pham, T.M. Mattox, and J.J. Urban, "Using Additives to Control the Decomposition Temperature of Sodium Borohydride." *Journal of Energy and Power Technology*, 2020. 2(2): p. 1-20.

[21] Kojima, Y., Y. Kawai, H. Nakanishi, and S. Matsumoto, "Compressed hydrogen generation using chemical hydride." *Journal of Power Sources*, 2004. 135(1-2): p. 36-41.

[22] Liu, B.H. and Z.P. Li, "A review: Hydrogen generation from borohydride hydrolysis reaction." *Journal of Power Sources*, 2009.

187(2): p. 527-534.

[23] Minkina, V.G., S.I. Shabunya, V.I. Kalinin, V.V. Martynenko, and A.L. Smirnova, "Long-term stability of sodium borohydrides for hydrogen generation." *International Journal of Hydrogen Energy*, 2008. 33(20): p. 5629-5635.

[24] Schlesinger, H., H.C. Brown, A. Finholt, J.R. Gilbreath, H.R. Hoekstra, and E.K. Hyde, "Sodium borohydride, its hydrolysis and its use as a reducing agent and in the generation of hydrogen1." *Journal of the American Chemical Society*, 1953. 75(1): p. 215-219.

[25] Abdelhamid, H.N., "A review on hydrogen generation from the hydrolysis of sodium borohydride." *International Journal of Hydrogen Energy*, 2021. 46(1): p. 726-765.

[26] Kojima, Y., K.-i. Suzuki, K. Fukumoto, M. Sasaki, T. Yamamoto, Y. Kawai, and H. Hayashi, "Hydrogen generation using sodium borohydride solution and metal catalyst coated on metal oxide." *International Journal of Hydrogen Energy*, 2002. 27(10): p. 1029-1034.

[27] Shang, Y. and R. Chen, "Hydrogen Storage via the Hydrolysis of NaBH4 Basic Solution: Optimization of NaBH4 Concentration." *Energy & Fuels*, 2006. 20(5): p. 2142-2148.

[28] Abdelhamid, H.N., "High performance and ultrafast reduction of 4-

nitrophenol using metal-organic frameworks." *Journal of Environmental Chemical Engineering*, 2021. 9(1): p. 104404.

[29] Kwon, S.-m., M.J. Kim, S. Kang, and T. Kim, "Development of a high-storage-density hydrogen generator using solid-state NaBH4 as a hydrogen source for unmanned aerial vehicles." *Applied Energy*, 2019. 251.

[30] Churikov, A.V., I.M. Gamayunova, K.V. Zapsis, M.A. Churikov, and A.V. Ivanishchev, "Influence of temperature and alkalinity on the hydrolysis rate of borohydride ions in aqueous solution." *International Journal of Hydrogen Energy*, 2012. 37(1): p. 335-344.

[31] "U.S Department of Energy Hydrogen Program, National Renewable Energy Laboratory, "Go/No-Go Recommendation for Sodium Borohydride for On-Board Vehicular Hydrogen Storage"." 2007; Available from: https://www1.eere.energy.gov/hydrogenandfuelcells/pdfs/42220.pdf.

[32] Principi, G., F. Agresti, A. Maddalena, and S. Lo Russo, "The problem of solid state hydrogen storage." *Energy*, 2009. 34(12): p. 2087-2091.

[33] Demirci, U.B. and P. Miele, "Cobalt-based catalysts for the hydrolysis of NaBH4 and NH3BH3." *Physical Chemistry Chemical Physics*, 2014. 16(15).

[34] Seven, F. and N. Sahiner, "Enhanced catalytic performance in hydrogen generation from NaBH4 hydrolysis by super porous cryogel supported Co and Ni catalysts." *Journal of Power Sources*, 2014. 272: p. 128-136.

[35] Netskina, O.V., E.S. Tayban, V.A. Rogov, A.M. Ozerova, S.A. Mukha, V.I. Simagina, and O.V. Komova, "Solid-state NaBH4 composites for hydrogen generation: Catalytic activity of nickel and cobalt catalysts." *International Journal of Hydrogen Energy*, 2021. 46(7): p. 5459-5471.

[36] Brown, H.C. and B.C.S. Rao, "A New Powerful Reducing Agent—Sodium Borohydride in the Presence of Aluminum Chloride and Other Polyvalent Metal Halides1,2." *Journal of the American Chemical Society*, 1956. 78(11): p. 2582-2588.

[37] Jung, S.C., S.W. Nahm, H.Y. Jung, Y.K. Park, S.G. Seo, and S.C. Kim, "Preparations of Platinum Nanoparticles and Their Catalytic Performances." *J Nanosci Nanotechnol*, 2015. 15(7): p. 5461-5.

[38] Soltani, M. and M. Zabihi, "Hydrogen generation by catalytic hydrolysis of sodium borohydride using the nano-bimetallic catalysts supported on the core-shell magnetic nanocomposite of activated carbon." *International Journal of Hydrogen Energy*, 2020. 45(22): p. 12331-12346.

[39] Brown, C.A., "Catalytic hydrogenation. V. Reaction of sodium

borohydride with aqueous nickel salts. P-1 nickel boride, a convenient, highly active nickel hydrogenation catalyst." *The Journal of Organic Chemistry*, 1970. 35(6): p. 1900-1904.

[40] Amendola, S.C.B., M.; Kelly, M.T.; Petillo, P.J.; Sharp-Goldman, S.L. , "A Novel Catalytic Process for Generating Hydrogen Gas from Aqueous Borohydride Solutions.", *Advances in Hydrogen Energy*, 2002.

[41] Paksoy, A., S.F. Kurtoğlu, A.K. Dizaji, Z. Altıntaş, S. Khoshsima, A. Uzun, and Ö. Balcı, "Nanocrystalline cobalt–nickel–boron (metal boride) catalysts for efficient hydrogen production from the hydrolysis of sodium borohydride." *International Journal of Hydrogen Energy*, 2021. 46(11): p. 7974-7988.

[42] Zhang, J.S., W.N. Delgass, T.S. Fisher, and J.P. Gore, "Kinetics of Ru-catalyzed sodium borohydride hydrolysis." *Journal of Power Sources*, 2007. 164(2): p. 772-781.

[43] Schlesinger, H.I., H.C. Brown, B. Abraham, A. Bond, N. Davidson, A. Finholt, J.R. Gilbreath, H. Hoekstra, L. Horvitz, and E.K. Hyde, "New developments in the chemistry of diborane and the borohydrides. I. General Summary1." *Journal of the American Chemical Society*, 1953. 75(1): p. 186-190.

[44] Liu, B.H., Z.P. Li, and S. Suda, "Nickel-and cobalt-based catalysts for hydrogen generation by hydrolysis of borohydride." *Journal of Alloys and Compounds*, 2006. 415(1-2): p. 288-293.

[45] Liu, B.H., Z.P. Li, and S. Suda, "Solid sodium borohydride as a hydrogen source for fuel cells." *Journal of Alloys and Compounds*, 2009. 468(1-2): p. 493-498.

[46] Liu, Z., B. Guo, S.H. Chan, E.H. Tang, and L. Hong, "Pt and Ru dispersed on LiCoO2 for hydrogen generation from sodium borohydride solutions." *Journal of Power Sources*, 2008. 176(1): p. 306-311.

[47] Singh, S.K., Y. Iizuka, and Q. Xu, "Nickel-palladium nanoparticle catalyzed hydrogen generation from hydrous hydrazine for chemical hydrogen storage." *International Journal of Hydrogen Energy*, 2011. 36(18): p. 11794-11801.

[48] Tuan, D.D. and K.-Y.A. Lin, "Ruthenium supported on ZIF-67 as an enhanced catalyst for hydrogen generation from hydrolysis of sodium borohydride." *Chemical Engineering Journal*, 2018. 351: p. 48-55.

[49] Larichev, Y.V., O.V. Netskina, O.V. Komova, and V.I. Simagina, "Comparative XPS study of Rh/Al2O3 and Rh/TiO2 as catalysts for NaBH4 hydrolysis." *International Journal of Hydrogen Energy*, 2010.

35(13): p. 6501-6507.

[50] Li, K., M. Ma, L. Xie, Y. Yao, R. Kong, G. Du, A.M. Asiri, and X. Sun, "Monolithically integrated NiCoP nanosheet array on Ti mesh: An efficient and reusable catalyst in NaBH4 alkaline media toward on-demand hydrogen generation." *International Journal of Hydrogen Energy*, 2017. 42(30): p. 19028-19034.

[51] Li, Y., X. Hou, J. Wang, X. Feng, L. Cheng, H. Zhang, and S. Han, "Co-Mo nanoparticles loaded on three–dimensional graphene oxide as efficient catalysts for hydrogen generation from catalytic hydrolysis of sodium borohydride." *International Journal of Hydrogen Energy*, 2019. 44(55): p. 29075-29082.

[52] Amendola, S.C., S.L. Sharp-Goldman, M.S. Janjua, N.C. Spencer, M.T. Kelly, P.J. Petillo, and M. Binder, "A safe, portable, hydrogen gas generator using aqueous borohydride solution and Ru catalyst." *International Journal of Hydrogen Energy*, 2000. 25(10): p. 969-975.

[53] Amendola, S.C., S.L. Sharp-Goldman, M.S. Janjua, M.T. Kelly, P.J. Petillo, and M. Binder, "An ultrasafe hydrogen generator: aqueous, alkaline borohydride solutions and Ru catalyst." *Journal of Power Sources*, 2000. 85(2): p. 186-189.

[54] Galli, S., M. De Francesco, G. Monteleone, R. Oronzio, and A. Pozio,

"Development of a compact hydrogen generator from sodium borohydride." *International Journal of Hydrogen Energy*, 2010. 35(14): p. 7344-7349.

[55] Richardson, B.S., J.F. Birdwell, F.G. Pin, J.F. Jansen, and R.F. Lind, "Sodium borohydride based hybrid power system." *Journal of Power Sources*, 2005. 145(1): p. 21-29.

[56] Zhang, J., Y. Zheng, J.P. Gore, and T.S. Fisher, "1kWe sodium borohydride hydrogen generation system: Part I: Experimental study." *Journal of Power Sources*, 2007. 165(2): p. 844-853.

[57] Li, S.-C. and F.-C. Wang, "The development of a sodium borohydride hydrogen generation system for proton exchange membrane fuel cell." *International Journal of Hydrogen Energy*, 2016. 41(4): p. 3038-3051.

[58] Kim, S.J., J. Lee, K.Y. Kong, C. Ryul Jung, I.-G. Min, S.-Y. Lee, H.-J. Kim, S.W. Nam, and T.-H. Lim, "Hydrogen generation system using sodium borohydride for operation of a 400W-scale polymer electrolyte fuel cell stack." *Journal of Power Sources*, 2007. 170(2): p. 412-418.

[59] Kim, J.-H., K.-H. Choi, and Y.S. Choi, "Hydrogen generation from solid NaBH4 with catalytic solution for planar air-breathing proton exchange membrane fuel cells." *International Journal of Hydrogen Energy*, 2010. 35(9): p. 4015-4019.

[60] Kojima, Y., K.-i. Suzuki, K. Fukumoto, Y. Kawai, M. Kimbara, H. Nakanishi, and S. Matsumoto, "Development of 10 kW-scale hydrogen generator using chemical hydride." *Journal of Power Sources*, 2004. 125(1): p. 22-26.

[61] Ferreira, M.J.F., L. Gales, V.R. Fernandes, C.M. Rangel, and A.M.F.R. Pinto, "Alkali free hydrolysis of sodium borohydride for hydrogen generation under pressure." *International Journal of Hydrogen Energy*, 2010. 35(18): p. 9869-9878.

[62] Chen, Y.-H. and J.-C. Lin, "Reactant Feeding Strategy Analysis of Sodium Borohydride Hydrolysis Reaction Systems for Instantaneous Hydrogen Generation." *Energies*, 2020. 13(18).

[63] Oronzio, R., G. Monteleone, A. Pozio, M. De Francesco, and S. Galli, "New reactor design for catalytic sodium borohydride hydrolysis." *International Journal of Hydrogen Energy*, 2009. 34(10): p. 4555-4560.

[64] Marchionni, A., M. Bevilacqua, J. Filippi, M.G. Folliero, M. Innocenti, A. Lavacchi, H.A. Miller, M.V. Pagliaro, and F. Vizza, "High volume hydrogen production from the hydrolysis of sodium borohydride using a cobalt catalyst supported on a honeycomb matrix." *Journal of Power Sources*, 2015. 299: p. 391-397.

[65] Murugesan, S. and V. Subramanian, "Effects of acid accelerators on

hydrogen generation from solid sodium borohydride using small scale devices." *Journal of Power Sources*, 2009. 187(1): p. 216-223.

[66] Akdim, O., U.B. Demirci, and P. Miele, "Acetic acid, a relatively green single-use catalyst for hydrogen generation from sodium borohydride." *International Journal of Hydrogen Energy*, 2009. 34(17): p. 7231-7238.

[67] Kim, H.J., K.-J. Shin, H.-J. Kim, M. Han, H. Kim, Y.-G. Shul, and K.T. Jung, "Hydrogen generation from aqueous acid-catalyzed hydrolysis of sodium borohydride." *International Journal of Hydrogen Energy*, 2010. 35(22): p. 12239-12245.

[68] Aiello, R., J. Sharp, and M.A. Matthews, "Production of hydrogen from chemical hydrides via hydrolysis with steam." *International Journal of Hydrogen Energy*, 1999. 24(12): p. 1123-1130.

[69] Beaird, A.M., T.A. Davis, and M.A. Matthews, "Deliquescence in the hydrolysis of sodium borohydride by water vapor." *Industrial & engineering chemistry research*, 2010. 49(20): p. 9596-9599.

[70] Liu, H., C.M. Boyd, A.M. Beaird, and M.A. Matthews, "Vapor phase batch hydrolysis of NaBH4 at elevated temperature and pressure." *International Journal of Hydrogen Energy*, 2011. 36(11): p. 6472-6477.

[71] Xi, S., X. Wang, D. Wu, X. Hu, S. Zhou, and H. Yu, "Efficient Hydrogen Generation From Hydrolysis of Sodium Borohydride in

Seawater Catalyzed by Polyoxometalate Supported on Activated Carbon." *Frontiers in Chemistry*, 2020. 8.

[72] Javed, U. and V. Subramanian, "Hydrogen generation using a borohydride-based semi-continuous milli-scale reactor: effects of physicochemical parameters on hydrogen yield." *Energy & fuels*, 2009. 23(1): p. 408-413.

[73] Zhang, Q. and R.M. Mohring, "Reaction chemistry between aqueous sulfuric acid and solid sodium borohydride." *Industrial & Engineering Chemistry Research*, 2009. 48(3): p. 1603-1607.

[74] Prosini, P.P. and P. Gislon, "A hydrogen refill for cellular phone." *Journal of Power Sources*, 2006. 161(1): p. 290-293.

[75] Akkuş, M.S., H.B. Murathan, D.Ö. Özgür, G. Özkan, and G. Özkan, "New insights on the mechanism of vapour phase hydrolysis of sodium borohydride in a fed-batch reactor." *International Journal of Hydrogen Energy*, 2018. 43(23): p. 10734-10740.

[76] Marrero-Alfonso, E.Y., J.R. Gray, T.A. Davis, and M.A. Matthews, "Hydrolysis of sodium borohydride with steam." *International Journal of Hydrogen Energy*, 2007. 32(18): p. 4717-4722.

[77] Lee, C.J. and T. Kim, "Hydrogen supply system employing direct decomposition of solid-state NaBH4." *International Journal of*

Hydrogen Energy, 2015. 40(5): p. 2274-2282.

[78] Özkan, G., M.S. Akkuş, and G. Özkan, "The effects of operating conditions on hydrogen production from sodium borohydride using Box-Wilson optimization technique." *International Journal of Hydrogen Energy*, 2019. 44(20): p. 9811-9816.

[79] Retnamma, R., A.Q. Novais, and C.M. Rangel, "Kinetics of hydrolysis of sodium borohydride for hydrogen production in fuel cell applications: A review." *International Journal of Hydrogen Energy*, 2011. 36(16): p. 9772-9790.

[80] Hung, A., S. Tsai, Y. Hsu, J. Ku, Y. Chen, and C. Yu, "Kinetics of sodium borohydride hydrolysis reaction for hydrogen generation." *International Journal of Hydrogen Energy*, 2008. 33(21): p. 6205-6215.

[81] Filiz, B.C. and A.K. Figen, "The Molecular-Kinetic Approach to Hydrolysis of Boron Hydrides for Hydrogen Production." *Kinetics and Catalysis*, 2019. 60(1): p. 37-43.

[82] Gardiner, J.A. and J.W. Collat, "Kinetics of the stepwise hydrolysis of tetrahydroborate ion." *Journal of the American Chemical Society*, 1965. 87(8): p. 1692-1700.

[83] Mesmer, R.E. and W.L. Jolly, "The hydrolysis of aqueous hydroborate." *Inorganic Chemistry*, 1962. 1(3): p. 608-612.

[84] Davis, R.E., E. Bromels, and C.L. Kibby, "Boron Hydrides. III. Hydrolysis of Sodium Borohydride in Aqueous Solution." *Journal of the American Chemical Society*, 1962. 84(6): p. 885-892.

[85] Shabunya, S.I., V.I. Kalinin, V.G. Minkina, and V.V. Martynenko, "Modeling of the Process of Hydrolysis of Sodium Borohydride in a Circulating Reactor." *Journal of Engineering Physics and Thermophysics*, 2018. 91(6): p. 1617-1622.

[86] Zhang, J., Y. Zheng, J.P. Gore, I. Mudawar, and T.S. Fisher, "1kWe sodium borohydride hydrogen generation system: Part II: Reactor modeling." *Journal of Power Sources*, 2007. 170(1): p. 150-159.

[87] Gonçalves, A., P. Castro, A.Q. Novais, C.M. Rangel, and H. Matos, "Modeling of catalytic hydrogen generation from sodium borohydride", in Computer Aided Chemical Engineering, B. Braunschweig and X. Joulia, Editors. 2008, Elsevier. p. 757-762.

[88] Carcadea, E., M. Varlam, I. Stefanescu, A. Marinoiu, and M. Raceanu, "Numerical analysis on the hydrogen generation from sodium borohydride hydrolysis." *Smart Energy and Sustainable Environment*, 2016. 19(1): p. 35.

[89] Sousa, T., V.R. Fernandes, P.J.R. Pinto, Y. Slavkov, L. Bosukov, and C.M. Rangel, "A sodium borohydride hydrogen generation reactor for

stationary applications: Experimental and reactor simulation studies." *Chemical Engineering Science*, 2012. 84: p. 70-79.

[90] Minkina, V.G., S.I. Shabunya, V.I. Kalinin, and V.V. Martynenko, "Stability of aqueous-alkaline sodium borohydride formulations." *Russian Journal of Applied Chemistry*, 2008. 81(3): p. 380-385.

[91] Kreevoy, M. and R. Jacobson, "The rate of decomposition of NaBH4 in basic aqueous solutions." *Ventron Alembic*, 1979. 15(2): p. 2-3.

[92] Geng, S., F.U. Shah, P. Liu, O.N. Antzutkin, and K. Oksman, "Plasticizing and crosslinking effects of borate additives on the structure and properties of poly(vinyl acetate)." *RSC Advances*, 2017. 7(13): p. 7483-7491.

[93] Ouyang, L., H. Zhong, H.-W. Li, and M. Zhu, "A Recycling Hydrogen Supply System of NaBH4 Based on a Facile Regeneration Process: A Review." *Inorganics*, 2018. 6(1).

[94] Kemmitt, T. and G. Gainsford, "Regeneration of sodium borohydride from sodium metaborate, and isolation of intermediate compounds." *international journal of hydrogen energy*, 2009. 34(14): p. 5726-5731.

[95] Lide, D.R., & Kehiaian, H.V., "CRC HANDBOOK of THERMOPHYSICAL and THERMOCHEMICAL DATA (1st ed.)." 1994: CRC Press.

[96] Maier, C.G. and K.K. Kelley, "An equation for the reprentation of high-temperature heat content data1." *Journal of the American Chemical Society*, 1932. 54(8): p. 3243-3246.

[97] Grimvall, G., "Thermophysical Properties of Materials." 1999: Elsevier Science.

[98] Lemmon, E.W., Bell, I.H., Huber, M.L., McLinden, M.O., "NIST Standard Reference Database 23: Reference Fluid Thermodynamic and Transport Properties-REFPROP, Version 10.0, National Institute of Standards and Technology, Standard Reference Data Program, Gaithersburg, 2018.", 2018.

[99] Akdim, O., U.B. Demirci, and P. Miele, "Acetic acid, a relatively green single-use catalyst for hydrogen generation from sodium borohydride." *International Journal of Hydrogen Energy*, 2009. 34(17): p. 7231-7238.

[100] Schmidt, E.F., "Wärmeübergang und Druckverlust in Rohrschlangen." *Chemie Ingenieur Technik*, 1967. 39(13): p. 781-789.

[101] Manlapaz, R.L. and S.W. Churchill, "FULLY DEVELOPED LAMINAR CONVECTION FROM A HELICAL COIL." *Chemical Engineering Communications*, 1981. 9(1-6): p. 185-200.

[102] Petukhov, B.S., "Heat transfer and friction in turbulent pipe flow with variable physical properties", in Advances in heat transfer. 1970,

Elsevier. p. 503-564.

[103] Mori, Y. and W. Nakayama, "Study on forced convective heat transfer in curved pipes:(3rd report, theoretical analysis under the condition of uniform wall temperature and practical formulae)." *International journal of heat and mass transfer*, 1967. 10(5): p. 681-695.

[104] Xin, R.C. and M.A. Ebadian, "The Effects of Prandtl Numbers on Local and Average Convective Heat Transfer Characteristics in Helical Pipes." *Journal of Heat Transfer*, 1997. 119(3): p. 467-473.

[105] Cioncolini, A. and L. Santini, "On the laminar to turbulent flow transition in diabatic helically coiled pipe flow." *Experimental Thermal and Fluid Science*, 2006. 30(7): p. 653-661.

[106] Pawar, S. and V.K. Sunnapwar, "Experimental studies on heat transfer to Newtonian and non-Newtonian fluids in helical coils with laminar and turbulent flow." *Experimental Thermal and Fluid Science*, 2013. 44: p. 792-804.

[107] Pimenta, T.A. and J. Campos, "Heat transfer coefficients from Newtonian and non-Newtonian fluids flowing in laminar regime in a helical coil." *International Journal of Heat and Mass Transfer*, 2013. 58(1-2): p. 676-690.

[108] Fernández-Seara, J., R. Diz, F.J. Uhia, J. Sieres, and A. Dopazo,

"Thermal analysis of a helically coiled tube in a domestic hot water storage tank." *HEFAT 2007*, 2007.

[109] Churchill, S.W. and H.H.S. Chu, "Correlating equations for laminar and turbulent free convection from a horizontal cylinder." *International Journal of Heat and Mass Transfer*, 1975. 18(9): p. 1049-1053.

[110] Ali, M.E., "Laminar natural convection from constant heat flux helical coiled tubes." *International Journal of Heat and Mass Transfer*, 1998. 41(14): p. 2175-2182.

[111] Ali, M.E., "Free convection heat transfer from the outer surface of vertically oriented helical coils in glycerol-water solution." *Heat and mass transfer*, 2004. 40(8): p. 615-620.

[112] Xin, R.C. and M.A. Ebadian, "Natural convection heat transfer from helicoidal pipes." *Journal of Thermophysics and Heat Transfer*, 1996. 10(2): p. 297-302.

[113] Rahul, S., "An experimental study for estimating heat transfer coefficient from coiled tube surfaces in cross-flow of air." in *Proceedings of the Third ISHMT-ASME Heat and Mass Transfer Conference and Fourth National Heat and Mass Transfer Conference, India, December, 1997*. 1997.

[114] Moawed, M., "Experimental study of forced convection from helical

coiled tubes with different parameters." *Energy Conversion and Management*, 2011. 52(2): p. 1150-1156.

[115] Kharat, R., N. Bhardwaj, and R. Jha, "Development of heat transfer coefficient correlation for concentric helical coil heat exchanger." *International Journal of Thermal Sciences*, 2009. 48(12): p. 2300-2308.

[116] Prabhanjan, D.G., T.J. Rennie, and G.S. Vijaya Raghavan, "Natural convection heat transfer from helical coiled tubes." *International Journal of Thermal Sciences*, 2004. 43(4): p. 359-365.

국 문 초 록

기후위기 극복을 위해 온실가스 절감 및 탄소중립 달성을 위한 범 지구적인 노력이 진행되고 있다. 탄소중립 달성을 위해서는 화석연료를 다른 에너지원으로 대체하는 것이 필수적이며, 수소는 현재 화석연료를 대체할 수 있는 에너지 운송체로써 가장 각광받고 있다. 따라서 휴대용 기기부터 대형 화물차, 발전 장치 등 고출력 기기에 이르기까지 수소를 에너지원으로 하는 다양한 에너지 시스템이 도입되고 있다. 하지만 현재 수소 공급에 주로 사용되는 고압기체저장, 액화수소저장 방식은 많은 에너지가 소비되고 대량 수송이 어려워 새로운 수소 저장, 운송 물질이 광범위하게 연구되고 있다. 화학수소화물, 그 중에서도 수소화붕소나트륨($NaBH_4$, SBH)은 높은 수소저장밀도와 운송의 편의성 등으로 미래 수소저장물질로써 각광받고 있다. SBH은 일반적으로 가수분해를 통해 수소를 생산하는데, 산촉매나 금속촉매를 필요로 한다. 일반적으로 상온 상압에서 연속적으로 반응을 수행할 수 있는 금속촉매를 사용한 연구가 많지만, 반응 생성물이 촉매 반응면을 차폐하는 것을 막기 위해 추가적인 물을 필요로 해 낮은 수소저장밀도를 갖게 되며, 고유량의 수소를 생산하기 어렵다. 이러한 한계를 극복하기 위해 본 연구에서는 고온 고압(최대 200 ℃, 40 기압), 산촉매 하에서

수행되는 SBH의 가수분해를 통해 고출력 연료전지 구동을 위한 충분한 유량의 수소를 생산할 수 있는 수소생산시스템을 제안하였다.

먼저 실험을 통해 본 연구의 수소생산시스템의 성능에 영향을 미치는 인자에 대해 분석하였다. 반응물 온도, 산용액 주입 속도, 당량비, 산용액 농도에 따른 본 수소생산시스템의 수소생산 특성을 분석하였다. 반응생성물은 ^{11}B 고체상 핵자기공명분석과 레오미터를 통해 그 조성과 점성을 분석하였다. 실험결과. 5% 농도 산용액을 통한 실험의 경우, 모든 조건에서 95% 이상의 전환율을 보였으며, 수소 발생 성능에 가장 큰 영향을 미치는 인자는 반응물 온도였다. 또한 추가적인 산용액 주입, 즉 당량비 증가를 통해 저온에서 수행된 반응의 낮은 전환율을 보완할 수 있으며, 겔-용액 상전이 온도를 낮춰 반응생성물의 배출을 용이하게 할 수 있음을 확인했다. 2.5% 농도 산용액을 통한 실험결과, 가장 고온(200 ℃)에서 반응한 경우에도 90% 미만의 전환율을 보였으며, 모든 실험에서 반응에 참여하지 않은 덩어리진 고체 SBH가 약 50 g 관측되었다. 따라서 2.5% 농도 산용액만을 통한 반응은 적절하지 않을 것으로 보인다.

SBH의 가수분해 반응은 발열반응으로 반응열을 제어하는 것이 중요하다. 하지만 기존의 SBH 기반 수소생산장치의 경우 주로 저출력 시스템을 대상으로 하였기 때문에 열관리에 대한 연구

필요성이 크지 않았다. 하지만 고출력 연료전지 구동을 위한 본 연구의 수소생산시스템의 경우 반응열이 크기 때문에 성능 및 한계출력 평가를 위해서는 반응 및 열관리에 대한 분석 및 예측이 필요하다. 따라서 본 연구의 수소생산시스템의 반응 및 열관리시스템에 대한 시뮬레이션을 수행하였다. 시뮬레이션에 대하여 실험 결과를 통한 검증을 수행한 결과, 5% 이하의 오차로 반응물 온도 및 냉각수 출구온도 거동을 모사하였다. 시뮬레이션을 토대로 실제 실험으로 검증하기 어려운 한계출력에 대해 평가하였다. 수소발생속도는 산용액 주입속도와 반응진행율의 함수로 계산되었으며, 반응물 온도를 특정온도 (220 ℃) 이하로 유지할 수 있는 최대 수소발생속도를 평가하였다. 결과 본 연구의 수소생산시스템을 통해 최대 13.2 g/min의 수소 발생이 가능하며, 이는 최대 12 kW의 연료전지를 구동할 수 있음을 의미한다.

마지막으로 본 연구의 수소생산시스템의 성능 및 수소저장밀도 최대화를 위한 운전전략에 대해 분석하였다. 저장 및 운송에 장점을 가지는 SBH의 특성상 SBH를 통한 수소생산장치는 수소 수요처에 직접 적용되는 것이 일반적이기 때문에, 수소 수요에 변화에 따른 유연한 수소생산이 필요하다. 이를 평가하기 위해 실험을 통해 단일 회분 반응에서 산용액 주입 속도를 변화시키길 때 수소발생속도 응답을 분석하였다. 실험결과, 용액 주입속도의 증감에 비례하여

수소발생속도가 증감하는 것을 확인하였다. 이를 통해 본 수소생산시스템을 통해 유연한 수소 생산이 가능함을 보였다. 또한 연료 비용을 절감하고 수소 저장 밀도를 높이기 위해 산 사용량 절감을 위한 운전 전략을 실험하였다. 2.5% 농도의 산용액을 사용한 실험은 낮은 전환율과 반응에 미참여한 고체 SBH를 보였으나, 반응 초기에는 5% 농도의 산용액을 통한 실험과 비슷한 수소발생 양상을 보였다. 이에 착안하여 반응 초기에는 2.5% 농도 산용액을 주입하고, 이후에는 5% 농도 산용액을 주입하여 산 사용량을 절감하면서 높은 전환율을 얻을 수 있는 지 확인하였다. 실험결과, 2.5% 농도 산용액 사용 비율이 늘어날수록 낮은 수소 저장 밀도와 전환율을 보였으며, 반응에 미참여한 고체 SBH의 양도 늘어났다. 하지만, 산용액에 사용되는 물은 그 비용이 저렴하고, 연료전지 반응 생성수를 활용할 수 있으므로 물을 제외한 수소저장밀도를 계산할 경우, 초기 25% 반응을 2.5% 농도 산용액을 사용할 경우 5% 농도 산용액만을 사용한 실험보다 1% 가량 낮은 전환율을 보이지만, 더 높은 수소 저장 밀도와 산 사용량을 12.5% 절감할 수 있어, 운영상의 필요에 따라서 적용할 수 있을 것으로 보인다.

본 연구를 통해 산촉매 하에서 고온 고압에서 수행되는 SBH 가수분해를 이용한 고출력 수소생산시스템을 제안하고 그 성능에 영향을 미치는 인자를 분석하였으며, 반응 및 열관리시스템

시뮬레이션을 통해 한계출력을 평가하고 수소저장밀도 향상을 위한 운전 전략에 대해 분석하였다. 본 연구의 수소생산시스템을 통해 수소 저장, 수송 등의 문제로 연료전지 적용이 어렵던 다양한 에너지 시스템에 활용될 경우 수소사회 실현에 기여할 수 있을 것으로 보인다.

주요어: 수소생산시스템, 수소화붕소나트륨 ($NaBH_4$), 개미산, 산촉매 가수분해, 반회분식 반응기 열관리, 운전최적화, 수소저장밀도, ^{11}B 고체상 핵자기공명분석법

학 번: 2013-20642